UNIVERSITY OF CAPE TOWN

Faculty of Engineering and the Built Environment

Department of Civil Engineering

MSc. Dissertation

Feroz Ahmed Mullajee

The Performance Assessment of Patch Repaired and CFRP Strengthened RC T-beams under Transverse Impact Loading

Supervisor

Prof. Pilate Moyo

1st April 2014

The Performance Assessment of Patch Repaired and CFRP Strengthened RC T-beams under Transverse Impact Loading

Feroz Ahmed Mullajee

Thesis submitted to the faculty of Engineering and the Built Environment, University of Cape Town, South Africa, in partial fulfilment of the requirements for the degree of Master of Science in Engineering

Cape Town, 2014

Declaration

I declare that this thesis is essentially my own, unaided work. It is being submitted for the degree of Masters of Science in Engineering in the University of Cape Town, Cape Town, South Africa. It has not been submitted before for any degree or examination in any other University.

……

Feroz Ahmed Mullajee

(1st April 2014)

Abstract

The collision of abnormally loaded vehicles into bridge beams is a frequent occurrence on many highways in South Africa. Structural damage due to such loading conditions requires repair and strengthening procedures that can return the structure to its original load bearing capacity. The use of patch repair mortar is common practice for the repair of impact damaged bridge beams and the use of carbon fibre reinforced polymers (CFRP) has become an established alternative to traditional strengthening materials. However, rehabilitated bridge beams may still be susceptible to the same adverse loading conditions.

The focus of the dissertation was to provide an in depth experimental investigation to determine the performance of patch repaired, CFRP strengthened T-beams subjected to consecutive, transverse, impact loading. The impact loading was applied in the transverse direction to simulate vehicular impact into repaired and strengthened bridge beams. The effect of the repair and strengthening systems on the dynamic response and damage progression was analysed. The possibility of enhancing the impact performance of the T-beams through the application of additional CFRP strengthening was also investigated. Finally, T-beams with varying stirrup spacing were selected in order to investigate the effects of stirrup spacing on the dynamic response and failure mechanisms under consecutive impact loading.

A total of five T-beams were tested. The beams were 1.9m long with identical cross-sectional dimensions and longitudinal reinforcement. The shear reinforcement, however, varied according to stirrup spacing. Four of the test specimens were damaged by exposing the tensile reinforcement and mechanically reducing the cross-sectional area of the reinforcement by approximately 25%. The damaged beams were repaired using patch repair mortar and subsequently strengthened for flexure with externally bonded CFRP laminates applied along the bottom of the T-beams. The remaining T-beam was used as an undamaged control specimen. Additional horizontal strengthening was applied to the side of one of the repaired and strengthened beams to provide additional resistance to the transverse impact loading.

A custom support system was manufactured to secure the T-beams horizontally so that the impact loading could be applied to the webs of the T-beam specimens. The impact loading

was induced at midspan, using a drop hammer impact machine. The beams were impacted consecutively from varying drop heights in order to analyze their behaviour as damage intensified. The contact force response, midspan deflection response and the progression of damage were recorded after each drop test.

The results indicated that the damage mechanisms varied according to stirrup spacing. High stirrup spacing resulted in low composite action between the flange and the web, which led to excessive cracking at the flange-web interface and a larger proportion of damage induced in the web. Conversely the damage observed in beams with low stirrup spacing showed a larger transfer of damage between the web and the flange, thus indicating a high degree of composite action. Increased stirrup spacing was also observed to result in an earlier deterioration of stiffness due to the consecutive impact tests.

The repaired and strengthened beams showed a greater capacity to withstand consecutive impact loading, although this improvement was considered minor. The slight increase in capacity was attributed to the combined effect of the patch repair concrete (which has superior tensile and compressive strengths than the substrate) and the transverse stiffness of the CFRP laminates. No cracking was observed to form along the interface between the repair mortar and the substrate thus indicating that the patch repair provided a continuous bond and did not have a noticeable effect on the damage progression.

The T-beam strengthened in the horizontal direction with additional CFRP laminates showed an increase in capacity to withstand transverse impact and an increase in transverse stiffness. The additional strengthening and stiffening also prevented delamination of the CFRP laminate applied to the bottom of the T-beam and minimised damage progression into the web, thus indicating the potential use of such a strengthening system as a means of energy absorption in bridge beams susceptible to transverse vehicular impact.

Acknowledgements

The author would like to thank the following people for their support and assistance during the dissertation period:

- My supervisor, Professor Pilate Moyo, for all the time he dedicated towards my study, the patience that he showed towards me and the manner in which he always challenged me to test the boundaries of CFRP investigations.
- A special thank you must go to Dr Steeve Chung Kim Yuen at the University of Cape Town, Blast and Impact Survivability Research Unit (BISRU), for supervising and ensuring my experimental program was successfully completed.
- Appreciation must also be given to the University of Cape Town laboratory and workshop staff. Mr Noor Hassen, Mr Charles Nicholas, Mr Charles May, Mr Elvino Witbooi and Mr Hector Mafungwa for all their assistance.
- Finally a special thank you to my parents, Muinuddin Mullajee and Ferial Mullajee, and my grandfather Taalib Sydney for all their encouragement and support throughout the dissertation period.

Table of Contents

List of Tables

List of Figures

List of Abbreviations

- **Amplitude** – The maximum value of a function as it varies with time.
- **Anisotropic** – A material with different mechanical properties in different directions.
- **Bar spacing** – The distance between parallel reinforcing bars, measured centre- to-centre of the bars perpendicular to their longitudinal axes.
- **Bond splitting** – Delamination of a FRP strengthened beam due to the separation of concrete from the tensile reinforcement.
- **Bond strength** – Resistance to separation of repair or strengthening materials from the substrate material.
- **Bonding agent** – A material applied to a suitable substrate to enhance bond between it and a new repair layer or CFRP laminate.
- **CFRP** – Carbon Fibre Reinforced Polymer
- **Compatibility of repair material and substrate** – The balancing of dimensional, permeable, chemical and electrochemical properties of the substrate and the repair material.
- **Composite** – A combination of two or more constituent materials.
- **Concrete Cracking** – When the structure has visible cracking on the surface, or dismemberment of the concrete as a whole.
- **Concrete substrate** – The original concrete surface to which repair mortar or CFRP strengthening is applied.
- **Contact force** – The maximum recorded force resulting from an impact load. The amplitude of the impact load.
- **Contact force response** – The variation of the impact force with respect to time.
- **Corrosion** – Destruction of metal by a chemical, electrochemical, or electrolytic reaction within its environment.
- **Creep** – The tendency of concrete to deform permanently under sustained loading conditions.
- **Cyclic Load** – A repetitive load at a constant frequency and amplitude.
- **Debonding** – A separation at the interface between the substrate and adherent material.
- **Deflection halfcycle** – The initial waveform/pulse of the deflection response.

- **Deflection response** – The variation of the deflection with respect to time.
- **Deformation** – A change in shape or size.
- **Delamination/Debonding** – When the CFRP laminate detaches from the original substrate or patch repair material, caused by excessive loading.
- **Deterioration** – Physical manifestation of failure of a material (e.g., cracking, delamination, flaking, pitting, scaling, spalling, staining) caused by service conditions or internal autogenous influences.
- **Drop hammer impact** – An impact load induced via a drop hammer impact machine.
- **Ductility** – A solid materials ability to deform under tensile stress.
- **Durability** – The ability of a structure or its components to maintain serviceability in a given environment over a specified time.
- **Dynamic increase factor (DIF)** – The ratio of the quasi-static ultimate stress to the dynamic ultimate stress.
- **Dynamic equilibrium** – When all the forces of an object in motion balance.
- **Dynamic response** – the response of a structural system to dynamic loading conditions.
- **Elastic deformation** – Deformation which is reversible.
- **Elastic Modulus** – Quantity describing the tendency of an object to deform under an applied load.
- **Energy dissipation** – The loss of energy introduced to a system to heat, sound, plastic deformation and other irreversible processes.
- **Fatigue life** – The number of cycles of fluctuating stress and strain that a material can sustain before failure.
- **Fibre reinforced polymer (FRP)** – A general term for a composite material that consists of a polymer matrix reinforced with cloth, strands, or any other fibre form.
- **Flexural rigidity** – The bending stiffness in beams
- **Flexure critical RC beams** – RC beams which have sufficient shear resistance
- **Global response** – Response phase due to the elastic-plastic deformation that occurs throughout a RC beam subjected to impact loading for a relatively long period after the induced impact

- **Grinding depth** – The depth to which the bottom tensile reinforcing bars were grinded in order to simulate flexural damage.
- **Heterogeneous material** – A material with different compositions.
- **Impact** – A time dependent load of high intensity occurring over a short duration of time which occurs when one object collides with another.
- **Impulse** – The change in momentum per unit time.
- **Interface** – The boundary between two materials, e.g., an existing concrete substrate and a bonded patch repair material or CFRP laminate.
- **Interfacial bond** – The bond between two different substances e.g. patch repair and CFRP
- **KFRP** – Kevlar Fibre Reinforced Polymer.
- **Laitance** – A weak layer of cement and concrete fines on a concrete surface.
- **Laminate** – One or more layers of fibre bound together in a cured resin matrix.
- **Laminate peeling** – Delamination of a FRP strengthened beam due to debonding of the FRP from the substrate surface.
- **Loading rate sensitivity** – The sensitivity of a material to loading rates.
- **Local failure** – Damage of a reinforced beam subjected impact characterised by concrete penetration and crushing.
- **Local response** – The development of a stress wave in the region of impact for a short duration after the impact.
- **Low velocity impact** – Impact of a high mass impactor travelling at a relatively low velocity.
- **NSMR** – Near Surface Mounted Strengthening.
- **Over-reinforced beams** – RC beams which fail due to crushing of concrete in the compression zone before the yielding of the tensile steel reinforcement, thus exhibiting abrupt failure.
- **Patch Repair** – A material used to substitute a portion of removed damaged concrete
- **Plastic deformation** – Deformation which is irreversible
- **Polymerization** – The process of converting a monomer into a polymer.

- **Propagate** – When a crack increases in length and size over time whilst under loading.
- **Pultrusion** – The process of pulling fibres through an unset binding resin.
- **Quasi static loading** – A load applied at a rate low enough to be considered static loading.
- **Repair** - The removal, cleaning, and replacement of damaged, deteriorating materials.
- **Scabbing** – Localised detachment of concrete along tensile reinforcing bars
- **Service life** – An estimate of the remaining useful life of a structure based on the current rate of deterioration or distress, assuming continued exposure to given service conditions without repairs.
- **Service load** – The load specified by general building codes that will not cause loss of serviceability of the structures.
- **Shear critical RC beams** – RC beams which have insufficient shear resistance
- **Shrinkage** – Volumetric change of concrete due to loss of moisture.
- **Spall** – A fragment of the cover concrete that is detached from the parent concrete.
- **Static load** – A single applied load at a constant rate or time.
- **Stiffness** – Resistance to deformation.
- **Stirrup** – Reinforcement used to resist shear and torsion stresses in a structural member.
- **Strain** – The change in length, per unit of length, in a linear dimension of a body.
- **Strain rate** – The rate of change in strain with respect to time.
- **Strengthening** – The structural enhancement of weakened structural elements in order to restore or improve their capacities in flexure, shear or direct tension and compression.
- **Stress** – Intensity of force per unit area.
- **Thermoplastics** – A polymer matrix which softens due to the application of heat and hardens due to cooling.
- **Thermosets** – A polymer matrix formed due to an irreversible chemical reaction between a resin and a hardener.

- **Time taken to rebound** – The total time taken from the point of initial contact of the drop hammer with the test specimen to the secondary contact due to the rebounding of the drop hammer.
- **Ultimate stress** – The stress at which failure of a material is observed.
- **Under-reinforced beams** – RC beams which fail due to yielding of the tensile steel reinforcement, exhibiting gradual failure.

List of Symbols

A_1	=	The area lost due to grinding subtracted from half the area of the reinforcing bar
A_l	=	Area lost due to grinding of steel reinforcing bar
A_s	=	Area of tensile steel reinforcement
F_{max}	=	Amplitude of contact force response (maximum contact force)
F_s	=	Internal compression force carried by the compression steel reinforcement
h	=	Drop height at which drop hammer is released
$I_{(t)}$	=	Impact force variation with respect to time
L	=	Length of RC beam specimen
$\bar{m}$	=	Equivalent mass of the drop hammer impactor
q	=	The grinding depth subtracted from the radius of the reinforcing bar
$R_{(t)}$	=	Reaction force variation with respect to time
s_f	=	Average spacing between flexural cracks
s_w	=	Average spacing between diagonal shear cracks on T-beam web
t_d	=	Duration of contact force
t_r	=	The total duration from the point of initial contact of the drop hammer with the test specimen to the secondary contact due to the rebounding of the drop hammer.
$\ddot{u}(x,t)$	=	Acceleration of beam and drop hammer mass system resulting from impact
Y_{max}	=	Maximum dynamic midspan deflection

Chapter 1: INTRODUCTION

1.1 Background to study

The deteriorating condition of concrete bridge infrastructure is a major problem worldwide. Deterioration can result from numerous factors including inadequate design, inappropriate material use, poor workmanship, prolonged environmental influences and adverse loading conditions. A particular problem, which is a frequent occurrence on many highways in South Africa, is vehicular impact of abnormally loaded trucks into bridge beams. The damage induced due to such loading conditions can vary in severity. Minor defects include the formation of surface cracks and minor spalling of concrete. Impact damage can also result in the exposure of reinforcing bars or prestressed tendons due to excessive spalling of concrete. In the most severe cases, reinforcing bars or prestressed tendons incur damage or complete rupture with the added possibility of beam misalignment. The exposure of reinforcement increases susceptibility to accelerated deterioration and damaged reinforcement may result in reduced load bearing capacity of the bridge beam. Figure 1 shows a bridge beam damaged due to transverse vehicular impact.

Figure 1: Bridge beam damaged as a result of transverse vehicular impact (SMEC, 2007)

Damaged concrete is usually repaired by the removal and replacement of the damaged volume with a cementitious patch repair mortar. The purpose of the patch repair is firstly to rebuild the damaged structure to its original surface profile and secondly to provide adequate protection against further deterioration, thus ensuring durability at the damage location. Any reduction in load carrying capacity also needs to be restored through the provision of a suitable strengthening system. The use of fibre reinforced polymers (FRP) for the strengthening of damaged bridge structures has become a viable alternative to traditional strengthening materials. Carbon-fibre reinforced polymer (CFRP) laminates can be bonded to a damaged bridge beam to increase or restore its load bearing capacity.

A bridge beam damaged due to vehicular impact and subsequently repaired and strengthened via patch repair and CFRP strengthening systems is still susceptible to the same impact loading conditions. Therefore there is a need to understand the behaviour of patch repaired RC beams, strengthened with CFRP laminates, subjected to transverse, low velocity, impact loading.

Transverse reinforcing stirrups in concrete bridge beams usually extend through the top of the beam in order to facilitate composite action between the bridge beam and the deck-slab, under normal loading conditions. However, under horizontal vehicular impact, the extension of the transverse stirrups into the deck-slab creates an additional boundary condition to resist transverse impact. The effect of stirrup spacing on the interaction between the bridge beam and deck under transverse impact loading is another area of research to be considered.

1.2 Statement of the problem

Limited research has been conducted to analyse the performance of RC beams, strengthened using CFRP laminates, subjected to low velocity impact loading. The few studies reported in the literature, such as Erki and Meier (1999) and Tang and Saadatmanesh (2003) focus on the potential use of FRP to enhance the impact behaviour of RC beams. This corresponds to vertically applied impact loading such that the strengthened beams undergo flexure about their major bending axis. The available studies also, only analyse the behaviour of strengthened beams without the presence of cementitious patch repair mortar.

In relation to the occurrence of transverse vehicular impact into bridge beams, currently no research has been identified which analyses the behaviour of patch repaired RC beams, strengthened with CFRP laminates, subjected to low velocity, transverse impact loading. In addition, no research has been conducted which analyses the effect of stirrup spacing on the degree of composite action between a bridge beam and deck-slab subjected to low velocity, transverse impact loading.

This study will address these issues experimentally by subjecting patch repaired RC T-beams, strengthened with CFRP laminates, to consecutive, transverse, impact loading tests. T-beams, with varying stirrup spacing, are selected in order to investigate the interaction between a bridge beam and deck-slab.

1.3 Dissertation objectives

The following objectives have been set for the study:

- Investigate the behaviour of the patch repair and the externally bonded CFRP laminates under consecutive impact loading. This will involve the identification and discussion of all possible failure modes resulting from the impact loading tests.
- Investigate the effects of the patch repair and CFRP strengthening on the dynamic response due to consecutive impact loading. The dynamic response includes the contact force response and the displacement response.
- Investigate the possibility of enhancing the impact performance through the application of additional transverse CFRP strengthening.
- Investigate the effect of stirrup spacing on the interaction between the flange and web of the T-beam specimens. Also, determine the effect of stirrup spacing on the progression of damage and the dynamic response of the beams under consecutive impact loading.

1.4 Outline of the thesis document

Chapter two provides an in depth analysis of existing research which focuses on the core aspects of the overall dissertation. These aspects include the behaviour of RC beams subjected to impact loading, repair methods for damaged RC structural elements, strengthening techniques for bridge beams damaged in flexure, the use of FRP as an

alternative strengthening material and finally the behaviour of RC beams strengthened with externally bonded FRP composites under impact loading.

Chapter three describes in detail the methodology followed for various stages of the experimental program. This includes a description of the procedure followed to induce damage, repair and strengthen each of the test specimens. The testing program is also described in detail.

Chapter four conveys all the test results and provides detailed discussions of all relevant observations. The results include detailed diagrams depicting the damage progression observed in the various test specimens due to consecutive impact tests as well as graphical representations of the contact force response and deflection response recorded after each impact test.

Chapter five focuses on providing conclusions based on the results obtained. Finally, recommendations for further studies related to the dissertation topic are provided.

2 Chapter 2: LITERATURE REVIEW

2.1 Introduction

This review provides an analysis of existing research which focuses on core aspects related to the overall objectives of this work. The review begins by discussing impact loading and loading rate effects on reinforced concrete beams particularly focusing on experimental procedures, damage mechanisms and failure modes. Thereafter, methods and aspects pertaining to the repair of damaged concrete structures are discussed in detail. Standard strengthening procedures for concrete bridge girders damaged in flexure are also discussed. The review then focuses on advantages of FRP composites as opposed to conventional strengthening materials as well as focusing on FRP strengthening systems for RC or pre-stressed concrete beams damaged in flexure. Finally the behaviour of RC beams, strengthened with FRP composites, subjected to impact loading, is analysed and discussed in detail.

2.2 Impact loading on RC beams

2.2.1 Introduction

Predicting the effects of impact loading on RC beams can be difficult due to the range of structural responses possible and the variability of material behaviour. Impact occurs over a short period of time and therefore causes the impacted structure to deform at strain rates greater than that induced due to quasi-static loading. The strain rate is a description of the rapidity of the deformation processes. Figure 2 shows varying strain rates associated with specific loading conditions. Vehicular impact is considered to be low velocity impact since it involves a high mass impactor travelling at a relatively low velocity (Kabir and Shafei, 2009). An analysis into the effects of impact loading on RC beams can provide insight into structural response of RC bridge beams subjected to transverse vehicular impact.

RC structures are composites consisting of plain concrete and steel reinforcement. Therefore the effect of loading rate on a RC element is influenced by the rate sensitivity of the constituent materials (Adhikary et al, 2012). In the following sections the behaviour of concrete and steel reinforcement under high loading rates will initially each be discussed.

This will be followed by a detailed discussion of the behaviour RC beams subjected to varying loading rates as well as impact load loading.

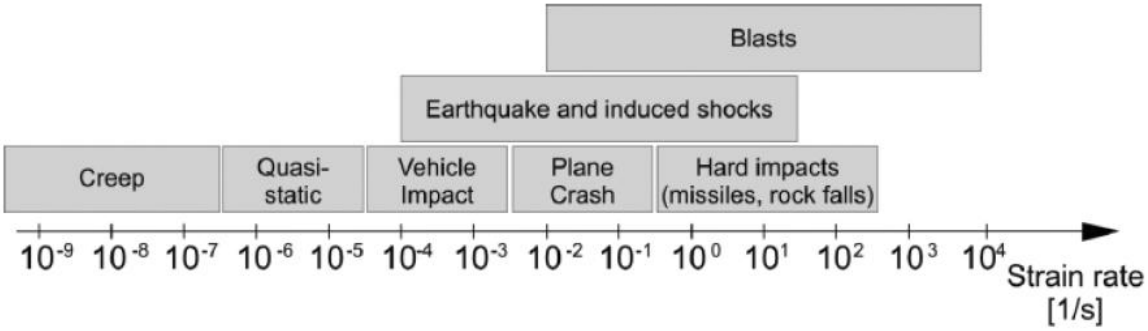

Figure 2: Typical strain rates associated with various loading conditions (Bischoff and Perry, 1991)

2.2.2 Strain rate sensitivity of concrete and reinforcing steel

The number of studies analysing the behaviour of concrete subjected to loading rates higher than that of quasi-static loading are limited. This is mainly due to difficulties associated with the development and operation of consistent, effective experimental techniques that can assure high rates of loading (Brara and Klepaczko, 2006). Results pertaining to the mechanical properties of concrete subjected to varying rates of strain have been reported to differ according to experimental technique and specimen dimensions (Pajak, 2012). However, an increase in strain rate has generally been reported to result in corresponding increases in the ultimate compressive stress, ultimate tensile stress, elastic modulus and the peak strain of concrete (Cusatis, 2011). The magnitude of strength increases are quantified by the dynamic increase factor (DIF), which represents the ratio of the quasi-static ultimate stress to the dynamic ultimate stress. Figure 3 is a scatter of DIF results from various experimental studies for concrete loaded in compression and tension at varying loading rates. The results of the various studies clearly indicate an increase in the DIF for specimens loaded in compression and tension (Cusatis, 2011). Specimens loaded in tension undergo a transition from low rate sensitivity to high rate sensitivity at a strain rate of approximately $1sec^{-1}$, whilst the transition rate for concrete in compression is approximately $10sec^{-1}$ (Brara, 2005). Strain rates above these transitional values result in large increases in ultimate stress. Loading rate also has an effect on the fracture behaviour of concrete, in that concrete

generally exhibits an increasingly brittle nature due to increasing loading rates (Adhikary et al, 2012).

As with concrete the principle effect of high loading rates on steel reinforcement is to increase yield stress to values beyond that of the static yield stress. High loading rates however have less of an effect on the ultimate stress of steel reinforcing bars (Norris, 1959). The strength properties of steel reinforcement can increase up to 60% for loading rates up to 10sec^{-1} , and up to 100% for loading rates up to 225sec^{-1} (Malvar and Crawford, 1998). The DIF for both yield and ultimate stress of steel reinforcement is inversely related to the static yield stress. Therefore the DIF is higher for mild steel than it is for high strength steel (Malvar and Crawford, 1998). Figure 4 is taken from a study conducted by Malvar and Crawford (1998) and represents a DIF formulation for varying grades of reinforcing steel, proposed for the American Society for Testing and Materials (ASTM).

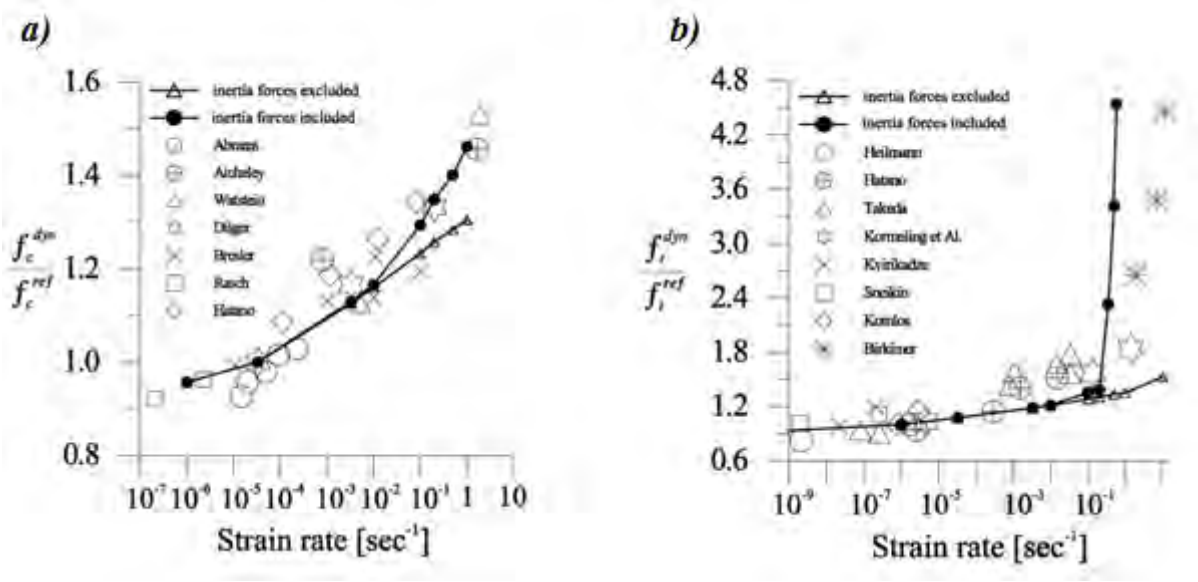

Figure 3: Dynamic increase factors observed by various researchers for (a) concrete in compression (b) concrete in tension at varying loading rates, (Malver and Crawford, 1998)

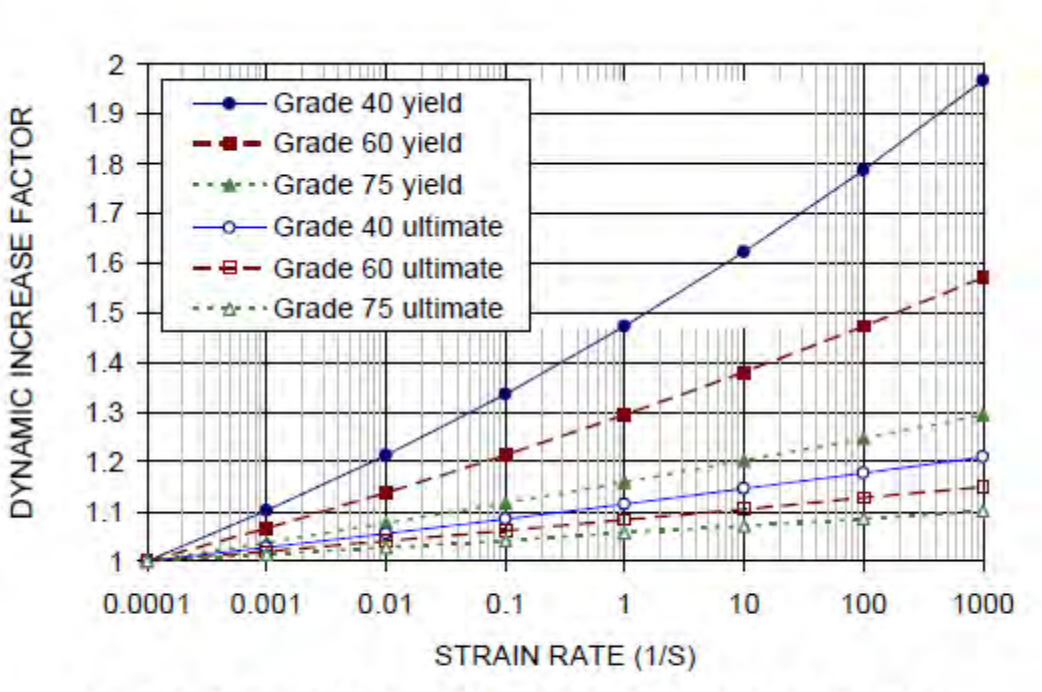

Figure 4: Proposed DIF for ASTM Grade, 40, 60 and 75 steel rebar (Assuming yield stresses of 48, 69 and 87 ksi respectfully), (Cusatis, 2011)

2.2.3 Behaviour of RC beams subjected to varying strain rates and drop hammer impact loading

Having briefly considered the effects of varying loading rates on the mechanical properties of concrete and reinforcing steel individually we now proceed to the overall behaviour of reinforced concrete beams subject to high loading rates and impact loading.

It has already been established that high loading rates result in an increase in ultimate compressive strength, ultimate tensile strength, elastic modulus and the peak strain of concrete. However, as loading rate increases concrete exhibits an increasingly brittle nature (Adhikary et al, 2012). It has also been established that steel subjected to high loading rates experience higher yield stress, whilst the increase in ultimate stress is less pronounced. Limited research has been conducted on the behaviour of RC beams subjected to high loading rates (Kulkarni and Shah, (1998); Fujikake et al, (2009); Mutsuyoshi and Machida, (1984); Adhikary et al, 2012). The findings of the few studies conducted on this subject indicate that the increases in the strength of concrete and steel due to increasing loading rates are reflected by corresponding increases in the ultimate load carrying capacity,

stiffness and energy absorption of RC beams subjected to increasing loading rates (Adhikary et al, 2012).

The behaviour of RC beams subjected to impact loading has been investigated experimentally, analytically and numerically. Initially, experimental studies were conducted in order to develop empirical and analytical models to predict the response of RC beams subjected to impact. Most of the analytical models were based on single degree of freedom systems using the basic principles of structural dynamics (Sangi, 2011). The development of numerical methods and in particular the finite element method, has led to the elimination of limitations associated with experimental methods. Such limitations include expensive material costs and the time needed for specimen preparation. Therefore most of the current experimental studies are carried out for the verification and validation of numerical simulations (Sangi, 2011). This study will focus on experimental methods and in particular the damage mechanisms and failure modes observed as a result of experimental impact tests on RC beams.

2.2.3.1 Drop hammer impact testing

Impact tests on RC beams are generally conducted via drop hammer impact apparatus such as that shown in Figure 5. The impact loading is induced via a drop weight which falls along guiding rails from a specified drop height.

The shape of the striking head differs according to the various experimental studies, however, they generally have blunt surfaces such as curved or hemispherical surfaces (Tachibana et al, 2010; Fujikake et al, 2009). Kishi et al (2001) conducted drop hammer impact tests with three different blunt hemispherical striking heads of radii r = 1407mm, 90mm, and 30mm to determine the effects of the loading area on the dynamic response of RC beams. The findings from this study indicated that varying loading areas had little effect on the time histories of the impact force, reaction force and the deflection.

Most of the drop hammer tests reported in literature utilized simply supported RC beams (Hughes and Beeby, 1982; Ishikawa et al, 2006; Fujikake et al, 2009). RC beams are typically simply supported through the provision of custom support systems that prevents uplift during impact without inducing restraint moments (Saatci and Vecchio, 2009).

The parameters measured during drop hammer impact tests generally include the following:

- The contact force and the reaction force response (generally measured using loadcells).
- Displacement response at the beam midspan (generally measured using laser displacement sensors).
- Strain measurements on the concrete surface and/or in the steel reinforcement (generally measured via electronic strain gages).

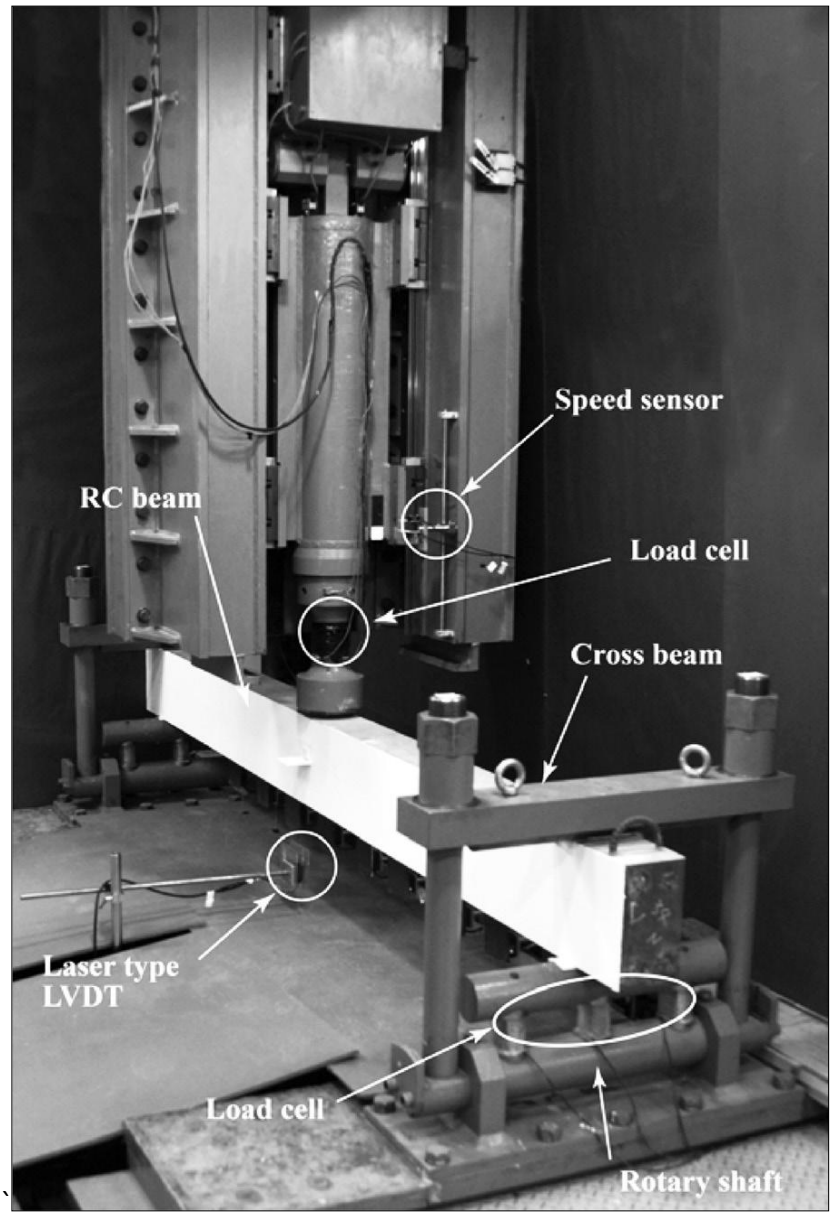

Figure 5: Typical drop hammer impact apparatus (Kishi et al, 2001)

2.2.3.2 Distribution of forces and dynamic equilibrium

A beam subjected to low velocity impact loading at its midspan is in a state of dynamic equilibrium as the load is applied and during the resulting dynamic response (Saatci and Vecchio, 2009). For dynamic equilibrium to exist, the inertia force must act in the direction opposite to the acceleration of the beam at a specific point in time. Figure 6 is a free body diagram depicting the forces resulting from low velocity impact on a beam.

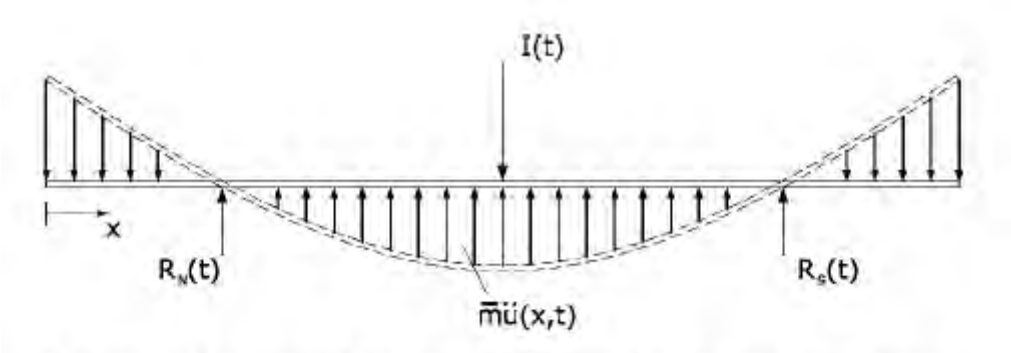

Figure 6: Free body diagram depicting dynamic equilibrium due to impact loading on a simply supported beam (Saatci and Vecchio, 2009)

The inertial force distribution is taken as being the same as the deflected shape of the beam (which coincides with the first mode shape of vibration response). All of the forces acting on the beam are functions of time. $\boldsymbol{I(t)}$ represents the impact force, $\boldsymbol{R_N(t)}$ and $\boldsymbol{R_S(t)}$ represent the support reactions at either end of the beam, and the Inertia force is equivalent to the mass of the impactor, $\boldsymbol{\bar{m}}$, multiplied by the acceleration, $\boldsymbol{\ddot{u}(x,t)}$, integrated over the entire volume of the beam (Saatci and Vecchio, 2009). The following equation represents the dynamic equilibrium of a beam subjected to impact loading at the midspan,

$$\int_0^L \bar{m}\ddot{u}(x,t)dx + R_A(t) + R_B(t) - I(t) = 0 \qquad (1)$$

where $\boldsymbol{L}$ is the total length of the specimen.

From Equation 1 it can be seen that the applied impact force is resisted by a combination of the inertia force and the reaction forces for a specific point in time. Figure 7 illustrates typical experimental data captured by Saacti and Vecchio (2009) which depicts the individual force components of the forces represented in Equation 1. From Figure 7 it is

clear that the impact force is immediately resisted by the development of the inertia force. As the impact force is imparted to the beam, the stress wave generated by the impact eventually reaches the reactions at which stage a negative inertia force is generated to ensure dynamic equilibrium. The time taken for the stress wave to reach the supports is dependent on the span of the beam as well as the beam cross-sectional dimensions.

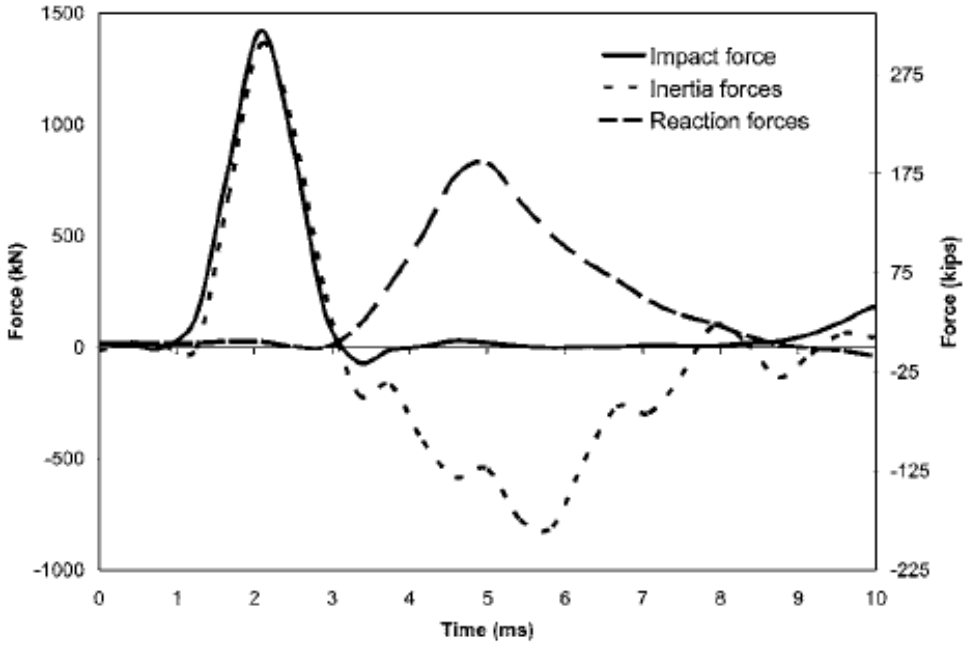

Figure 7: Experimental data depicting impact force, inertia force and reaction force responses (Saatci and Vecchio, 2009)

2.2.3.3 Damage mechanisms and Failure modes

Damage induced in drop hammer impact tests on RC beams can generally be categorised according to two response phases, namely the local response phase and the global response phase (Fujikake et al, 2009).

The local response phase is caused by the development of a stress wave at the position of contact for a short duration after the impact. Local failure is characterised by concrete penetration and crushing and is more commonly a concern when dealing with RC plates subjected to impact loading (Fujikake et al, 2009). Thabet and Haldane (2000) have described the following damage mechanisms related to the local response phase:

- **Surface crushing:**

  As the drop hammer makes contact with the beam, compressive stress waves are transmitted in the region of contact within the initial microseconds of the impact. Energy is dissipated through localised crushing of concrete forming a crater on the contact surface (refer to Figure 8 (b & c)).

- **Scabbing:**

  The compressive stress waves are eventually reflected resulting in tension failure on the tensile surface. Such failure is characterized by localized detachment of concrete along the flexural reinforcing bars (refer to Figure 8 (d)).

- **Concrete plug formation:**

  Upon the application of the impact load, the stress wave travels through the beam and is reflected by aggregate, reinforcement, voids and cement paste (Sangi, 2011). The downward acceleration of the beam results in the development of inertia forces and a build up of momentum as the stress wave is dissipated. If the momentum is large enough a shear crack formation, known as a shear plug forms in the initial stage of the impact before the beam has time to respond in flexure (refer to Figure 8 (e)) (Sangi, 2011).

The global response phase is due to the elastic-plastic deformation that occurs throughout the RC beam for a relatively long period after the induced impact (refer to Figure 8 (a)). The overall response of RC beams subjected to impact loading is usually a combination of local and global response phases, however the global response is considered to be the main concern for RC beams subjected to impact loading (Hughes and Beeby, 1982; Fujikake et al, 2009).

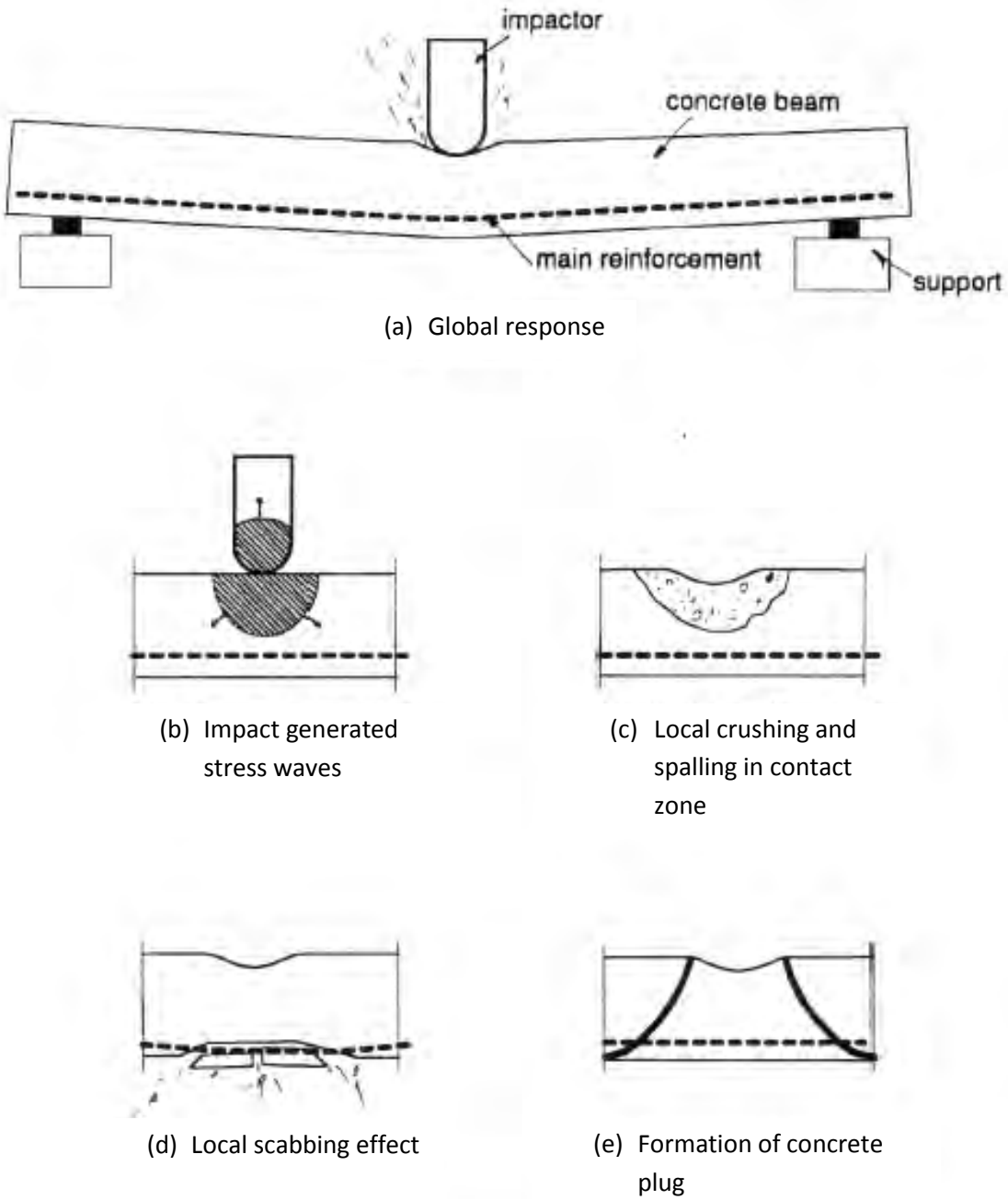

Figure 8: Damage mechanisms due to low velocity impact on a RC beam (Thabet, 1994)

2.2.3.4 Experimental studies conducted on RC beams subjected to varying loading rates and drop hammer impact loading

A reinforced concrete beam subjected to static loading will exhibit either ductile flexure-critical behaviour or brittle shear-critical behaviour. Characteristic flexural behaviour begins with the development of vertical flexural cracks at the central region of the beam. As the beam continues to deform the flexural cracks widen and propagate towards the top of the

beam. A shear-critical beam will exhibit brittle failure under static loading characterised by the formation and rapid propagation of diagonal cracks at the support regions on either side of the beam. Experimental studies on the impact behaviour of RC beams indicate that the capacity and the mode of failure observed in RC beams are influenced by their static behaviour, i.e. whether the beams are critical in flexure or in shear (Sangi, 2011).

Saatci and Vecchio (2009) conducted static loading tests and drop hammer impact loading tests on a total of 12 RC beams. Eight (8) of the beams were subjected to drop hammer impact at their midspans, whilst the remaining 4 beams were subjected to static loading. All of the specimens had identical longitudinal reinforcement, but varying shear reinforcement ratios. The primary aim of the study was therefore to investigate the effects of shear capacity on impact behaviour. A total of 20 impact tests were conducted with multiple impact tests conducted on some of the beams. Figure 9 illustrates the beam dimensions and the reinforcement layout.

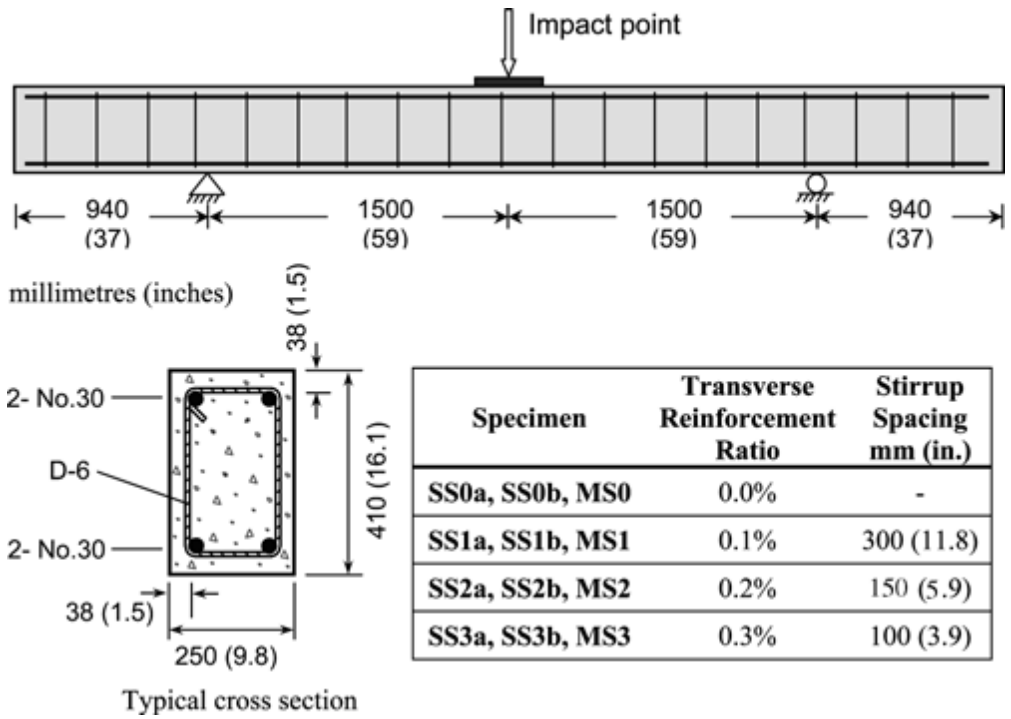

Specimen	Transverse Reinforcement Ratio	Stirrup Spacing mm (in.)
SS0a, SS0b, MS0	0.0%	-
SS1a, SS1b, MS1	0.1%	300 (11.8)
SS2a, SS2b, MS2	0.2%	150 (5.9)
SS3a, SS3b, MS3	0.3%	100 (3.9)

Figure 9: Specimen details (Saatci and Vecchio, 2009)

The findings of the drop hammer impact tests indicated clear differences in the RC beam behaviour depending on the shear capacity of the beams. Beams with higher shear capacities (flexure-critical beams) sustained more impact loads and absorbed more energy,

whereas beams with lower shear capacity exhibited extensive damage as a result of similar or smaller loads.

Figures 10 and 11 show the damage observed in the shear-critical and flexure-critical beams. The flexure-critical beams (SS2a, SS2b, SS3a and SS3b) exhibited some crushing in the contact region and a shear plug formation under the point of impact. Vertical flexural cracks were observed in the central region and near the supports. The flexural crack formations were dense, indicating high ductility. The shear critical beams also exhibited crushing in the contact zone and the formation of a shear plug under the point of impact. However, additional diagonal cracks were observed to develop alongside the shear plug originating from the supports and propagating at 45 degrees towards the top surface before becoming horizontal close to the top.

The capacities of the flexural-critical beams were observed to be higher based on a comparison of the damage sustained under repeated impact tests. The shear-critical beams failed due to excessive shear crack formation at the support regions whereas the flexure-critical beams had sufficient shear strength to carry the shear forces beyond the shear plug to the supports. The shear-critical beams also sustained higher residual deflections as well as delamination of concrete at the steel-concrete interface on the top and bottom surfaces of the beams.

Saacti and Vecchio (2009) thus concluded that the extent of the damage observed due to impact loading decreases with increasing shear capacity. It was also concluded that the load carrying and energy absorbing capacity increases with increasing shear capacity while the maximum dynamic and residual deflection decreases.

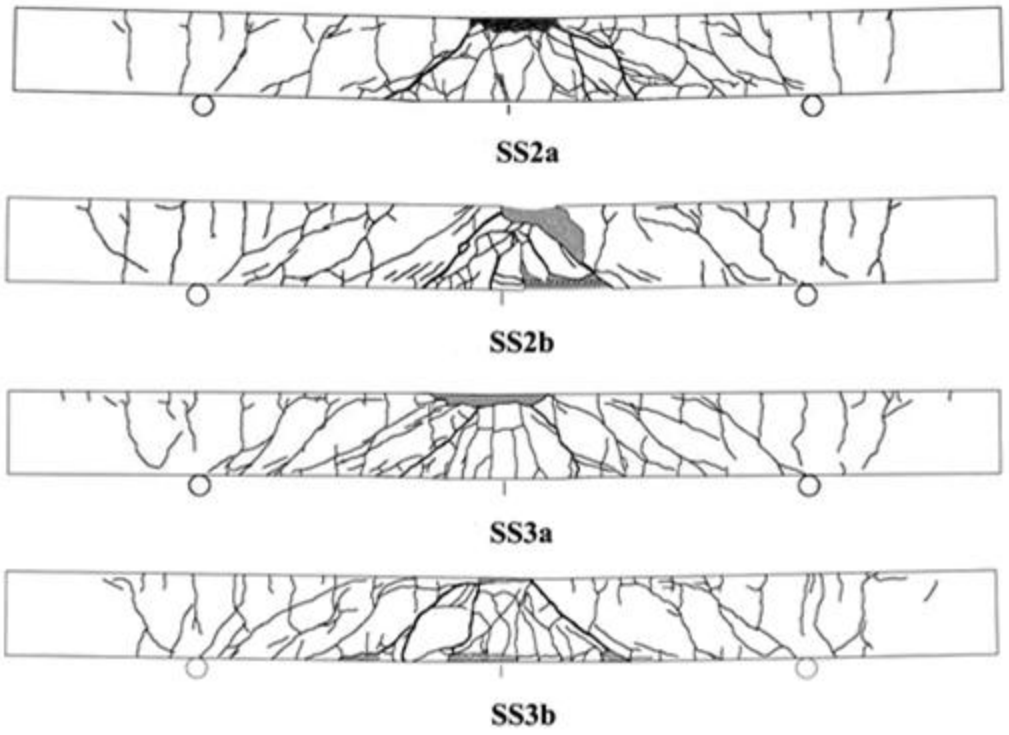

Figure 10: Damage induced in flexure-critical beams (Saacti and Vecchio, 2009)

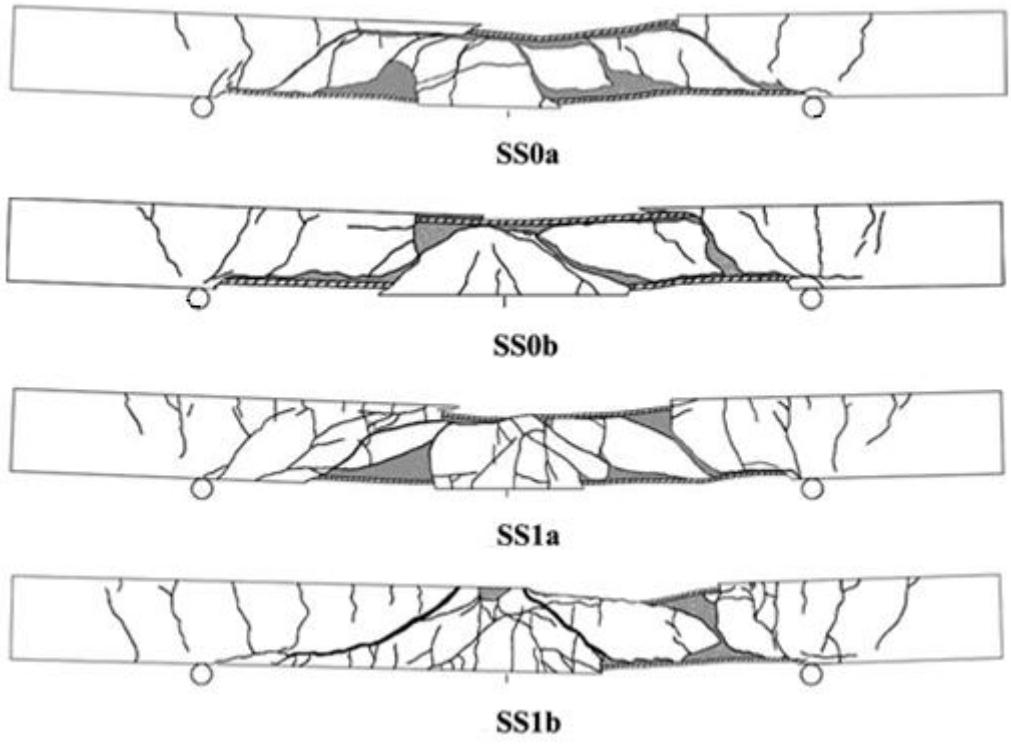

Figure 11: Damage induced in shear-critical beams (Saacti and Vecchio, 2009)

Adhikary et al (2012) tested a total of 24 RC beams with identical longitudinal reinforcement and varying shear reinforcement ratios. The beams were divided into three groups distinguished in terms of their shear reinforcement ratios (0%, 0.12% and 0.56%). Each group consisted of 4 pairs of specimens and each pair was subjected to a different loading rate (static: $4x10^{-4}$m/s, low: $4x10^{-2}$m/s, medium: 0.4m/s, high: 2m/s). Figure 12 shows the reinforcement layouts and the beam dimensions for each group of specimens.

Figure 13 shows the difference in load carrying capacity between the shear-critical beams and the flexure-critical beams for varying loading rates. The findings indicated that the load carrying capacity of the RC beams subjected to loading rates greater than that of static loading increased with an increase in shear reinforcement ratio. It was also observed that shear-critical RC beams exhibited more catastrophic failure modes at high loading rates. The flexure-critical beams were observed to resist catastrophic failure by providing confinement to the core concrete and lateral restraint against buckling of longitudinal reinforcement. Figure 14 shows the shear critical and flexure critical RC beams after being subjected to the varying loading rates.

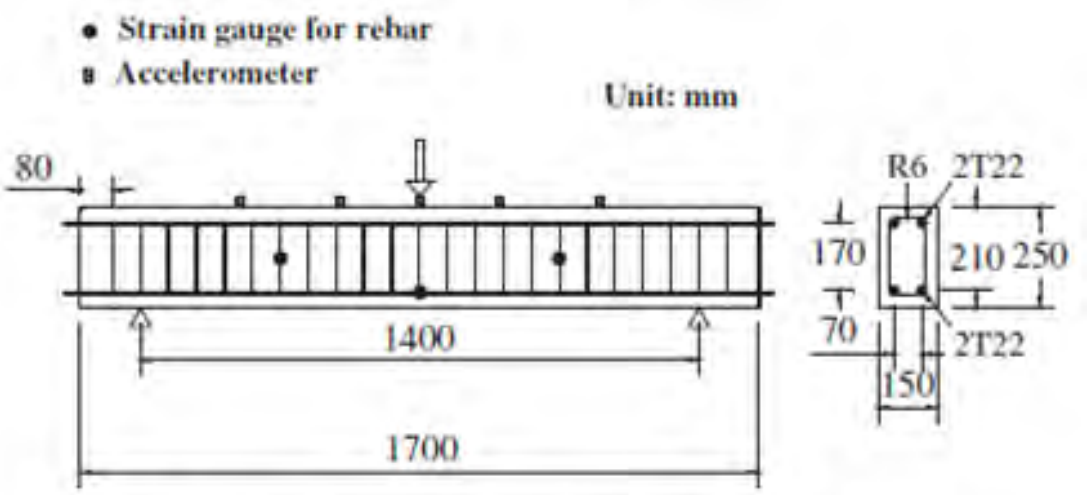

Group allocation	Shear reinforcement ratio	Stirrup spacing (mm)
RC3_S0	0%	-
RC3_S12	0.12%	350
RC3_S56	0.56%	70

Figure 12: Specimen details (Adhikary et al, 2012)

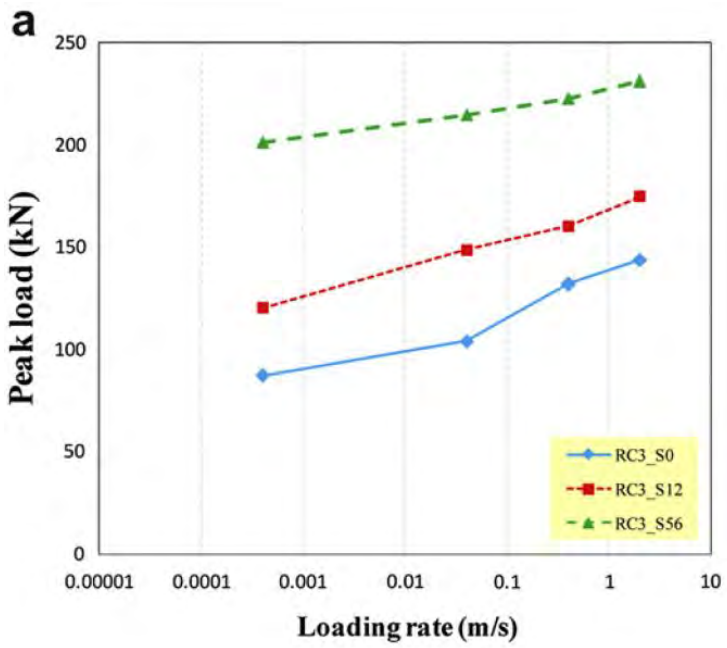

Figure 13: Variation of peak load and DIF of RC beams with varying stirrup spacing subjected to varying loading rates (Adhikary et al, 2012)

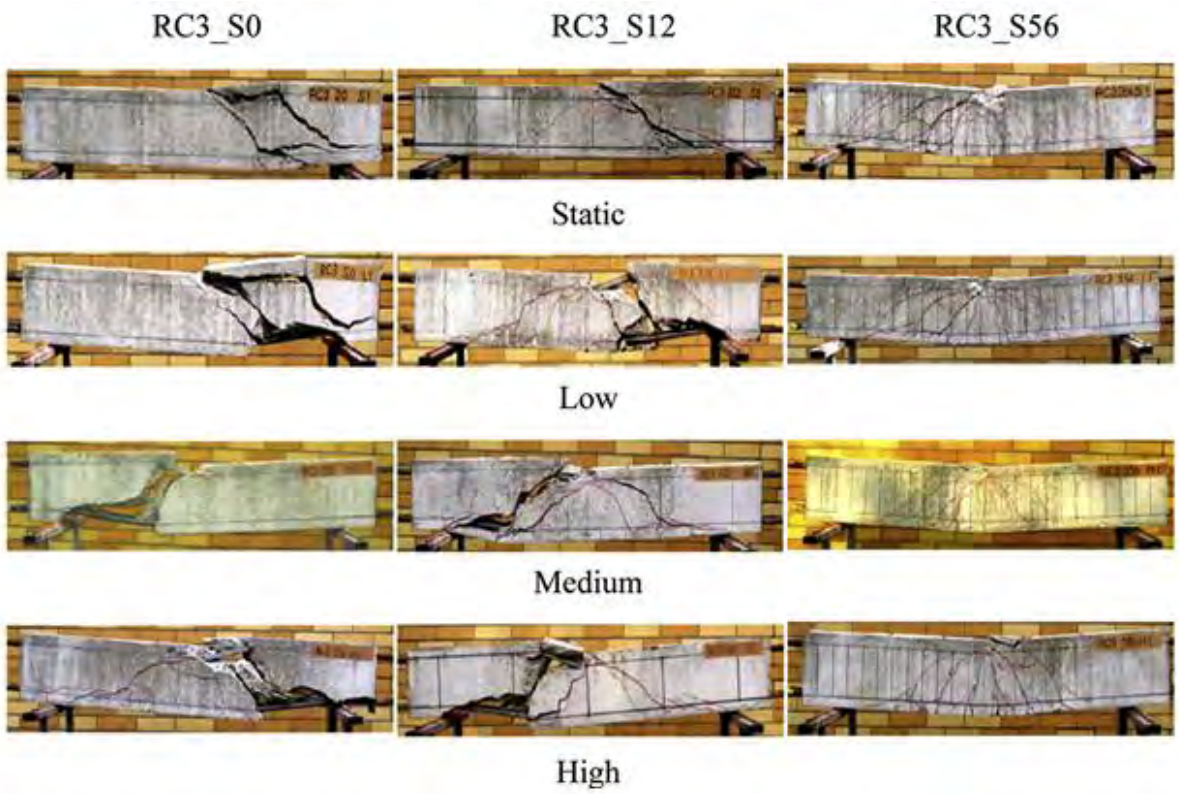

Figure 14: Damage observed due to varying loading rates (Adhikary et al, 2012)

Fujikake et al (2009) conducted drop hammer impact tests on 12 RC beams from varying drop heights in order to determine the influence that longitudinal reinforcement ratio has on the impact response. The beams were therefore all flexure-critical with varying flexural capacities. The beams were divided into three groups of four according to the degree of longitudinal reinforcement provided. The RC beams in a specific group, each had identical longitudinal and shear reinforcement. All beams were of equal span of 1.4m and each beam was subjected to a single drop test from a specified drop height (0.15m, 0.3m, 0.6m and 1.2m). Figure 15 shows the dimensions and reinforcement ratios of each group of RC beams.

Figure 16 is a summary of the findings observed as a result of the impact tests. The maximum contact force, the duration of the impact load, the magnitude of the impulse, the maximum midspan deflection and the time taken to reach maximum deflection all increased with an increase in drop height. The over-reinforced beams experienced larger maximum contact forces, and smaller midspan displacements. The failure modes were also shown to be dependent on the degree of longitudinal reinforcement provided. Under-reinforced beams exhibited ductile failure characterised by flexural crack formation and propagation. Over reinforced beams exhibited a comparatively dense flexural crack formation as well as localised damage in the form of crushing under the point of impact. The findings suggested further that beams with higher amounts of compression reinforcement experienced lower degrees of localised damage. Figure 17 shows the damage induced in the test specimens after the impact tests had been conducted.

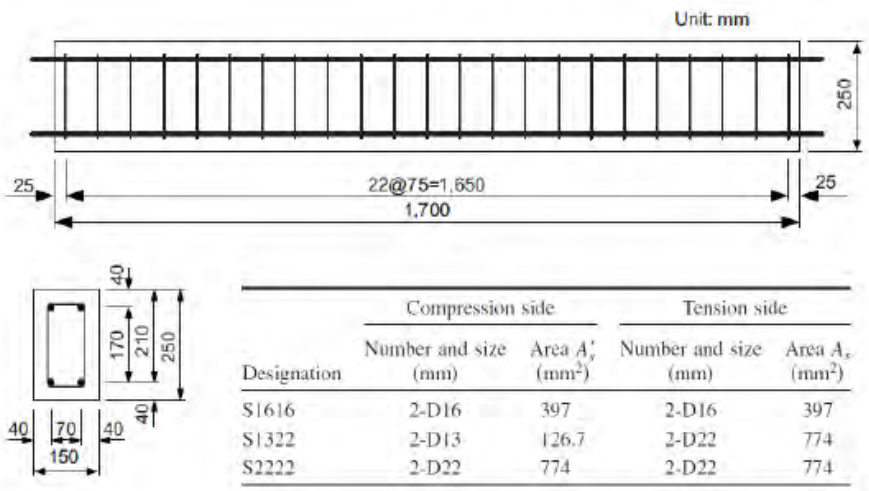

Designation	Compression side		Tension side	
	Number and size (mm)	Area A'_s (mm^2)	Number and size (mm)	Area A_s (mm^2)
S1616	2-D16	397	2-D16	397
S1322	2-D13	126.7	2-D22	774
S2222	2-D22	774	2-D22	774

Figure 15: Specimen details (Fujikake et al, 2009)

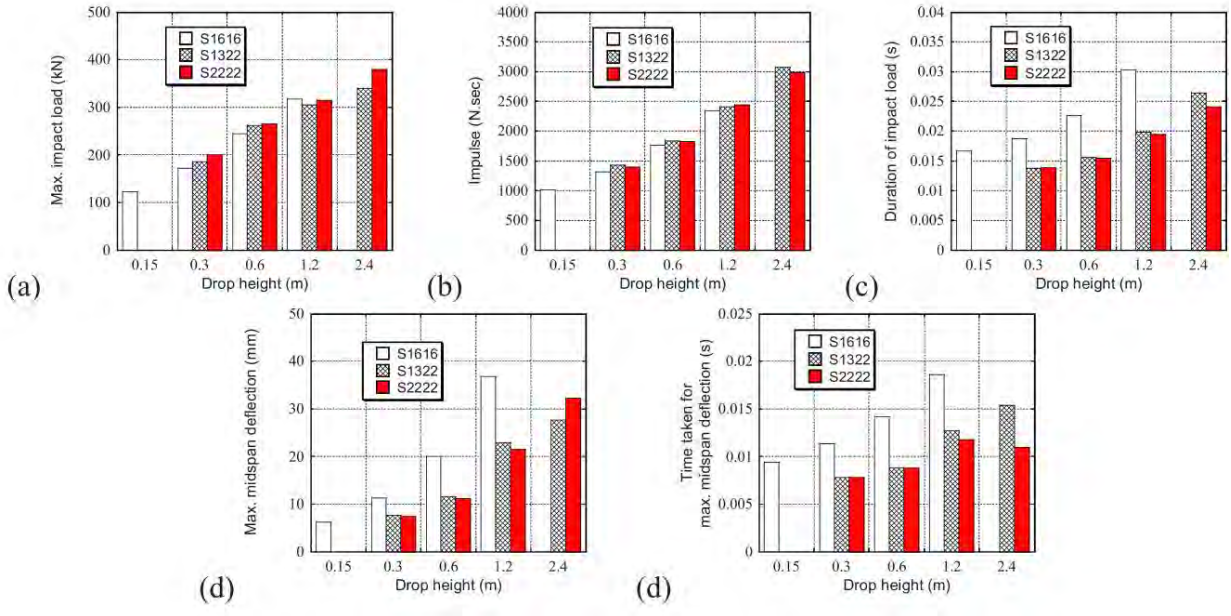

Figure 16: Summary of test findings (Fujikake et al, 2009)

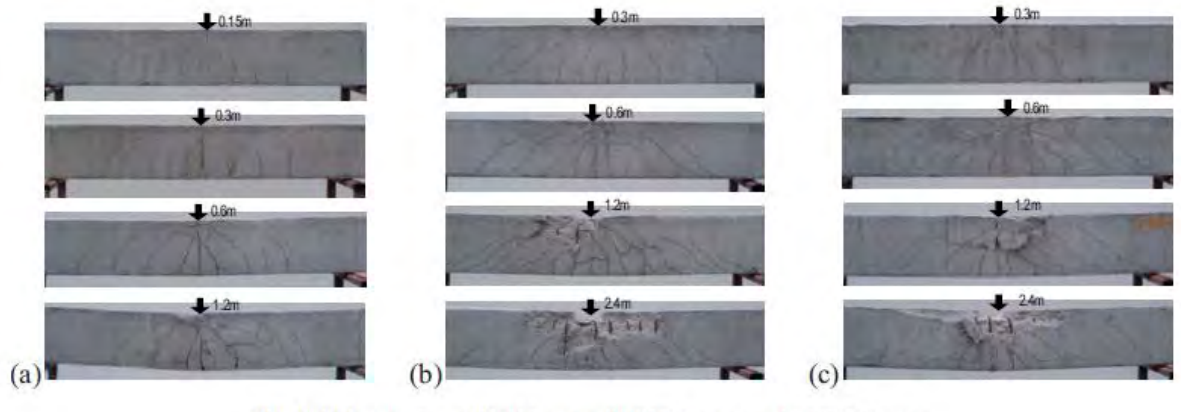

Figure 17: Damage observed in various specimen groups: a) S1616, b) S1322, c)S2222 (Fujikake et al, 2009)

The experimental studies referred to herein deal with the behaviour of RC beams subjected to impact loading applied via drop hammer impact testing apparatus. These studies provide useful insight into the effects of varying reinforcement layouts on the response of rectangular concrete beams subjected to vertically applied impact loading.

The current study will, in part, investigate the effect that varying stirrup spacing has on the response of RC T-beams subjected to horizontally applied impact loading. Transverse reinforcing stirrups in RC bridge beams usually extend through the top of the beam in order to facilitate composite action between the beam and the slab. The current study therefore aims to provide insight into the effects of stirrup spacing on the composite action between the flange and the web of a T-beam, repaired and strengthened with CFRP, subjected to horizontally applied impact loading.

2.3 Repair of damaged RC beams

In this study, the term 'repair' refers to the removal, cleaning, and replacement of damaged, deteriorating materials. Repair works therefore do not add extra strength to a damaged structure. If an increase in capacity is required various 'strengthening' techniques can be adopted.

Impact damage on concrete bridge beams is a common occurrence which can range in severity. Minor defects include non-structural cracks and gaps, surface cavities and minor voids (Ryall, 2010). Moderate damage can result in significant spalling of concrete to the extent that prestressed tendons and reinforcing bars are exposed. Such damage may not result in an immediate reduction of flexural capacity however, major patch repair works would be necessary to protect exposed tendons or bars from accelerated deterioration (Waheed et al, 2005). Severe damage results in an immediate reduction in structural capacity due to significant spalling of concrete and damage or complete rupture of reinforcing bars or prestressed strands. In such cases both patch repair works and additional strengthening would be required (Waheed et al, 2005). Severe impact damage may also result in permanent beam distortion and misalignment (Waheed et al, 2005).

A thorough condition assessment of the structure is important to identify the extent of damage and the type of repair and/or strengthening required. Figures 18 to 20 are examples of impact damaged bridge beams.

Figure 18: Bridge beam damaged due to transverse vehicular impact (SMEC, 2007)

Figure 19: Bridge beam damaged due to transverse vehicular impact (SMEC, 2007)

Figure 20: Severely impact damaged bridge beam (Chhabra, 2014)

2.3.1 Repair Techniques

Minor defects can usually be repaired via crack injection techniques or minor patch repair works (Ryall, 2010). Major patch repair works are required for moderate and severe impact damage. Various application methods can be implemented for patch repair depending on the extent of the repair required and the accessibility of the damage location, each of which utilises different patch repair materials.

Examples of patch repair application methods and the corresponding repair materials are:

- **Hand/trowel application:**
  This method of application is only suitable for small areas, less than 0.1m^3, and for repair works in accessible locations. The following materials are available for patch repair works using the hand trowel method of application:
  - Plain cementitious material:
    The main advantage of these repair materials is that durability can be provided through the use of ad-mixtures that reduce permeability (Beushausen, 2009). The major concern is ensuring compatibility between the repair material and the substrate material. Therefore the cementitious repair should have similar thermal, shrinkage and permeability properties as the substrate material. The modulus of elasticity should also be similar to the substrate (Tigelli, 2010).
  - Polymer materials (such as epoxies and acrylics):
    These materials are usually used for thin applications of repair and have an advantage of having high chemical resistance. However, they are only suitable for small areas due to the deformational incompatibility with substrate materials. The thermal coefficient of these materials is usually a lot higher than conventional concrete. Differences in thermal deformation may result in high stress development and cracking (Beushausen, 2009).
  - Polymer modified repair mortars:
    These materials are advantageous due to their high strength and resistance to abrasion, chemical and environmental influences. They can be applied over larger areas than regular epoxies and they can also be applied over small thicknesses. Another advantage is their high bond strength. As with regular polymer materials the main disadvantage is deformational compatibility with

the substrate. The coefficient of thermal expansion for polymer modified repair mortars are generally 2-5 times that of conventional concrete. The elastic modulus of these materials is also higher than conventional concrete which could lead to restrained substrate deformation and the development of high stresses at the repair interface (Beushausen, 2009).

- **Fluid application**
  Fluid application is suited for large areas or areas where access is difficult (Ryall, 2010). The fluidity of the mix enhances capillary suction in the substrate thereby improving bond strength between the substrate and the repair (Beushausen, 2009). The repair mortar used for such application usually consists of a cementitious, free-flowing, micro-concrete which is self compacting, shrinkage compensated, has high strength, high chloride and carbon resistance, and low alkalinity (Ryall, 2010).
- **Spraying application**
  Sprayed concrete (shotcrete or gunite) can be used over large areas with relatively shallow depths whether vertical, horizontal or inclined application is required. The concrete is sprayed onto the substrate using high amounts of energy. The concrete can be described as a fine aggregate paste with good bond strength if applied correctly (Beushausen, 2009).

2.3.2 Patch Repair

Concrete bridge beams damaged due to transverse vehicular impact are most commonly repaired via patch repair methods (Zobel et al, 1997; Yail et al, 2008). Figure 21 shows the successful application of cementitious patch repair mortar to a severely spalled bridge beam. The purpose of the patch repair is firstly to rebuild the damaged structure to its original surface profile and secondly to provide adequate protection against further accelerated deterioration, thus ensuring durability at the damage location. Although this method of repair has become standard practice, premature failure is often observed in the form of excess cracking and debonding of the repair mortar from the substrate (Beushausen, 2009). The reasons for such failure varies, however, it is generally accepted that poor workmanship and incompatibility between the repair material and the substrate material are the main contributing factors to the premature failure. Therefore proper

surface preparation, application procedures, curing techniques and the selection of adequate repair materials are important to ensure the repair serves its prescribed purpose.

Figure 21: a) severely spalled bridge beam b) patch repair of spalled concrete (SMEC, 2007)

Compatibility refers to the balancing of dimensional, permeability, chemical and electrochemical properties of the substrate and the repair mortar, in order to ensure that the repair system is able to withstand stresses induced due to volumetric changes and chemical or electrochemical effects (Vaysburd, 2006). Figure 22 shows the various factors which influence compatibility of the repair material and the substrate.

Research pertaining to the interaction of the repair mortar and the substrate focuses mainly on factors influencing dimensional compatibility, issuing particular importance on the following factors (Vaysburd, 2006):

- Drying shrinkage of the repair material
- Thermal expansion or contraction differences between the repair and substrate materials
- Differences in the modulus of elasticity causing unequal load sharing and strains resulting in interface stresses
- Creep properties
- Relative fatigue performance which may result in interface stresses that could initiate crack formation or debonding of the repair material from the substrate.

A suitable repair mortar may therefore require similar shrinkage characteristics, thermal deformation characteristics and elastic properties to the existing substrate material. Low creep properties between the substrate and the repair are also advantages, especially if the

repair mortar is to be subjected to load induced deformations (Beushausen, 2009). Standards require that the minimum shear resistance at the interface of the patch repair and the substrate, commonly referred to as the bond strength, should be between 1 – 1.5MPa in order to facilitate composite behaviour between the repair mortar and the structure (Beushausen, 2009).

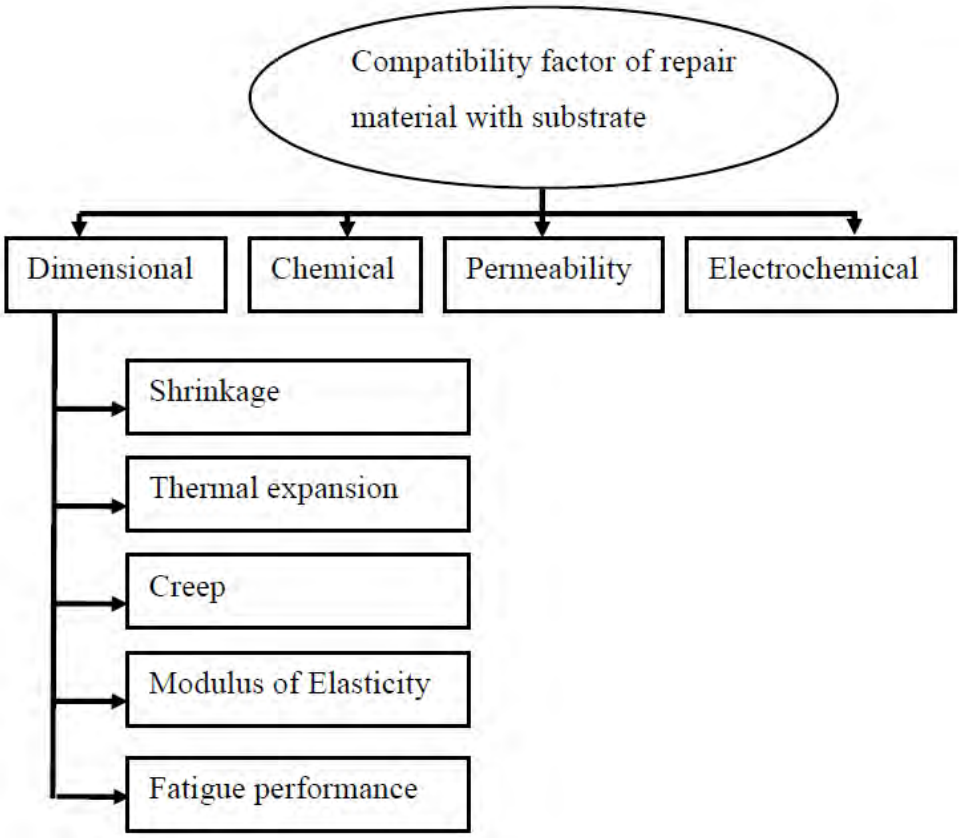

Figure 22: Compatibility factors between repair material and substrate (Vaysburd, 2006)

Common patch repair practice begins with the identification of the damage area and removal of all fractured concrete at the damage location. Depending on the extent of the damage, common methods of removal include the use of hammer and chisel, pneumatic hammers, sand blasting and water jetting (Ryall, 2010). In order to analyze the extent of damage in the reinforcement, concrete can be removed approximately 15mm above the damaged bars (Ryall, 2010). The boundaries of the repair patches should be cut straight and normal to free surfaces to avoid feather edges that may result in localized patch repair failure (Beushausen, 2009). The method of concrete removal can affect the quality and strength of the substrate. Studies have shown that mechanical methods of removal such as the use of pneumatic hammers are likely to induce micro-cracking along the substrate

surface which could adversely affect the surface bond strength, whereas water jetting or sandblasting produce sound substrate surfaces with sufficient roughness for adequate bond strength provision (Beushausen, 2009).

Upon the successful removal of the fractured concrete, the substrate should be cleaned thoroughly to remove dust particles and surface contaminants. Bonding agents are normally specified by commercial repair mortar suppliers to improve bond strength between the repair mortar and the substrate; alternatively, if bonding agents are not used the substrate surface should be dampened to prevent suction of water from the applied repair mortar which could result in a weak interfacial layer and low bond strength (Beushausen, 2009). Once the repair material is cast, adequate curing procedures can reduce rapid moisture loss and drying shrinkage. Standards stipulate that the repair material should be kept moist for at least 3 days after casting (Beushausen, 2009).

The prompt repair of structural members damaged due to mechanical loading such as transverse vehicular impact can provide protection against accelerated deterioration. However, such members are still susceptible to the same loading conditions. Currently, no research has been found which investigates the influence of loading rate on the interfacial bond between the repair material and the substrate. Additionally, there have been no studies which investigate the behaviour of patch repaired RC beams subjected to impact loading. The current research aims, in part, to investigate the behaviour of patch repaired and strengthened RC beams subjected to horizontally applied impact loading.

2.4 Strengthening of RC beams

Strengthening refers to the structural enhancement of weakened structural elements in order to restore or improve their capacities in flexure, shear or direct tension and compression (Ryall, 2010). In the case of bridge structures, strengthening may be required to accommodate increasingly large traffic loads or to compensate for damage and deterioration. Various strengthening methods are available for damaged or under-designed concrete bridges including the application of external load bearing elements such as bonded steel plates or FRP composites. Other methods include jacketing and external post-tensioning systems. The effectiveness of the strengthening method depends on the sufficient enhancement of strength properties where enhancement is required, ease of

application, cost effectiveness, durability and reliability, and the visual appearance of the strengthening solution (Ryall, 2010).

2.4.1 Steel plate bonding

Externally epoxy-bonded steel plates have traditionally been used as a means of enhancing the flexural strength, load carrying capacity and stiffness of under-designed or damaged concrete bridge structures (Beushausen, 2009). Although this is an established and relatively simple method of strengthening there are certain deficiencies related to application difficulties and long term durability. Steel plates are generally heavy and bulky and therefore pose problems in transport, delivery and handling. Application requires the use of scaffolding and expensive auxiliary bolting to support the self weight of the plates during the curing process (Ryall, 2010). Additionally the steel plates are susceptible to corrosion damage which could result in bond deterioration at the steel-concrete interface (Bakis et al, 2002). Figure 23 shows steel plates externally bonded to damaged bridge beams.

Figure 23: Damaged bridge beams strengthened using externally bonded steel plates a) scaffolding required for placement b) after completion (SMEC, 2007)

2.4.2 Jacketing systems

The use of jacketing systems is another common method of structural strengthening. Jacketing is an effective method of improving the flexural strength, stiffness and ductility of structural elements; however it also has certain deficiencies. One major disadvantage is that it is a particularly labor intensive procedure. The method also results in increased cross-sectional dimensions of strengthened elements and corresponding increases in dead-loads.

Additionally, the jacketing system may result in unwanted stiffness increases which could adversely affect the bridge structure (Bakis et al, 2002). Highway bridge beams strengthened via the jacketing system could result in a reduction of head room for traffic travelling under the bridge, which is unacceptable for low lying bridge structures (Ryall, 2010).

2.4.3 External post tensioning

External post-tensioning is a more specialized method utilized for the strengthening of bridge beams, decks or girders. This method is effective in increasing both flexural and shear strength, and is usually utilized to compensate for prestress losses or deficiencies. However, the primary purpose of this procedure is to restore serviceability by relieving dead-load bending effects resulting in reduced deflections and cracking (Ryall, 2010).

Figure 24: External post tensioning use (Chhabra, 2014)

2.4.4 Fibre reinforced polymer (FRP) systems

Fibre reinforced polymer composites have become a viable alternative to conventional strengthening materials due to a range of advantages properties. The section to follow will review in detail the properties of FRP composites as well as the application of these materials for the flexural strengthening of bridge structures in particular.

2.5 Fibre Reinforced Polymer

Historically FRP composites were first applied as flexural strengthening materials for reinforced concrete bridges in the late 1980's (Bakis et al, 2002). Since then the number

applications utilizing FRP composites has increased tremendously. In the construction industry the most common uses of FRP include the use of externally bonded FRP laminates/plates and fabrics. FRP composites are formed by combining high strength polymer fibres with a binding matrix and are therefore considered to be heterogeneous and anisotropic materials. Common applications of FRP composites include the strengthening and repair of various structural elements, such as, beams, columns, slabs and load bearing walls. They are generally applied to structural elements to enhance any of the following properties (Buyukozturk *et al.*, 2004; Taljsten and Elfgren, 2000):

- Axial, shear and flexural load capacities for ultimate limit state design
- Ductility and concrete confinement for improved seismic performance
- Durability in harsh environmental conditions
- Fatigue life
- Structural stiffness for reduced deflections for serviceability limit state design

The reasons for the increasing interest into the use of FRP composites as opposed to traditional materials are primarily due to the following useful properties that FRP composites exhibit (Keller, 2003):

- High strength to weight ratio in the direction of the fibres (approximately 40-50 times higher than structural steel)
- High corrosion resistance and durability
- High fatigue resistance
- Ease of handling and application
- Ability to tailor manufacture composites to achieve the most desirable effects

2.5.1 Constituent materials

As has already been mentioned FRP composites consist of high strength polymer fibres embedded in a binding matrix. Both the reinforcing fibres and the matrix perform specific functions in order to ensure that the composite performs satisfactory as a whole. The purpose of the fibres is to provide the required strength and stiffness to the composite whereas the matrix binds the fibres together and enables the transfer of stress and strain between the fibres. The matrix also provides environmental protection resulting in the characteristic FRP durability (Taljsten, 2006).

2.5.1.1 Fibres

The most common fibre reinforcements used in FRP composites for the strengthening of civil engineering structures are glass, aramid and carbon fibres. The physical and mechanical properties of each of these fibre types range over a wide spectrum. Therefore the properties of FRP composites can vary considerably (Balaguru et al, 2009). Figure 25 illustrates the stress-strain relation of unidirectional carbon, aramid and glass FRPs as compared to structural steel.

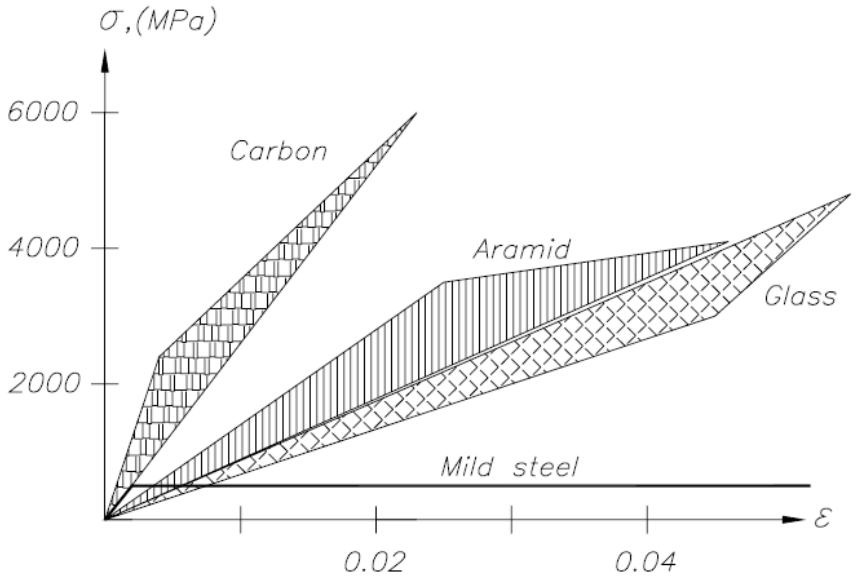

Figure 25: Stress versus strain properties of common FRP composites as compared to mild steel (Taljsten, 2006)

The shaded areas of the various FRPs illustrate the variability of mechanical properties of each fibre type. FRP composites exhibit superior strength and stiffness properties to steel and are also considered superior in terms of weight, durability and resistance to fatigue. A major advantage of FRP strengthening systems is their relative ease of application. The reduction in cost due to the ease of construction counter acts the high material cost of the FRP. Also the superior durability of the FRP laminates lead to longer service life and therefore lowers long term maintenance costs (Keller, 2003).

Glass fibres are the most commonly used of all the reinforcing fibres, however majority of its usage is outside of the building industry. The major advantages of glass fibres include their low cost, high tensile strength, resistance to certain chemicals and their high

temperature resistance. The general disadvantages of glass fibres include the relatively low tensile-modulus, brittleness, sensitivity to abrasion while handling, low fatigue resistance, low humidity resistance and their low alkaline resistance. The susceptibility to alkaline attack is of particular concern due to the high alkalinity of concrete structures. This has led to the development of alkali-resistant glass fibres (AR-glass) (Balaguru et al, 2009).

Carbon fibre has the highest tensile-modulus of all the reinforcing fibres. The major advantages of carbon fibres include their high strength to weight ratios, high tensile-modulus to weight ratios, high fatigue resistance, high temperature resistance and low coefficient of thermal expansion. In addition to this carbon fibres have extremely high chemical resistance (including high alkaline resistance) at temperatures below 400°C (Balaguru et al, 2009). Major disadvantages of carbon fibres include their relatively low impact resistance and their high manufacturing costs (due to high energy requirements) (Balaguru et al, 2009).

Aramid fibres (which include Kevlar© and Twaron© fibres) are synthetic. Although aramid fibres generally have lower tensile strength than carbon fibres their strength to weight ratio is the highest of all the common reinforcing fibres. In addition to high strength, these fibres also exhibit high thermal and chemical resistance. Another major advantage of aramid fibres is that they tend to have higher fracture toughnesses than carbon and glass fibres. Due to this property, aramid fibres have relatively high impact resistance. Disadvantages of aramid fibres include their low ultraviolet radiation resistance, low compressive strength and relatively high manufacturing costs (Balaguru et al, 2009).

2.5.1.2 Matrix

Fibrous materials alone have limited use for strengthening applications since there is no medium to transmit loads from one fibre to another (Taljsten, 2006). FRP composites are formed when fibres are embedded in a binding matrix. As has already been mentioned, in addition to binding the fibres together, the matrix also enables force transfer as well as providing sufficient environmental protection. The failure strain of the matrix should be greater than that of the reinforcing fibres to avoid the formation of micro cracks in the matrix under working loads (Keller, 2003). Binding matrices also enhance certain mechanical

properties of FRP composites, such as the transverse strength and stiffness as well as the compression resistance (Taljsten, 2006).

Polymer matrices can be separated into two groups based on how they respond to the application of heat, namely thermoplastics and thermosets. Thermoplastics soften due to the application of heat and harden due to cooling. Repeated softening and hardening has little effect on the material properties (Balaguru et al, 2009). Thermosets are formed chemically due to a reaction between a resin and a hardener. The chemical reaction is irreversible and upon setting the thermoset remains in a hardened state (Balaguru et al, 2009). In the building industry, thermosets are mainly utilised (Keller, 2003). The three main types of thermoset polymers used as matrices for FRP composites are polyester, epoxy and vinylester resins. Epoxies are more commonly used due to their superior mechanical and durability properties. However epoxy is also the most expensive (Taljsten, 2006).

2.5.1.3 Fibre-matrix bond

The mechanical properties of FRP composites depend on the adhesion between the fibres and the matrix; the mechanical compatibility between the fibres and the matrix; and the orientation of the fibres with respect to loading (Keller, 2003).

FRP composites generally have high strength properties in the direction of the fibres in tension and to a lesser extent in compression. The strength properties in the transverse direction, through the cross-section of the composite, are however considerably weaker which results in susceptibility to transverse shear forces and impact forces (Reid and Zhou, 2000). When a composite is subjected to compressive stresses the matrix must provide sufficient resistance to ensure that the fibres do not buckle (Keller, 2003).

When describing FRP composites one needs to distinguish between built-up insitu composites and prefabricated composites. In the building industry insitu composites usually consist of wrap strengthening systems. The fibrous wraps can be unidirectional or multi-directional fabrics which are applied insitu through the use of impregnating resins. These resins act as both the binding matrix and the adhesive between the structure and the fabric. The fibre volume fraction of insitu systems can range from between 25% to 35% (Taljsten, 2006). Prefabricated composites are formed through a process called pultrusion. During this process fibres are pulled through the unset binding resin. Heat is applied to initiate

polymerization and the composite is left to cure. Such prefabricated composites are plate like laminates and are available as unidirectional or multidirectional composites. The fibre volume fraction of prefabricated laminates ranges from 50% to 70% (Taljsten, 2006).

Table 1 provides a quantitative evaluation of glass, Carbon and Aramid unidirectional, prefabricated laminates. The criteria and weighting is based on the use of these laminates, specifically for the repair and strengthening of bridge structures (Keller, 2003).

Table 1: Quantitative rating of fibres (ratings: 3=very good, 2=good, 1=adequate, 0=inadequate) (Keller, 2003)

Criterion	**Weighting factor**	**Weighted rating of laminates with fibres of:**		
Range of weighting factor	1-3	Carbon	Aramid	E-glass
Tensile strength	3	9	9	9
Compressive strength	2	6	0	4
Young's Modulus	3	9	6	3
Long-term behaviour	3	9	6	3
Fatigue resistance	2	6	4	2
Bulk density	2	4	6	2
Alkaline resistance	2	6	4	0
Cost	3	6	6	9
Total points		55	41	32
Ranking		1st	2nd	3rd

Carbon fibre polymer composites have been proven to be favourable for the strengthening of concrete bridge structures and will therefore be used as strengthening for the experimental work of this study.

2.5.2 CFRP Strengthening Systems

There are various CFRP systems available for the strengthening of bridge structures. The scope of this research covers only the application of CFRP for flexural strengthening.

Laminate system

Laminate systems are prefabricated systems and are available in varying grades and cross-sectional areas. This system is most suitable for flat surfaces such as beams, walls and slabs. The length of a laminate is limited to 20 meters to ensure practicality during the application process (Taljsten, 2006). Laminates are bonded to the structural element in need of strengthening via an epoxy bonding adhesive. The thickness of the adhesive is typically between 1-2mm (Balaguru et al, 2009). The adhesive is only applied once the concrete surface has been adequately prepared. This usually entails the removal of the cement laitance and the thorough cleaning of the substrate surface. In order to facilitate adequate bond strength between the laminate and the substrate an epoxy based bonding adhesive is applied to the CFRP or the substrate surface. Thereafter the laminate is applied to the substrate through the application of light pressure and the system is left to harden (Taljsten, 2006). The laminate system was first applied for the strengthening of a bridge structure in Switzerland in the late 1980s which had been subjected to vehicular impact that resulted in the rupture of pre-stressing tendons. Since then this system has gained widespread use all over the world (Taljsten, 2006). Figure 26 illustrates the use of externally bonded CFRP laminate for the strengthening purposes.

Sheet system

Sheet systems typically consist of an epoxy primer, putty or pre-impregnation fibre and resin system. Sheets used for flexural strengthening are usually unidirectional; however multi-directional fibres are often used for other strengthening applications (Taljsten, 2006). The flexibility of the sheets make it suitable for seismic retrofitting, the strengthening of curved surfaces, and the strengthening of walls or slabs with openings. The sheets are bonded to the substrate via a high strength epoxy adhesive. Post treatment is often required such as painting, plastering or application of a thin layer polymer concrete (Taljsten, 2006). The sheet system often requires more surface preparation since it is more sensitive to irregularities along the concrete surface (Taljsten, 2006).

NSMR system

Near Surface Mounted Strengthening (NSMR) systems utilize circular or rectangular rods that are bonded underneath the concrete surface in slots so as to provide cover. NSMR systems are favourable in cases where protection from mechanical damage is needed (Taljsten, 2006). A minimum cover depth of 25mm is usually required. Surface preparation initially requires the sawing of slots for the CFRP rods. These slots need to be cleaned thoroughly to ensure adequate adhesion of the CFRP. The rods are typically bonded via epoxy adhesive or a high quality cementitious grout (Taljsten, 2006). Figure 27 illustrates the use of a NSMR for the strengthening of a bridge structure.

Prestressed laminate systems

The prestressing of laminate strips prior to bonding can result in more economical use of materials since the same strengthening can be achieved with lower material usage as compared to strengthening with non-prestressed laminates (Bakis et al, 2002). The prestressing system reduces crack formation and propagation and improves the serviceability of the structure by reducing deflections and improving durability (Taljsten, 2006). However, the system is more expensive than the non-prestressed laminate system due to the requirement of prestressing equipment and the time and expertise needed for application. Also, special clamping devices are required (Taljsten, 2006).

Figure 26: Externally bonded CFRP plate system (Structural strengthening, n.d.)

Figure 27: NSMR strengthening system (Taljsten, 2006)

2.5.3 CFRP Application

CFRP application procedures for flexural strengthening place particular importance on the linear elastic nature of FRP materials and the quality and strength of the bond between the substrate and the CFRP (Bakis et al, 2002). An under-reinforced RC beam is designed such that the tensile steel yields before the concrete crushes in compression, thus avoiding abrupt brittle failure. The behaviour of a CFRP strengthened RC beam is governed by the linear elastic, brittle nature of the CFRP and the limitations of the bond between CFRP and the substrate. For this reason traditional under-reinforced failure cannot be reached (Taljisten, 2006). However, a strengthened section can be designed such that considerable deformation takes place before failure is achieved. Balaguru et al (2009) describe the following failure modes associated with unstressed FRP laminates or sheets applied for flexural strengthening:

1. Crushing of concrete in compression before yielding of steel:

   This occurs if a beam is over-reinforced and the concrete reaches its failure strain before that of the steel reinforcement.
2. Steel yielding followed by FRP rupture:

   The reinforcing steel is fully utilised which allows for ductility. After the yielding of the steel the flexural rigidity is provided mainly by the FRP. Eventual rupture of the FRP results brittle failure.

3. Steel yielding followed by crushing of the concrete in compression (while FRP remains bonded):

   Such failure occurs when the FRP is sufficient to provide higher resistance than the concrete in compression after the steel has yielded. In such cases the failure mode is changed from under-reinforced failure to over-reinforced failure.
4. Bond splitting failure due to the separation of the concrete from the tensile reinforcement due to excess cracking; or laminate peeling due to the debonding of the FRP from the concrete substrate. This can be separated further into the following failure modes (Bakis et al, 2002):
   i. Bond-splitting due to shear failure of concrete at the FRP cut off end
   ii. Laminate peeling at the cut off end or at a flexural crack due to high stress development in the adhesive
   iii. Laminate peeling at the FRP-substrate interface due faulty bonding or uneven surface bonding

The failure of strengthened beams should preferably be preceded by ductile deformation. Therefore, it is preferable that a strengthened beam experiences yielding of the tensile steel reinforcement before failure of the strengthening system. If this is not the case then the FRP utilization is low and failure can be considered to be premature (Taljsten, 2006). Of all the failure modes described above, mode 3 is considered to be the most desirable, as failure of the strengthening system is preceded by yielding of the steel reinforcement and crushing of the concrete in compression, thereby providing ample warning before failure of the strengthening system (Bakis et al, 2002). Mode 4(i) can be prevented by providing adequate shear strengthening, whilst mode 4(ii) can be avoided by limiting the strain in the FRP to roughly 0.008 (Bakis et al, 2002). Laminate peeling at the cut off ends can also be prevented by providing sufficient anchorage lengths or by providing additional anchorage systems such as anchorage end strips. Mode 4(iii) can be prevented by adhering to established application procedures (Bakis et al, 2002).

2.6 Behaviour of FRP strengthened beams subject to impact loading

2.6.1 FRP properties under impact loading

FRP Composites generally have high strength properties and have reasonable impact resistance when stress is applied in the direction of the fibres (Balaguru et al, 2009). The performance in the transverse direction, through the thickness of the composite is however, poorer which results in susceptibility to impact loading applied directly to FRP composite surfaces (Balaguru et al, 2009). Generally, the mechanical properties of FRP composites in transverse directions are governed by the matrix, and properties which are matrix dependent are much lower than those which are governed by the fibre (Reid and Zhou, 2000). The poor performance of FRP subjected to direct impact is partly due to a lack of plastic deformation ability. Unlike metals, FRP is unable to retain a level of integrity after being stressed to yield point. Any damage incurred is permanent and could lead to further damage due to low material toughness (Reid and Zhou, 2000).

Caprino et al (1999) performed drop hammer impact tests on square, CFRP laminates with 70mm sides and varying thicknesses, in order to investigate the influence of laminate thickness on the response to low velocity impact. The laminates were prepared by bonding CFRP fabric layers with an epoxy resin. The thickness of the laminates varied according to the number of fabric layers bonded together. A total of four laminates were tested consisting of 4, 8, 12 and 16 CFRP fabric layers respectively. The force and absorbed energy at the point of delamination initiation, the maximum force and related energy, and the penetration energy were evaluated. From the experimental results they concluded that each of the recorded quantities, with the exception of the energy required for delamination initiation, followed the same trend, increasing to the power of approximately 1.5 with increasing plate thickness. Caprino et al (1999) also observed that the energy at delamination could be divided into energy dissipated due to flexural deformation and energy dissipated due to local deformation at the point of contact. The latter was observed to increase with specimen thickness. Figure 28 shows the force displacement curves recorded in the impact tests carried out up to penetration for the different laminate thicknesses.

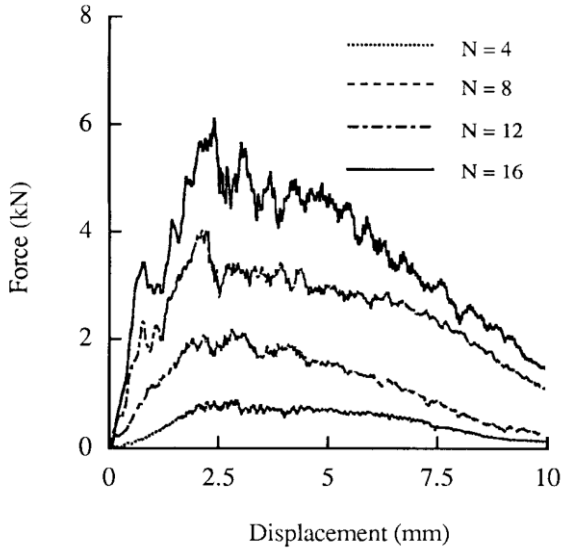

Figure 28: Force versus displacement curves recorded during impact for different specimen thicknesses. N = number of layers (Caprino et al, 1999)

2.6.2 Studies conducted on strengthened beams

Limited research has been conducted to understand the effect of sudden impact loading on FRP strengthened RC beams (Erki and Meier, 1999; White et al, 2001; Tang and Saadatmanesh, 2003). The available research focuses on the potential use of FRP to enhance impact resistance. This corresponds to vertically applied impact loading such that the strengthened beams undergo flexure about their major bending axis and the FRP strengthening is stressed in the direction of the fibres. Currently no research work is reported in technical literature that analyses the performance of FRP strengthened beams subjected to transverse impact. Additionally, the available research focuses on FRP strengthened RC beams as opposed to patch repaired and FRP strengthened RC beams.

The literature cited below provides useful insight into the overall performance of FRP strengthened RC beams subjected to impact loading and varying loading rates as well as providing insight into experimental procedures and the research parameters used to analyse the behaviour of FRP strengthened RC beams under impact loading conditions.

Erki and Meier (1999)

Erki and Meier (1999) tested the behaviour of two identical RC beams strengthened with CFRP laminates subjected to impact loading tests. The impact loads were induced by lifting

one end of the simply supported beam and dropping it from varying heights onto a critically dampened support. One of the CFRP-retrofitted test beams (beam BF1) was subjected to consecutive impact loading tests from varying beam drop heights (0.5m, 1m, 1.5m). The remaining test beam (beam BF2) was dropped once from a height of 2m. The results from the impact tests were compared to that of a previous study conducted by Weder and Ladner (1981), which analysed the behaviour of two RC beams (beams G1 and G2) strengthened with externally bonded steel plates, subjected to impact loading.

Beams BF1 and BF2 were identical in length and cross-section. Two CFRP laminate strips were bonded to the bottom surface of the RC beams. The cross-sectional areas of the laminates were chosen to have approximately the same tensile yield strength as the steel plates externally bonded to beams G1 and G2 from the previous comparative study. The dimensions and reinforcing details of beams BF1, BF2, G1 and G2 are shown in Figure 29.

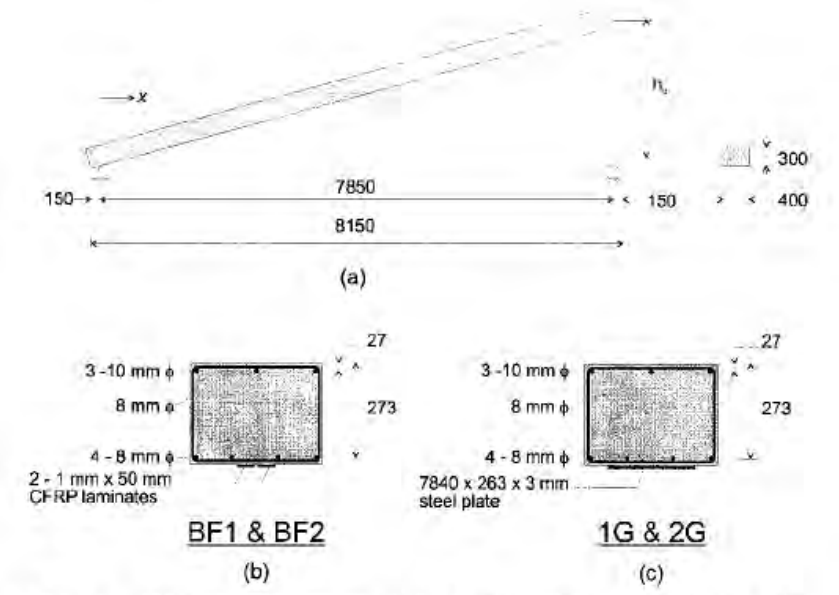

Figure 29: (a) Test set up and beam dimensions (b) BF-beam reinforcement layout (c) G-beam reinforcement layout used by Weder and Ladner (1981). (Erki and Meier, 1999)

The behaviour of the CFRP-retrofitted beams under the applied impact loading was determined by recording and analysing the following parameters:

- The reaction force response at both ends of the beams
- The midspan dynamic and residual deflections

- The longitudinal strain along the CFRP laminates
- The progression of damage and failure mechanisms within the beams

The progression of damage and the failure mechanisms were analysed based on observations made after each drop test. Crack formation and propagation was recorded in the concrete, the epoxy adhesive and the CFRP laminates. High speed camera (HSC) footage of each impact test was also used to monitor failure mechanisms. The deflection response at midspan was recorded with an optical sensor. A damping unit at the contact support end was instrumented to record the deflection response and the contact force response at the damper. The pin support at the stationary end was instrumented to record the reaction force response. Two accelerometers were used to record the beam acceleration at the free end that was raised and dropped. Strain gauges were used to record dynamic and residual strain along the CFRP laminates.

The first beam, BF1, was subjected to three consecutive impact tests. The first test involved dropping the free end of the beam from a height of 0.5m. This led to the formation of flexural cracks spread over the middle two thirds of the beam length with the most severe flexural cracks observed at the central region of the beam. Additional longitudinal cracks were observed to form in the epoxy adhesive layer between the CFRP and the concrete. The second drop test conducted from a height of 1m resulted in an increase in the spread of flexural cracks along the bottom surface of the beam. The cracking in the epoxy was also observed to extend. During the final drop test conducted from a height of 1.5m the beam sustained a large midspan defection followed by complete rupture at the midspan. Prior to rupture, the HSC captured the initial debonding of one of the CFRP laminates followed by the tensile rupture of the second adjacent CFRP laminate.

The second beam, BF2, was dropped only once from a drop height of 2m. Flexural cracking was observed over the entire beam length. The most severe cracks at the central region of the beam extended to approximately 90% of the beam height. The ends of these flexural cracks indicated horizontal branching which suggests that the concrete was approaching crushing strain (Erki and Meier, 1999). The CFRP behaved similar to that of the first beam tested in that one of the laminates initially debonded followed by the tensile rupture of the remaining laminate. The beam did not rupture, however yielding of the tensile steel was observed.

Erki and Meier (1999) compared the failure mechanisms and maximum deflection observed in beam BF2 to that of beam G2 tested by Weder and Ladner (1981). The maximum displacement observed in beam BF2, before delamination, was less than that of beam G2. It was also observed that while beam BF2 failed due to premature delamination, beam G2 failed due to yielding of the externally bonded steel plate followed by delamination. It was thus suggested that the capacity of beam BF2 could have been improved if premature delamination was prevented through the provision of adequate anchorage.

The energy absorbing capacities of beams BF1 and BF2 were also compared to those of beams G1 and G2. For both pairs of beams the impact energy was initially absorbed by the damper and then by the beam itself through crack formation in the concrete and yielding of the steel reinforcement. For the beams G1 and G2, energy was absorbed further through the yielding and delamination of the steel plates. The CFRP retrofitted beams, BF1 and BF2, absorbed energy through the formation of longitudinal cracks in the epoxy resin, the delamination of one of the laminates and finally through the rupture of the remaining CFRP-laminate. The tensile failure and delamination of the CFRP laminates were likened to that of a highly stretched elastic band. Strain energy is stored in the laminates as they are stretched due to beam deformation; this is followed by a sudden explosive release of energy during delamination and tensile failure.

It was concluded that the CFRP-retrofitted beams performed well under impact. However, they could not provide the same energy absorption as the beams strengthened with the steel plates. It was also concluded that additional anchorage at the ends of the laminates would improve impact resistance and reduce the risk of early delamination.

White et al, (2001)

White et al (2001) investigated experimentally and analytically the effect of varying loading rates on the performance of CFRP-retrofitted RC beams. The beams were subjected to various loading rates ranging from slow: 0.0167mm/s to fast: 36mm/s.

A total of nine beams were tested. Each beam was identical in length and geometry and was reinforced with high strength longitudinal steel. The shear reinforcement was provided in excess to prevent shear failure and premature delamination. Four of the beams were

strengthened with S-type CFRP laminates and four beams were strengthened with R-type CFRP sheets. The S-type CFRP laminates were 50mm wide and 1.2mm thick with a maximum strength of 2400MPa and a tensile modulus of 155GPa. The R-type CFRP sheets were, 135mm wide and 0.11mm thick with a maximum strength of 3000MPa and a tensile modulus of 160GPa. The remaining beam was an un-strengthened control specimen. The beam dimensions and reinforcement layout are shown in Figure 30.

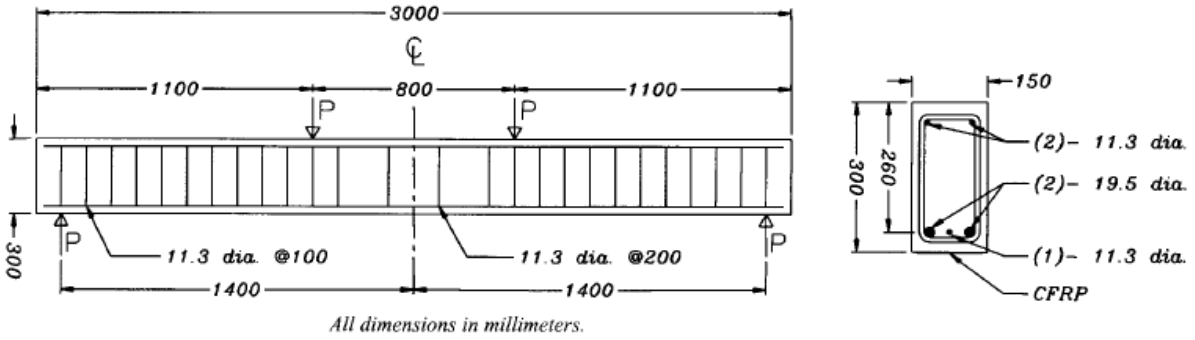

Figure 30: Beam dimensions and reinforcement layout (White et al, 2001)

The CFRP was bonded to the bottom faces of the beams so that the eight beams would have the same tangential stiffness (despite the different mechanical properties of the R-type and S-type CFRP). Various loading rates were applied to the beams via four point bending test apparatus. The tests were performed in order to determine the behaviour of the two types of retrofitted beams under slow loading rates, fast loading rates and various combinations of slow and fast loading rates to simulate the behaviour of damaged beams and beams under service load conditions. Table 2 shows the type of loading applied to each of the test specimens.

The behaviour of the CFRP-retrofitted beams under the applied loading rates was determined by recording and analysing the following parameters:

i. Beam deflection
ii. Flexural capacity (comparison of bending moment capacities for the various beam types)
iii. Tangential stiffness
iv. Energy absorption
v. CFRP longitudinal strain
vi. Cracking behaviour and failure mechanism

Table 2: Loading schemes for various test specimens

Beam	CFRP strengthening	Load type*
C-B (Control specimen)	-	B
S-A	S-type pultruded laminates	A
S-B	S-type pultruded laminates	B
S-C	S-type pultruded laminates	C
S-D	S-type pultruded laminates	D
R-A	R-type FRP sheets	A
R-B	R-type FRP sheets	B
R-C	R-type FRP sheets	C
R-D	R-type Prepreg sheets	D
*Note: A-slow load to failure; B-rapid load to failure; C- slow load to 150kN; D-rapid load to 120kN for 12 cycles		

Strain gauges were used to measure strain along the CFRP laminates. LVDTs were located at the end supports to measure beam settlement during testing and at the midspan to measure the midspan deflection. Comparisons were made between the performance of the rapidly loaded CFRP-strengthened beams and the rapidly loaded control beam. The individual performances of the S-type and R-type CFRP strengthened beams were also compared. Finally the performances of the rapidly loaded CFRP strengthened beams were compared to beams loaded at slower rates. These comparisons were based on the parameters listed.

Figures 31 and 32 show the load deflection results for the various test specimens. In comparing the results of the rapidly loaded CFRP strengthened beams to that of the control specimen it was found that the CFRP strengthened beams experienced higher yield loads, ultimate loads and greater pre-yield and post-yield stiffness. However the maximum energy absorbed by the CFRP strengthened beams was significantly less than that of the control beam. The strengthened beams showed an increase in capacity until failure occurred which was mainly due to premature delamination. The maximum deflections of the CFRP strengthened beams were observed to be less than the control specimen. In comparing the slow loaded CFRP-strengthened beams to the fast loaded beams it was found that the yield

and ultimate strengths of the beams increased with increasing loading rates. The pre-cycled beams behaved similarly to the other strengthened beams. In some cases noticeable increases in pre-yield stiffness was observed in the pre-cycled beams, thus indicating the possibility of strain memory. In comparing the performance of the two types of CFRP strengthened beams the S-type CFRP exhibited the highest increase in flexural capacity.

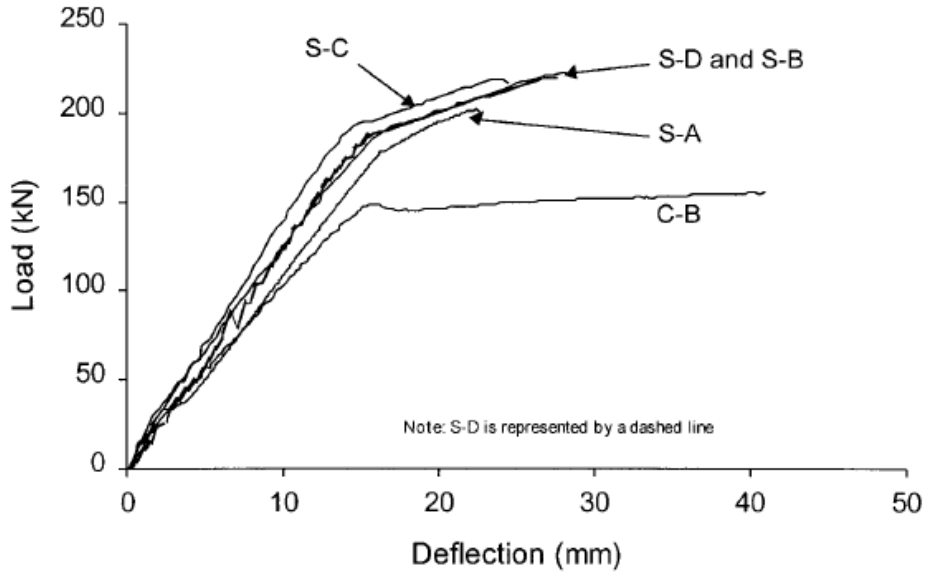

Figure 31: Load-deflection results for S-type CFRP strengthened beams (White et al, 2001)

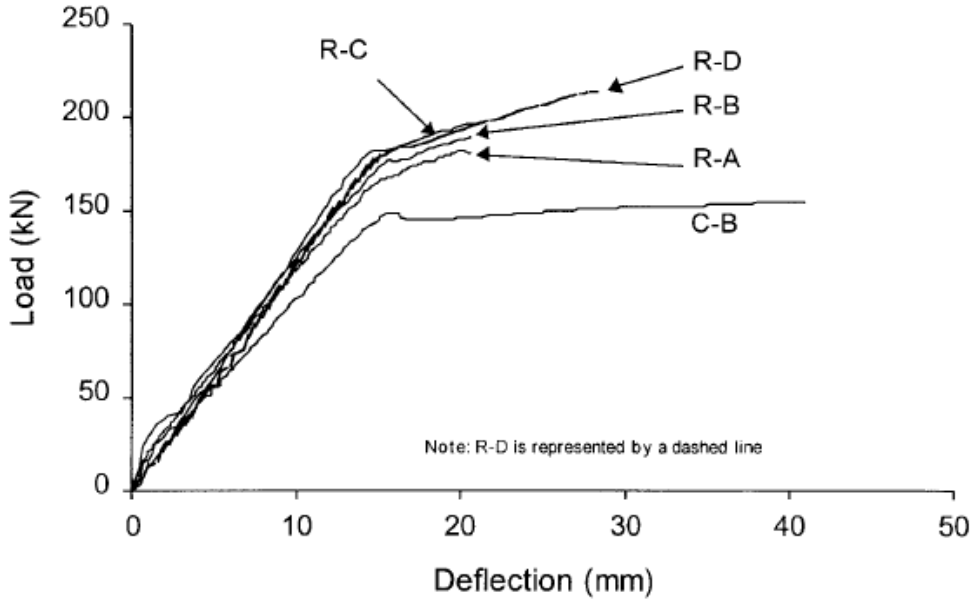

Figure 32: Load-deflection results for R-type CFRP strengthened beams (White et al, 2001)

The failure modes of the retrofitted beams were attributed firstly to the formation of either flexural cracks or a combination of flexural and shear cracks followed by delamination. The study distinguishes between two types of delamination, namely laminate peeling and bond splitting failure. Laminate peeling occurs when the CFRP debonds from the concrete surface, whereas bond splitting occurs when the concrete between the tensile reinforcement and the CFRP laminate fails due to excessive shearing (White et al, 2001). Bond splitting failure suggests that the bond between the concrete and the CFRP laminate is strong and that failure can more accurately be attributed to excessive cracking in the concrete along the tensile reinforcement (White et al, 2001). The S-type CFRP retrofitted beams that failed due to bond splitting exhibited higher maximum midspan deflections and therefore higher energy absorption than the other CFRP retrofitted beams. Figure 33 illustrates the bond splitting failure of an S-type CFRP retrofitted beam where both flexural and shear cracks were observed. Figure 34 illustrates the laminate peeling failure of an R-type beam where only flexural cracks are present. The strain along the CFRP also revealed useful information in relation to the mode of failure. Beams which failed due to bond splitting showed higher strain at failure than beams which failed due to laminated peeling.

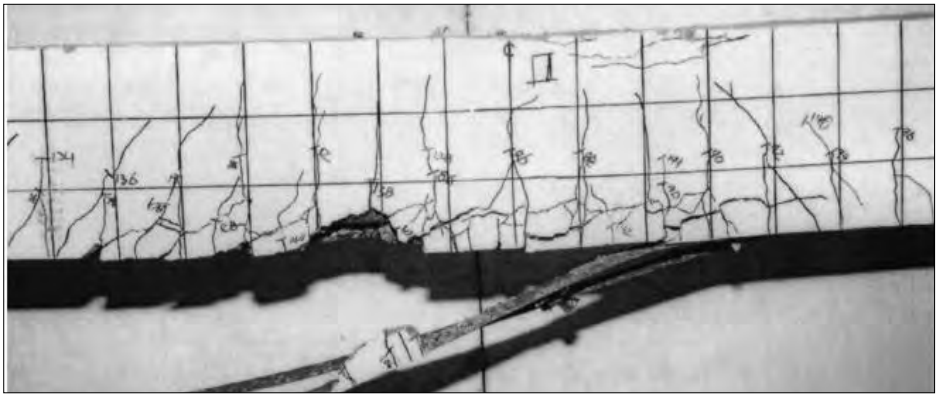

Figure 33: Beam S-A bond splitting failure (White et al, 2001)

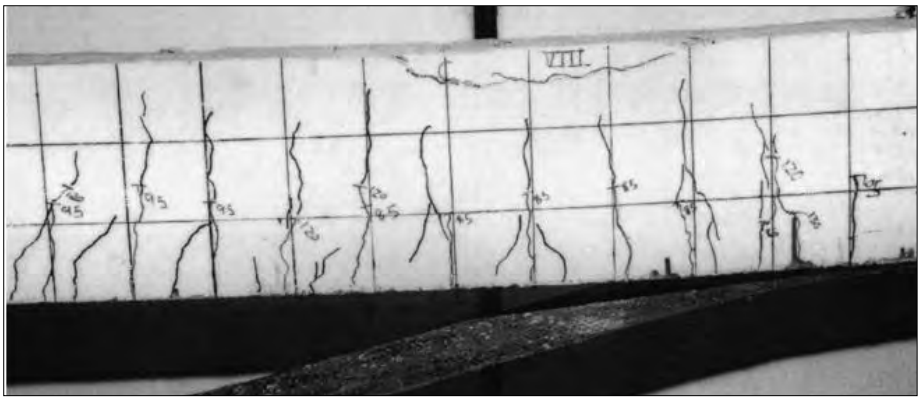

Figure 34: Beam R-A laminate peeling failure (White et al, 2001)

The study concluded that strengthening with CFRP increases flexural capacity and stiffness. The extent of these changes is dependent on the amount of CFRP provided. However, strengthening with CFRP also results in a significant decrease in maximum energy absorption. It was confirmed that rapidly loaded CFRP retrofitted beams exhibit increased flexural capacity, stiffness and energy absorption as compared to beams loaded slowly. Preloading the beams to simulate service load conditions did not have an adverse effect on the load bearing capacity.

Tang and Saadatmanesh, 2003

Tang and Saadatmanesh (2003) tested the impact resistance of RC beams strengthened with CFRP and KFRP fabrics. A total of five beams were tested. Two beams were strengthened on their top and bottom faces with CFRP laminates and two were strengthened the same way with KFRP (Kevlar fibre reinforced polymer). The remaining beam was an un-strengthened control specimen. The impact was induced via a steel drop weight, dropped from varying heights.

Each beam was identical in cross-section and length. The beams also had identical longitudinal reinforcement of mild strength. No shear reinforcement was provided since the span to depth ratio was considered large enough to provide adequate shear resistance. Unidirectional CFRP and KFRP fabrics were bonded to the top and bottom surfaces of the beams. The CFRP was bonded along the entire width of the beam and had a thickness of 0.67mm, an ultimate strength of 1035MPa and an elastic modulus of 85.7GPa. The KFRP was also bonded along the entire width of the beam and had a thickness of 0.43mm, an

ultimate strength of 460MPa and modules of elasticity of 37.7GPa. Figure 35 illustrates the beam dimensions and reinforcement layout.

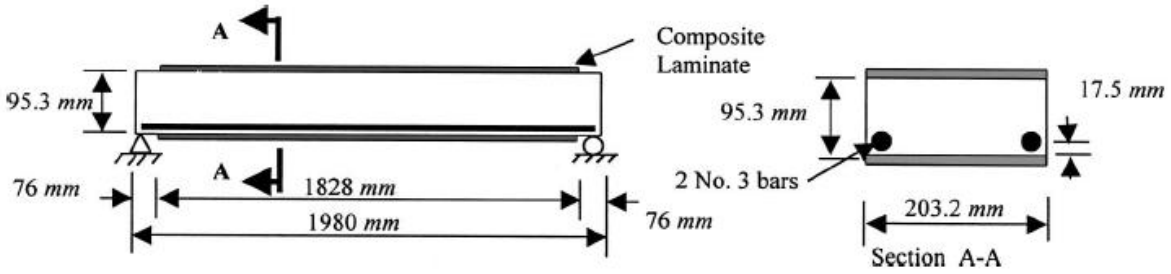

Figure 35: Beam dimensions and reinforcement layout (Tang and Saadatmanesh, 2003)

The beams were simply supported and secured against uplift. Three beams were subjected to consecutive impact loading tests from varying drop heights. After each successive drop test the drop height was increased. These beams included one CFRP retrofitted beam (TB2), one KFRP retrofitted beam (TB1) and an un-strengthened control specimen (TB5). The remaining CFRP retrofitted beam (TB4) and the KFRP retrofitted beam (TB3) were tested by dropping the steel cylinder from a constant height until beam failure was achieved.

The following research parameters were identified:

- Reaction force response
- Deflection response at midspan
- The longitudinal strain distribution in the FRP fabrics.
- Progression of damage and failure mechanisms

The overall behaviour of the various beams were interpreted and compared based on the analysis of these parameters

Figure 36 is a comparison of the maximum reaction forces observed after successive drop tests conducted on TB1, TB2 and TB5. The KFRP and CFRP strengthened beams (TB1 and TB2) exhibited reaction forces greater than that of the un-strengthened control beam (TB5). The stiffer, CFRP strengthened beams exhibited the largest reaction forces. An analysis of the deflection response indicated that the maximum deflection as well as the period of vibration increased after successive impact tests. This was attributed to reductions in beam stiffness and overall beam softening. Figure 37 shows the maximum deflections observed in

TB1, TB2 and TB5 for the various drop tests. The FRP laminates were found to significantly reduce the maximum and residual deflections for similar impact energies.

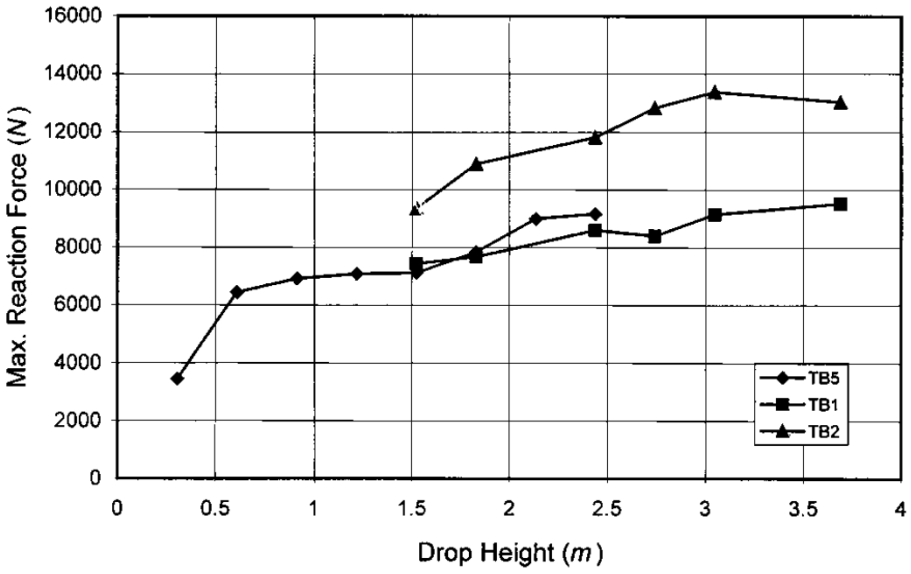

Figure 36: Comparison of maximum reaction forces observed for TB1, TB2 and TB3. (Tang and Saadatmanesh, 2003)

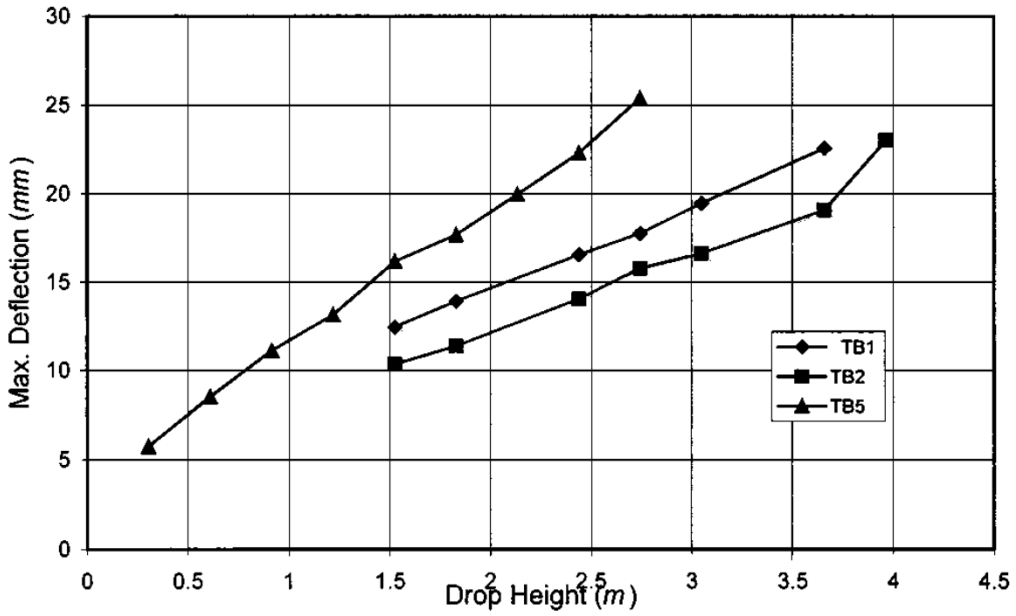

Figure 37: Comparison of maximum deflection forces observed for TB1, TB2 and TB3. (Tang and Saadatmanesh, 2003)

In analysing the damage progression in the strengthened beams, it was observed that the formation of flexural cracks preceded the formation of diagonal shear cracks. Since none of

the beams were reinforced with shear reinforcement the shear cracks extended to the concrete-laminate interface on the top surface of the strengthened beams. Thereafter the cracks continued along the interface, ultimately leading to delamination. The tensile strain along the surface of the FRP laminates was determined to be dependent on the formation and propagation of flexural and shear cracks. The CFRP strengthened beam, TB2, exhibited the least amount of cracks and therefore displayed a more linear strain variation until delamination. The maximum strain recorded in all the strengthened beams was observed to be less than the ultimate strain of both the KFRP and CFRP laminates. The failure mode of the strengthened beams was attributed to shear accompanied by local concrete crushing and ultimately delamination. Longitudinal cracks were also recorded in the KFRP and CFRP laminates.

Tang and Saadatmanesh concluded that the overall effect of the FRP strengthening was to increase the capacity of the beams to resist impact loading since the strengthened beams were able to resist higher impact energies before failure than the un-strengthened control beam. It was found that the CFRP strengthened beams experienced a larger increase in capacity than the KFRP strengthened beams. It was therefore concluded that the magnitude of the increase in capacity to resist impact is dependent on the type, thickness, weight and strength of the FRP laminate. The FRP also reduced maximum deflections and residual deflections, and was observed to increase the beams shear capacity firstly by delaying and limiting crack propagation and secondly by providing concrete confinement. In comparison to the performance of the strengthened beams, the un-strengthened control beam failed shortly after the formation of shear cracks. Figure 38 captures the failure modes of the test specimens.

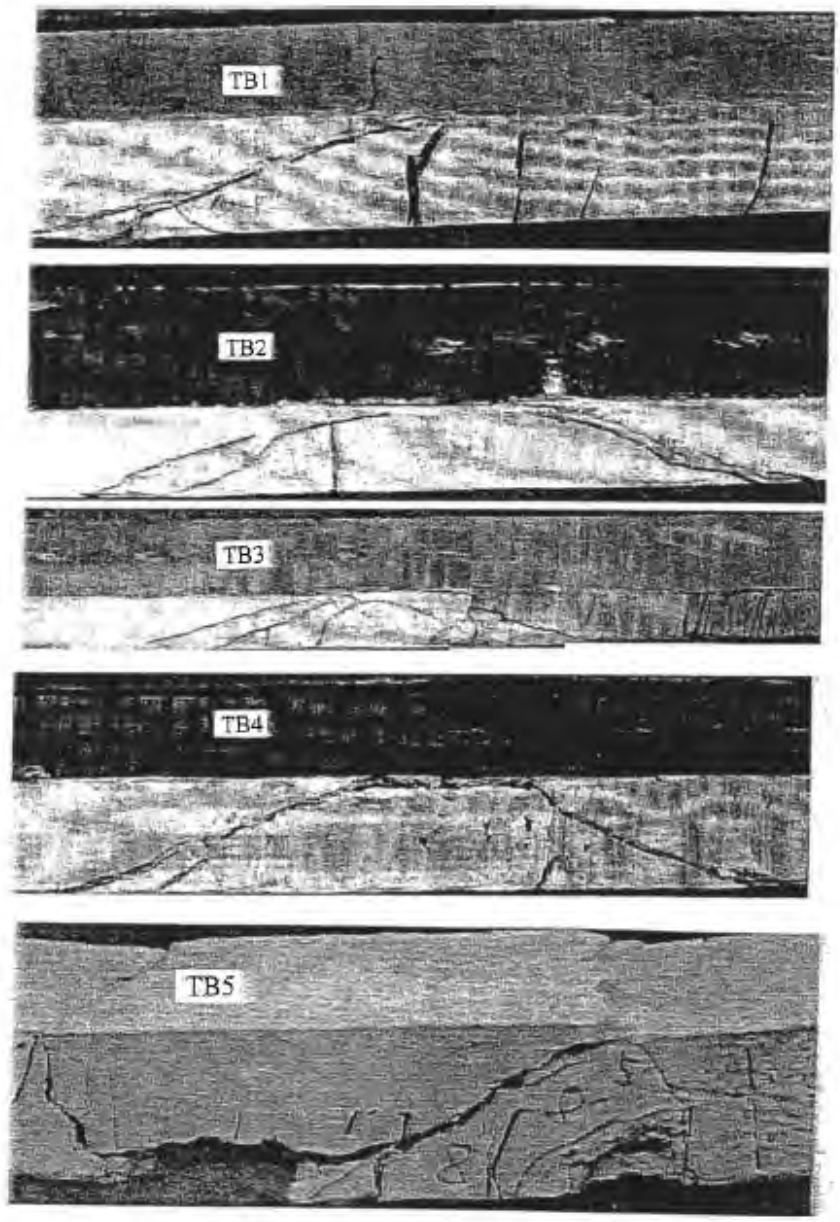

Figure 38: Damage observed in test specimens after impact loading tests (Tang and Saadatmanesh, 2003)

2.7 Summary

Vehicular impact of abnormally loaded trucks with concrete bridge beams is a frequent occurrence and cause of damage which perpetuates the need for structural repair and strengthening. However, upon the application of repair and strengthening procedures the rehabilitated structure is still susceptible to the same loading conditions. In relation to this common occurrence the literature reviewed herein focused on the various components of the problem described above including the application and analysis of impact loading on RC

beams, common repair and strengthening methods for damaged concrete bridge beams, the use of FRP as an alternative strengthening material and the behaviour of FRP strengthened beams subject to impact loading and high loading rates.

Concrete and steel, both exhibit an increase in mechanical properties when subjected to loading rates greater than that of quasi-static loading. This is reflected by corresponding increases in the ultimate load carrying capacity, stiffness and energy absorption of RC beams subjected to increasing loading rates (Adhikary et al, 2012). Experimental studies conducted to analyse the behaviour of RC beams subjected to low velocity impact indicate that failure modes vary depending on the static behaviour of the RC beams, i.e. whether the beams are shear-critical or flexure-critical. Shear-critical beams tend to exhibit lower impact resistance and comparatively catastrophic failure modes characterised by extreme widening of diagonal shear cracks at the support regions (Saatci and Vecchio, 2009). The experimental studies reviewed provide useful insight into the effects of varying reinforcement layouts on the response of RC beams to vertically applied impact loads. However, in relation to analysing the effects of horizontal vehicular impact on concrete bridge beams, the boundary at the interface between a bridge beam and deck needs to be compensated for. Transverse reinforcing stirrups in typical concrete bridge beams usually extend into the deck in order to facilitate composite action under normal loading conditions. Under horizontal impact loading, these stirrups could also facilitate a degree of composite action resulting in damage induced in both the bridge beam and the bridge deck. This study will therefore attempt to simulate the bridge beam-deck interaction by subjecting RC T-beams with varying stirrup spacing to horizontal impact loading. The T-beam flange is analogous of a bridge deck and the web is analogous of a bridge beam.

Impact damaged bridge beams are commonly repaired using patch repair methods. The purpose of the patch repair is firstly to rebuild the damaged structure to its original surface profile and secondly to provide adequate protection against further accelerated deterioration, thus ensuring durability at the damage location (Beushausen and Alexander, 2009).

Strengthening refers to the structural enhancement of weakened structural elements in order to restore or improve their capacities. The effectiveness of the strengthening method

depends on the sufficient enhancement of strength properties where enhancement is required, ease of application, cost effectiveness, durability and reliability, and the visual appearance of the strengthening solution. The use of externally bonded CFRP laminates has become an established alternative to conventional strengthening techniques due to useful properties that CFRP composites exhibit; such as high strength to weight ratios, high durability and resistance to chemical attack, high fatigue resistance and the relative ease of handling and application (Keller, 2003).

The prompt repair and strengthening of structural members damaged due to mechanical loading conditions such as transverse vehicular impact can prevent accelerated deterioration and can return the structure to its original load bearing capacity. However, such members are still susceptible to the same loading conditions after successful repair and strengthening procedures.

Current research on the behaviour of FRP strengthened RC beams subjected to low velocity impact loading is limited and has mainly been conducted to investigate the possibility of enhancing the capacity of RC beams subjected to impact (Erki and Meier, 1999; White et al, 2001; Tang and Saadatmanesh, 2003). These studies indicate that the provision of FRP increases the flexural capacity and stiffness whilst reducing maximum and residual deflections. The magnitudes of these changes are dependent on the type, thickness, weight and strength of the FRP laminates. The studies indicate further that the provision of FRP reduces crack formation and propagation. However, composites generally have reasonable impact resistance when stress is applied in the direction of the fibres. The mechanical properties of composites in other directions are considerably weaker.

The existing literature has focused on vertically applied impact such that the FRP is stressed in the fibre direction. Currently, no studies have been conducted on the behaviour of RC beams strengthened in flexure subjected to horizontal impact loading. Also, no research has been conducted on the behaviour of patch repaired beams subjected to any form of impact loading or loading induced at rates greater than that of quasi-static loading rates. The current study will address these issues by inducing transverse impact on RC T-beams, intentionally damaged, patch repaired, and strengthened for flexure with CFRP composite laminates. Therefore, in addition to analyzing the effect of varying stirrup spacing on the

composite action between the flange and web of the T-beams, this study will also focus on analyzing the behaviour of the repair and strengthening materials under consecutive horizontal impact loading and additionally determine the effect that these materials have on the impact response.

3 *Chapter 3:* Experimental Investigation

3.1 Introduction

This experimental program was undertaken in order to investigate the behaviour of reinforced concrete beams, intentionally damaged, repaired and strengthened for flexure, subjected to horizontally induced impact loading. In addition to this the effect of stirrup spacing on impact behaviour was also analysed.

Highway bridges susceptible to vehicular impact loading often have T-beam superstructure cross-sections. The experimental program hence included the testing of 5 T-beam specimens in order to simulate the interaction between the beam and deck slab of such bridge structures during impact. Figure 39 illustrates the basic concept behind the experimental program selected to simulate horizontal impact on a typical bridge beam structure.

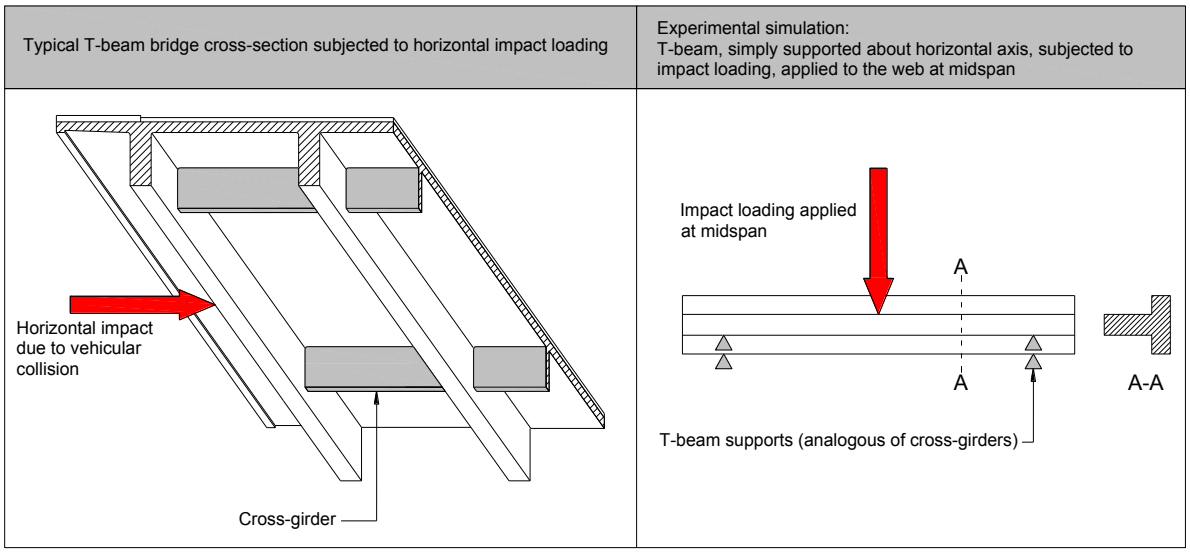

Figure 39: Experimental simulation

The T-beams had identical dimensions and longitudinal reinforcement and varying stirrup spacing. Four of the beams were damaged through the exposure and grinding of the tensile steel reinforcement in order to reduce their flexural capacities. These beams were repaired using self-levelling patch repair mortar across the entire damaged section and strengthened with externally bonded CFRP laminates in order to recover the reduced capacity. The remaining T-beam was undamaged and used as a control specimen.

Consecutive horizontal impact was applied to the sides of the T-beams at the web location from varying drop heights. This was accomplished using standard drop hammer impact testing machinery and by supporting each of the T-beam specimens on their sides using a custom made support system.

3.1.1 Specimen Details

Figure 40 is a schematic diagram illustrating the reinforcement details for the test specimens. The test specimens had identical cross-sectional dimensions and were limited to 1.9m in length for practical reasons (see Figure 40). Each of the specimens also had identical longitudinal reinforcement and was cast using the same concrete mix proportions. The shear reinforcement consisted of 8mm diameter stirrups with varying stirrup spacing. Damage was induced in the central region of the beams and the repair lengths and depths were kept constant.

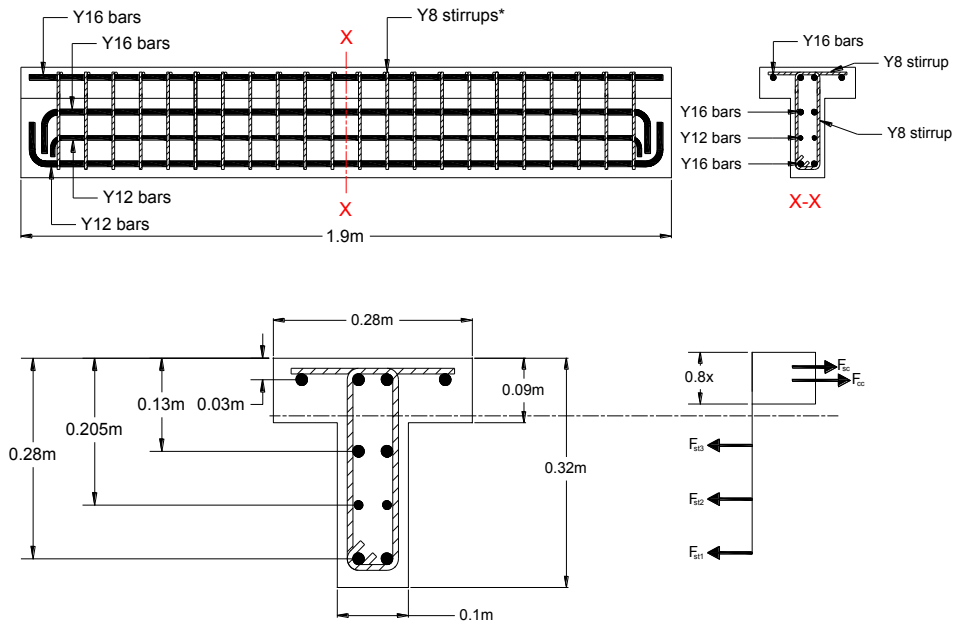

Figure 40: T-Beam dimensions and reinforcement layout (stirrup spacing varies)

Four of the test specimens were mechanically damaged by reducing the cross-sectional area of the bottom tensile reinforcement through grinding. The damaged reinforcement was exposed and the beams were repaired using patch repair mortar. Thereafter the beams were strengthened for flexure with CFRP laminates. The remaining beam was used as a control specimen. Table 3 indicates the annotation used and the distinguishing details of each test specimen.

The control beam, C-80, was undamaged and had a stirrup spacing of 80mm. Beams R-80, RS-80, R-160 and R-240 were all damaged, repaired and strengthened. Beams R-80 and RS-80 both had 80mm stirrup spacing while beam R-160 and R-240 had 160mm and 240mm stirrup spacing respectively. Additional strengthening was applied to the side of the web of beam RS-80. These laminates were applied for additional resistance to the impact load. Since the impact is applied to the side of the web, the resulting stresses in the additional laminates, applied to beam RS-80, should be in the direction of their fibres.

Table 3: Specimen notation and description

Beam Code	Description	Diagram
C-80	- Undamaged control specimen - 80mm stirrup spacing	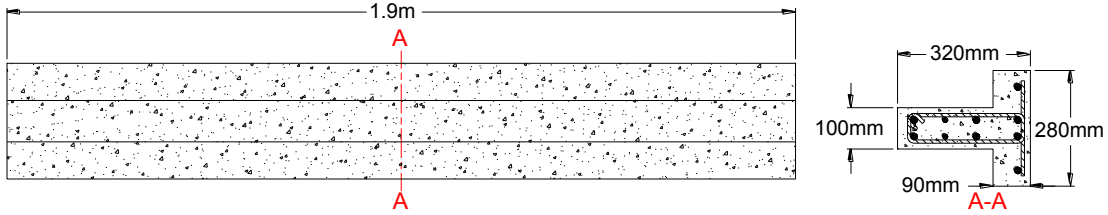
R-80	- Mechanically damaged by grinding tensile reinforcement - repaired with patch repair mortar - Strengthened for flexure with CFRP - 80mm stirrup spacing	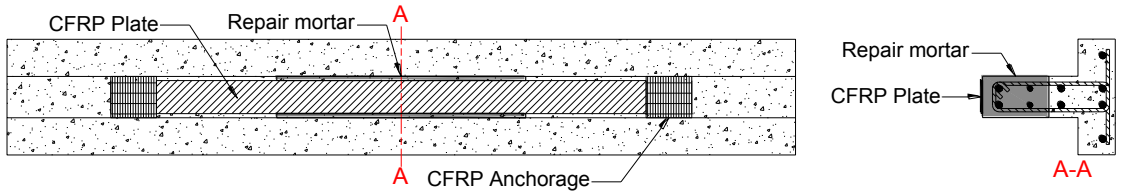
RS-80	-Mechanically damaged by grinding tensile reinforcement - repaired with patch repair mortar - Strengthened for flexure with CFRP - Additionally strengthened along web with CFRP - 80mm stirrup spacing	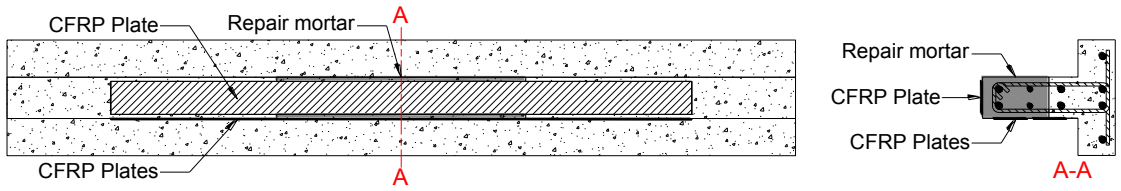
R-160	- Mechanically damaged by grinding tensile reinforcement - repaired with patch repair mortar - Strengthened for flexure with CFRP - 160mm stirrup spacing	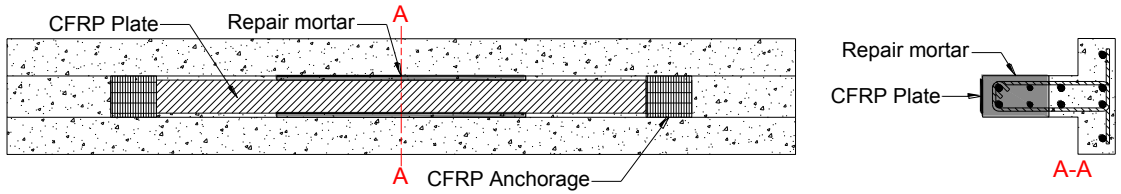
R-240	- Mechanically damaged by grinding tensile reinforcement - repaired with patch repair mortar - Strengthened for flexure with CFRP - 240mm stirrup spacing	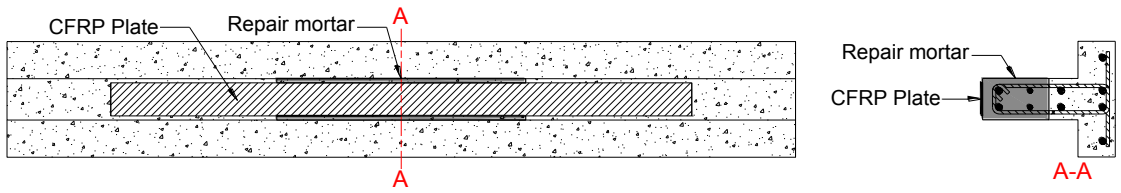

3.1.2 Material Properties

3.1.2.1 Concrete and steel reinforcement properties

Each of the specimens was cast using CEM I, 52.5N (OPC), with a w/c ratio of 0.45; Klipheuwel sand and 9mm Greywacke aggregate. Table 4 is a summary of the material quantities per m^3 of concrete.

Table 4: Concrete mix proportions per m^3

Concrete constituent materials	Material mass kg per m^3
CEM I 52.5 (kg/m^3)	467
Water (l/m^3)	210
9mm Greywacke aggregate (kg/m^3)	958
Klipheuwel sand (kg/m^3)	777

The concrete was mixed in a 100*l* concrete mixer and cast into the steel T-beam moulds shown in Figure 41.

Figure 41: T-beam moulds

Figure 42: Demoulded T-beams

The concrete was compacted using a poker vibrator during casting and levelled with a trowel. Immediately after casting, the exposed surfaces of the beams were covered in

polythene sheets for two days before demoulding. Once the beams were demoulded they were covered with damp hessian cloth for a 28 day period to ensure adequate curing. Concrete cubes were also cast simultaneously and were left to cure under the hessian cloth with the beams. Table 5 shows the results of compressive cube strength tests conducted after 7 days and 28 days. The average 28 day compressive cube strength was determined to be 50.7 MPa.

Table 5: Concrete compressive strength

Age days	Cube no.	Mass (kg) 100x100mm cube	Compressive strength (MPa)	Average compressive strength (MPa)
7	1	2.456	41.3	41.3
	2	2.434	40.6	
	3	2.453	41.9	
28	1	2.428	51.9	50.7
	2	2.412	49.8	
	3	2.431	50.5	

The compression, tensile and shear reinforcing steel was of high yield strength. The steel had a documented yield and ultimate strength of 450MPa and 585MPa.

3.1.2.2 Repair and strengthening materials

The following materials were used during the patch repair and CFRP strengthening stages:

Repair products

- Repair mortar:

  A free flowing, high strength cement based repair concrete with a maximum aggregate size of 9mm was used. The mortar had high strength development and documented compressive cube strength of 75MPa.
- Bonding agent:

  A two component structural epoxy bonding agent was used for bonding the fresh repair concrete to the existing concrete substrate.

Strengthening products

- CFRP Laminates:

  CFRP laminates were used to strengthen beams R-80, RS-80, R-160, and R-240. The laminates had a reported ultimate strain at failure of 1.7%, a modulus of elasticity of approximately 165GPa, and a theoretical tensile strength of 1000MPa at 0.6% elongation (the recommended % elongation limit for design in order to prevent premature delamination). The CFRP laminates had a thickness of 1.4mm and a width of 80mm.

- Laminate bonding agent

  A two component structural epoxy bonding agent was used to bond the CFRP laminates to the concrete substrate. The bonding agent was also used to level uneven substrate surfaces before bonding the CFRP laminates.

- Unidirectional CFRP fabric

  The fabric was used to provide anchorage to beams R-80 and R-160. The manufacturer stipulates an ultimate strain at failure of 1.8%, a nominal modulus of elasticity of 234GPa and a nominal tensile strength of 4300MPa.

- Fabric bonding agent:

  A two component epoxy impregnation resin specifically manufactured for the wet application and bonding of CFRP fabrics to concrete substrates was used to bond the CFRP fabric anchorage strips at the support ends of beams R-80 and R-160.

3.1.3 Damage Procedure

The collision of overloaded trucks into bridge beams often results in the spalling of concrete and the damage or complete rupture of steel reinforcing bars or prestressing tendons at the region of contact. This type of damage often results in a reduction in the beams flexural capacity which facilitates the need for adequate repair and flexural strengthening. Beams R-80, RS-80, R-160 and R-240 were intentionally damaged in order to simulate the effects of vehicular collision. This was achieved by exposing the bottom, tensile reinforcing steel and by reducing the reinforcing steel area through grinding. Damage was only induced at the centre of the T-beams to simulate localised damage.

3.1.3.1 Exposure of reinforcement

In practice, standard repair procedure entails that once the damaged location has been identified, the surrounding concrete in the location of the contact area should be removed and replaced with standard patch repair concrete. The removal of concrete in the contact zone requires the use of machinery which was not provided by the university. Therefore an alternative method to simulate the removal of the concrete was devised. Before specimens R-80, RS-80, R-160 and R-240 were cast they were fitted with rectangular polystyrene plugs to prevent concrete from hardening in the repair zone. The polystyrene plugs were 600mm in length, 140mm in height and 100mm wide (same width as the web). Once the concrete had set the polystyrene plugs were removed leaving a prismatic void at the centre of each beam with the same dimensions as the polystyrene plug. Figure 43 shows one of the T-beams fitted with a polystyrene plug after the T-beam was removed from the mould. Figure 44 shows the void left in the T-beam after the removal of the polystyrene plug.

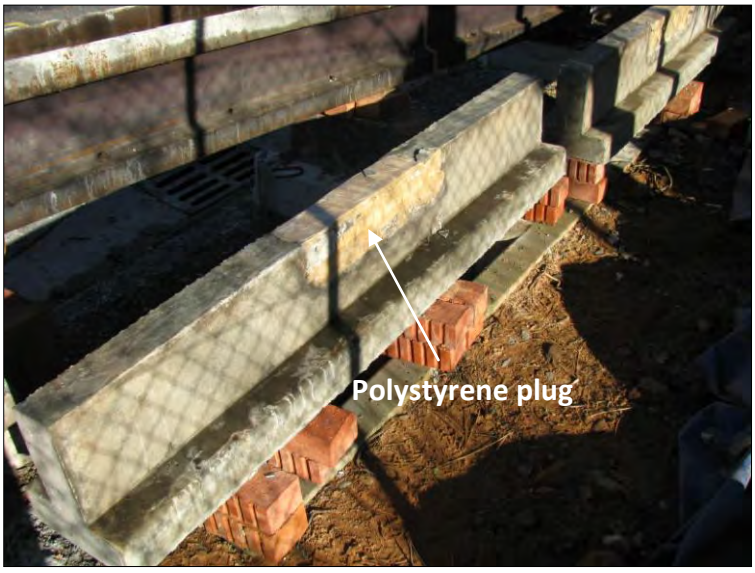

Figure 43: Demoulded beam with polystyrene plug

Figure 44: Exposure of bottom steel reinforcement

3.1.3.2 Reduction of flexural capacity

In order to simulate flexural damage, the cross-sectional areas of the bottom tensile steel reinforcement (two Y16 reinforcing steel bars) were reduced by 25%. This was accomplished through the grinding of the reinforcing bars to an average depth of 4.8mm. The method of determining the grinding depth which corresponds to a 25% reduction of cross-sectional area is presented below.

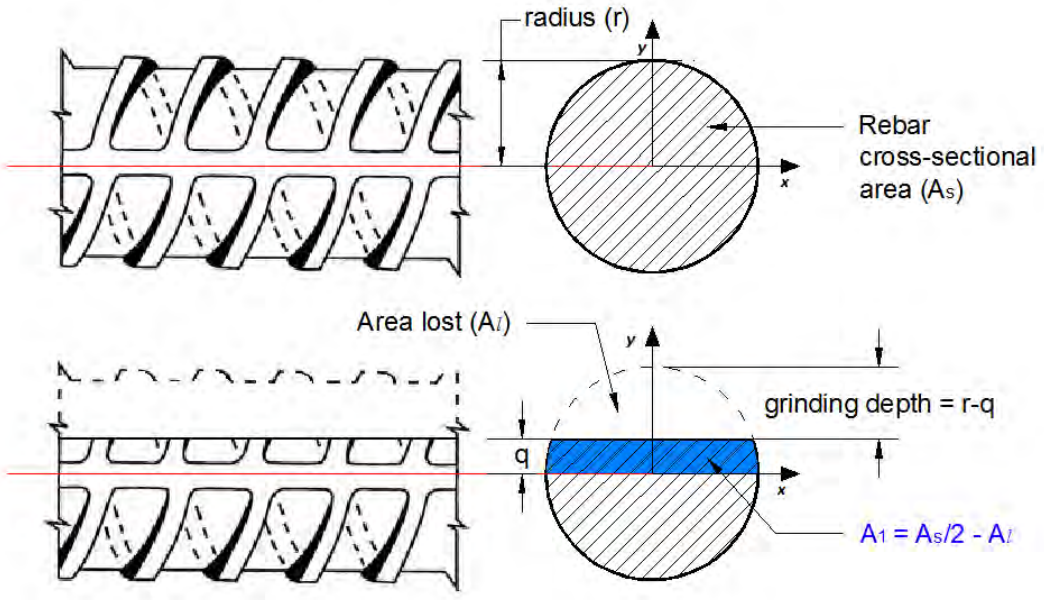

Figure 45: Reduction of rebar cross-sectional area due to grinding

Determination of grinding depth for 25% loss of cross-sectional area:

$A_s = rebar\ \emptyset\ area$

$$A_1 = \int_0^q r\sqrt{1-\frac{y^2}{q^2}}.dy$$

$$= r^2 arcsin\left(\frac{y}{r}\right) + y\sqrt{r^2-y^2}\ \Big]_0^q$$

$$= r^2 \arcsin\left(\frac{q}{r}\right) + y\sqrt{r^2-q^2} \quad (1)$$

$A_l = area\ lost\ due\ to\ grinding$

$$= \frac{A_s}{2} - A_1 \quad (2)$$

Sub equation (1) into equation (2) and rearrange

$$\frac{A_s}{2} - A_l = r^2 arcsin\left(\frac{q}{r}\right) + q\sqrt{r^2-q^2} \quad (3)$$

Consider r = 8mm and $A_l = \frac{A_s}{4}$ = 25% loss of rebar ∅ area, and sub into equation (3):

$$\therefore \frac{A_s}{4} = 64 arcsin\left(\frac{q}{8}\right) + q\sqrt{64-q^2}$$

Solving for q, with $A_s = \pi r^2 = \pi 8^2 = 201.06$

$$\therefore q = 3.23$$

$$\therefore grinding\ depth = r - q = 8 - 3.23 = 4.77 \approx 4.8mm$$

Table 6: Steel reinforcement grinding depth

Rebar radius (mm)	Rebar cross-sectional area (mm^2)	Grinding depth (mm)	Reduced cross-sectional area (mm^2)	% Area lost
8	201	4.8	150.75	25

The longitudinal grinding length varied between 140mm and 160mm, however, the targeted depth was kept constant at 4.8mm. Figure 46 shows one of the T-beams after grinding.

Figure 46: Reduced cross-sectional area of steel reinforcement

3.2 Repair Process

3.2.1 Repair preparation

Before the patch repair concrete was poured the surface of the substrate was prepared mechanically by removing the cement laitance and exposing the aggregate. This was done using an impact drill over the entire substrate area. Additionally the substrate was hosed down and scrubbed with a wire brush in order to remove all surface contaminants and loose material. The substrate was wetted and kept damp over night in order to ensure full saturation before the application of the patch repair concrete.

3.2.2 Patch Repair

The voids left after the removal of the polystyrene plugs were filled using a high strength, free flowing repair mortar. Prior to casting, the substrate was air blasted with a compression gun and rinsed before being thoroughly coated with the epoxy bonding agent. The repair mortar was mixed with 3.1/ of water per 25kg bag and subsequently poured into the formwork. Silicone sealant was used to ensure that the formwork was grout tight. The sides

of the formwork were only briefly vibrated to remove air bubbles. Since uneven surfaces require levelling before the application of CFRP laminates, special care was taken in order to ensure that the repair mortar was at the same level as the existing concrete. Immediately after casting the repair mortar, the beams were covered with polythene sheets. 2 hours after casting (the reported duration required for the initial set to be reached), damp hessian cloth was applied over the exposed surface of the repair mortar before being covered once again with polythene sheets. The formwork was removed after 24 hours and the entire surface of the repair was covered with the damp hessian cloth, which was kept damp for an additional 48 hours in order to ensure proper curing. Compressive cube strength tests were conducted on the repair mortar after 7 days, the results of which are presented in Table 7. Figure 47 is a picture of beam R-80 after repair and strengthening procedures. The region of patch repair is clearly identifiable.

Table 7: Cube strength tests conducted on repair mortar

Cube no. (100mm cubes)	7 day Compressive strength (MPa)	Average 7day compressive strength (MPa)
1	61.2	62
2	60.8	
3	64.0	

Table 8: Repair mortar strength properties as supplied by Sika product manual

Age days	Compressive strength (MPa)	Flexural strength (MPa)	Tensile strength (MPa)
1	34	3.8	-
7	55	5.7	-
28	75	7.5	5.5

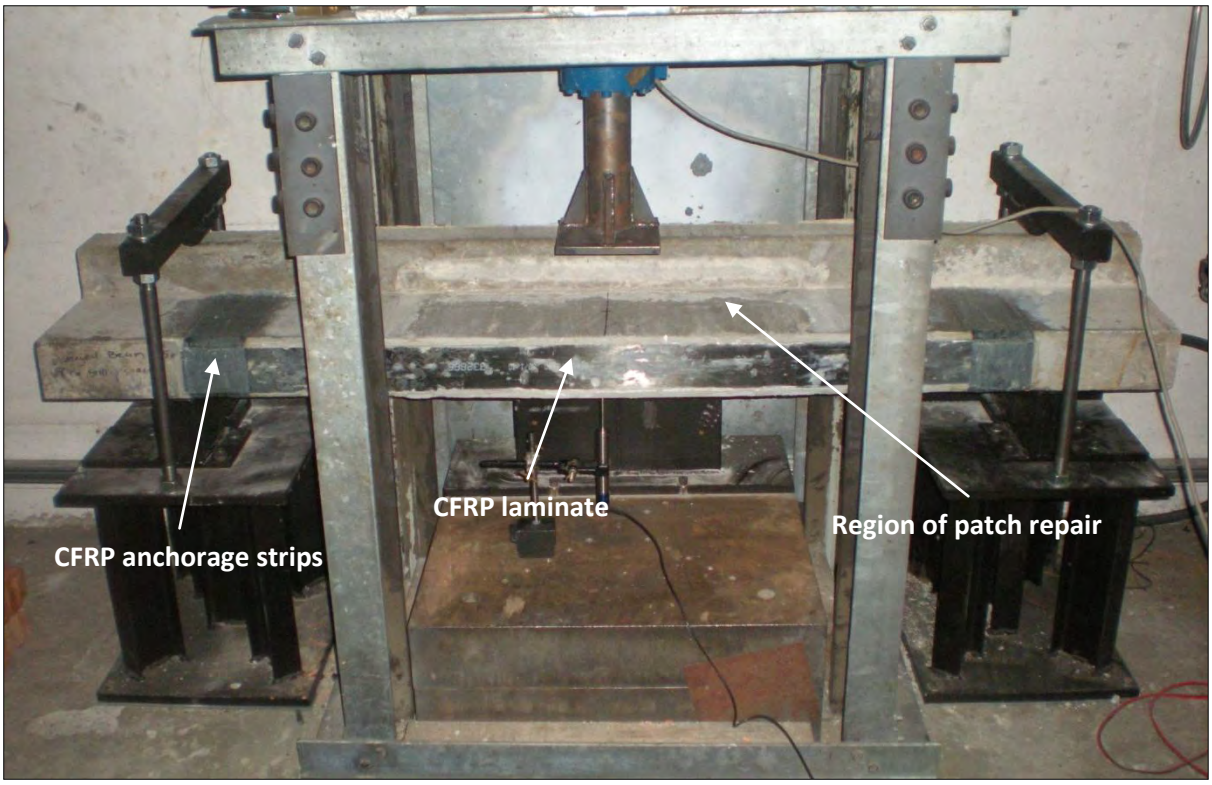

Figure 47: Beam R-80, repaired and strengthened before testing

3.2.3 CFRP Strengthening Procedure

The repaired beams were left for a total of seven days before the application of the CFRP laminates. The primary purpose of the CFRP was to restore the load carrying capacity of the beams lost due to the grinding of the steel reinforcement. Correct application of the CFRP is considered vital in order to ensure proper performance. Improper application can reduce the long term bond performance and result in premature failure. Therefore, a high standard of surface preparation and CFRP application must be adhered to in order to ensure long term performance.

All of the beams, with the exception of the control specimen, C-80, were retrofitted with CFRP laminates along the bottom of their webs. Beam RS-80 was retrofitted identically to the other beams; however it also had two additional CFRP laminates bonded to the side of the web in order to provide additional horizontal stiffness (see Table 3).

Before the CFRP laminates could be applied the bonding surfaces were checked for unevenness. The product manual allowed for a tolerance of 4mm unevenness per 0.3m in length. Where leveling was required an epoxy adhesive was used to even out the surface.

Thereafter the epoxy was left to harden for 24 hours (leveling was only required for beam R-240).

The bonding surface was also prepared mechanically in order to remove laitance and to ensure an open textured surface. Loose materials were removed by air blasting and fine dust particles were removed with a damp cloth. The CFRP laminates were cut to 1.4m panels and the bonding surfaces of the laminates were cleaned to remove any fine dust particles.

The laminate bonding agent was prepared by mixing the two components thoroughly until a uniform light grey mixture was obtained. The adhesive was then immediately applied to the clean surface of the CFRP laminates with a trowel. Thereafter the laminates were gently applied to the bonding surface and pressed down so that the thickness of the epoxy layer was approximately 2.5mm along the entire laminate length. A roller and a spirit level were used to ensure an even bond. Immediately after applying the CFRP laminates the beams were covered with polythene sheets to protect the beams from sunlight and moisture. The laminates were left to set and harden before testing.

Unidirectional 110mm wide CFRP material was bonded around the edges of the CFRP laminates applied to beams R-80 and R-160 in order to provide anchorage. The CFRP laminates and anchorage strips are indicated in Figure 47.

3.3 Impact testing

Consecutive impact loading was induced on the sides of the T-beam specimens from varying drop heights. The beams were repeatedly impacted on their sides in order to analyze the behaviour of the varying beams as damage intensified. Practical applications of such loading situations can include repeated vehicular collision against bridge beams or girders. The impact loading was induced via a drop hammer impact machine. The recorded parameters include the contact force response, the deflection response of the beams and the progression of damage observed as a result of the consecutive impact loading. The procedure and the instrumentation used to acquire the relevant data are discussed below.

3.3.1 Drop hammer machine and T-beam support system

In order to carry out this experimental study, a custom support system was designed and manufactured so that the impact loads could successfully be applied to the webs of the T-beam specimens. Figures A1 to A3 in Appendix A are diagrams which indicate the detailed design of the support system as well as the relevant support dimensions. Figures 48 and 49 show the drop hammer testing machine and the complete support system after manufacturing.

The drop hammer fell along four guiding rails and had a recorded total mass of 261kg. The striking head of the drop hammer had a curved contact surface with a length of 170mm and a radius of 500mm. The relevant dimensions of the striking head are shown in Figure A4 in Appendix A. The T-beams were simply supported over a 1.4m span on their sides so that impact could be applied to the web at midspan. Figure 49 shows one of the end supports with the control specimen, C-80, in place. Special steel clamps were designed and installed at each end in order to prevent the beam from bouncing or moving out of displacement, without inducing restraint moments. A guiding back plate was also installed behind the beam in the central region in order to limit torsion during impact (see Figure A3 of Appendix A). Special care was taken in order to ensure that the test beams rested level on the support structure. This was important to ensure an even contact area between the striker head and the contact surface of the beams.

Figure 48: Impact machine and support system

Figure 49: Simply supported right end of beam C-80

3.3.2 Contact force response measurement

The contact force response was recorded via a 200kN capacity loadcell, rigidly attached between the striker head and the drop hammer mass (see Figure 50). The loadcell showed consistency in its ability to record the contact force response. The output data from the

loadcell was recorded at a sampling rate of 10,240 kHz. The data captured was processed using *Matlab* graphic analysis and *Microsoft Excel*. Figure 51 shows the data acquisition set up.

Figure 50: Striker head and loadcell *Figure 51: Data acquisition set up*

3.3.3 Deflection response measurement

The recording of the deflection response proved a difficult task due to limitations of the available equipment. Initially a linear variable differential transducer (LVDT) was mounted at the midspan of beam C-80 in order to record the dynamic response. However, the LVDT was inadequate for recording the high rate response resulting from the impact loading. This was evident due to the unrealistic deflection response recorded. Analysis of HSC footage of the initial impact tests indicated that the LVDT tip lost contact with the beam immediately after the beam reached maximum deflection. Despite attempts to secure the LVDT tip, the problem persisted. Therefore an alternative approach to record the displacement response was developed using the HSC footage. The HSC was set to a recording frequency of 25000 frames per second. This enabled the precise tracking of the midspan deflection of the repaired and strengthened beams with respect to time. The HSC was kept in a constant position while recording each of the impact tests conducted on the various test specimens. For the purpose of determining the midspan deflection response, the following individual frames were isolated from the HSC footage:

- Frame 1: The instant at which the beam and the striker head displace together immediately after initial contact is made
- Frame 2: The frame capturing maximum midspan deflection.
- Frame 3: The frame at which instant the beam returned to its original position before contact.

For every drop test, each of the above mentioned frames from the HSC was scaled precisely so that the beam dimensions in the frames were identical to the actual specimen dimensions. This enabled precise measuring of the maximum dynamic midspan deflection and the recording of the initial deflection halfcycle duration. The method described above is illustrated in Figure 52.

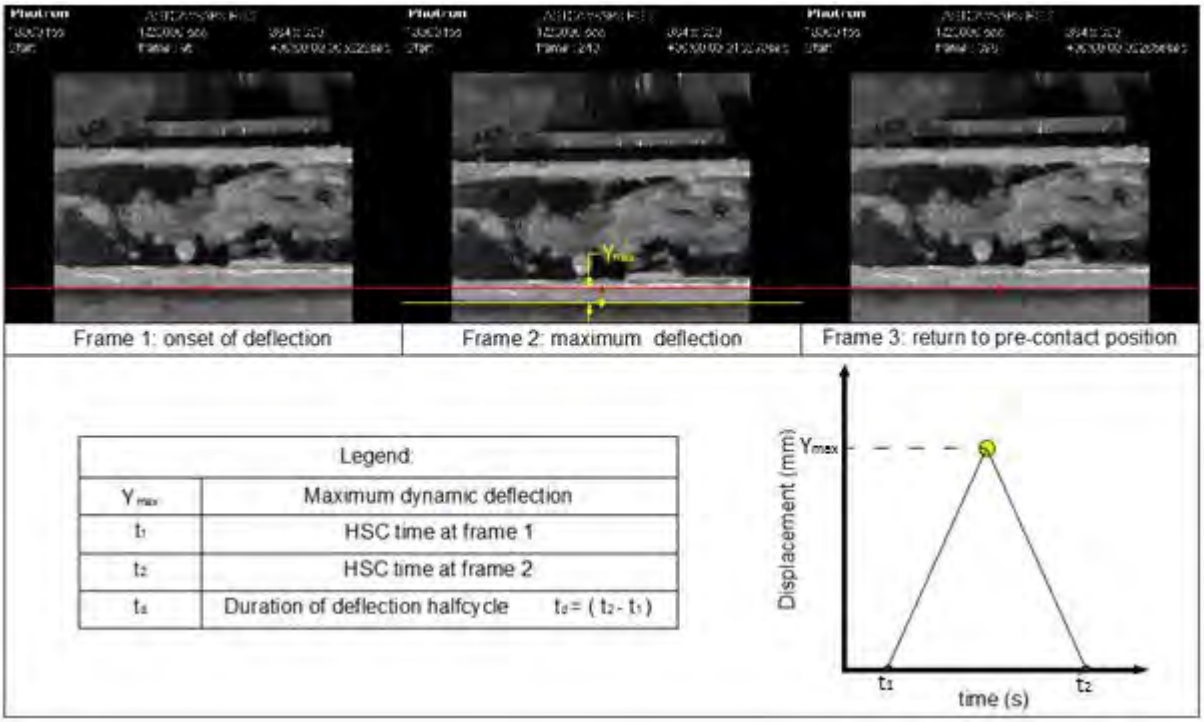

Figure 52: Determination of deflection response data

The residual midspan deflection was recorded after each drop test via a laser distance meter and was confirmed via the HSC footage.

3.3.4 Test program

The test program involved impacting the various test specimens consecutively from increasing drop heights. The control specimen, C-80, was initially tested in order to determine a suitable drop height range which would not result in contact forces above the

suggested limit of the loadcell (200kN). The damage observed in the control specimen and the recorded contact force responses due to consecutive impact loading led to the selection of a standard drop height range for the tests to be conducted on the various repaired and strengthened beams. The test program selected therefore involved performing eight consecutive impact tests on each of the beams from the following increasing drop heights: drop height (***h***) = 150mm; ***h*** =300mm; ***h*** =450mm; ***h*** =600mm; ***h*** =750mm; ***h*** =1000mm; ***h*** =1200mm; and ***h*** =1400mm. This drop height range was selected since it enables gradual progression of damage from that of low intensity to high intensity. This in turn enables thorough analysis of the damage behaviour of the various test specimens. A laser distance meter was used to position the drop hammer to within a few millimeters of the specified drop height. After each drop test was conducted the loadcell data and the HSC footage was saved and the specimen being tested was thoroughly observed for the presence of cracks and other forms of damage. Photographs were taken of any damage observed. The HSC footage was also used to analyze the damage progression and the failure mechanisms of the CFRP laminates.

3.4 Summary

The experimental methodology described in this chapter was designed in order to test the performance of damaged, patch repaired and CFRP strengthened RC T-beams, with varying stirrup spacing, subjected to consecutive impact loading tests.

The specimen preparation is discussed in detail. This includes the damage, patch repair and CFRP strengthening procedures. A detailed description of the test set up is also presented including a description of the designed support system.

Finally the method of testing and the data acquisition process is described. The drop hammer impact testing scheme was set up so as to achieve the objectives of this dissertation. The results of the proposed methodology are discussed and analyzed in the chapter to follow.

4 Chapter 4: RESULTS

4.1 Introduction

The impact loading experimentation was carried out according to the procedure presented in the methodology. This enabled the successful analysis of the repaired and strengthened beams. The relevant data is presented and discussed according to the following research parameters: progression of damage observed during testing, the contact force response and the recorded displacement response.

4.2 Progression of Damage

4.2.1 Introduction

Damage progression due to consecutive impact loading, observed during testing, varied according to the specimen being tested. Observations made during testing were used to record damage evolution after successive drop tests. High speed camera footage obtained during the testing of beams R-80, RS-80, R-160 and R-240 also revealed important information relating to the failure mechanisms of the CFRP laminates. Figure 53 is an idealisation depicting the various forms of damage encountered during testing. These forms can broadly be categorized as follows:

- Flexural damage due to the overall response of the beam (Figure 53 (a))
- Horizontal shear cracking along the flange-web interface (Figure 53 (b))
- Shear damage at the support ends (Figure 53 (c))
- Shear cracking on the impacted surface (Figure 53 (d))
- Compression damage in the form of cracking and crushing in the extreme compression region during flexure (Figure 53 (e))
- Localised damage in the contact zone of the applied impact load (Figure 53 (f))
- Damage observed in the strengthening material (Figure 53 (g))

Photographs taken of the beams during testing will be presented and used to discuss aspects of the damage progression. Detailed diagrams illustrating the damage observed after successive drop tests will also be presented for each of the beams with the exception of the control beam, C-80. The behaviour of each beam with respect to damage progression

will initially be discussed. This will be followed by a comparative analysis of all the beams tested.

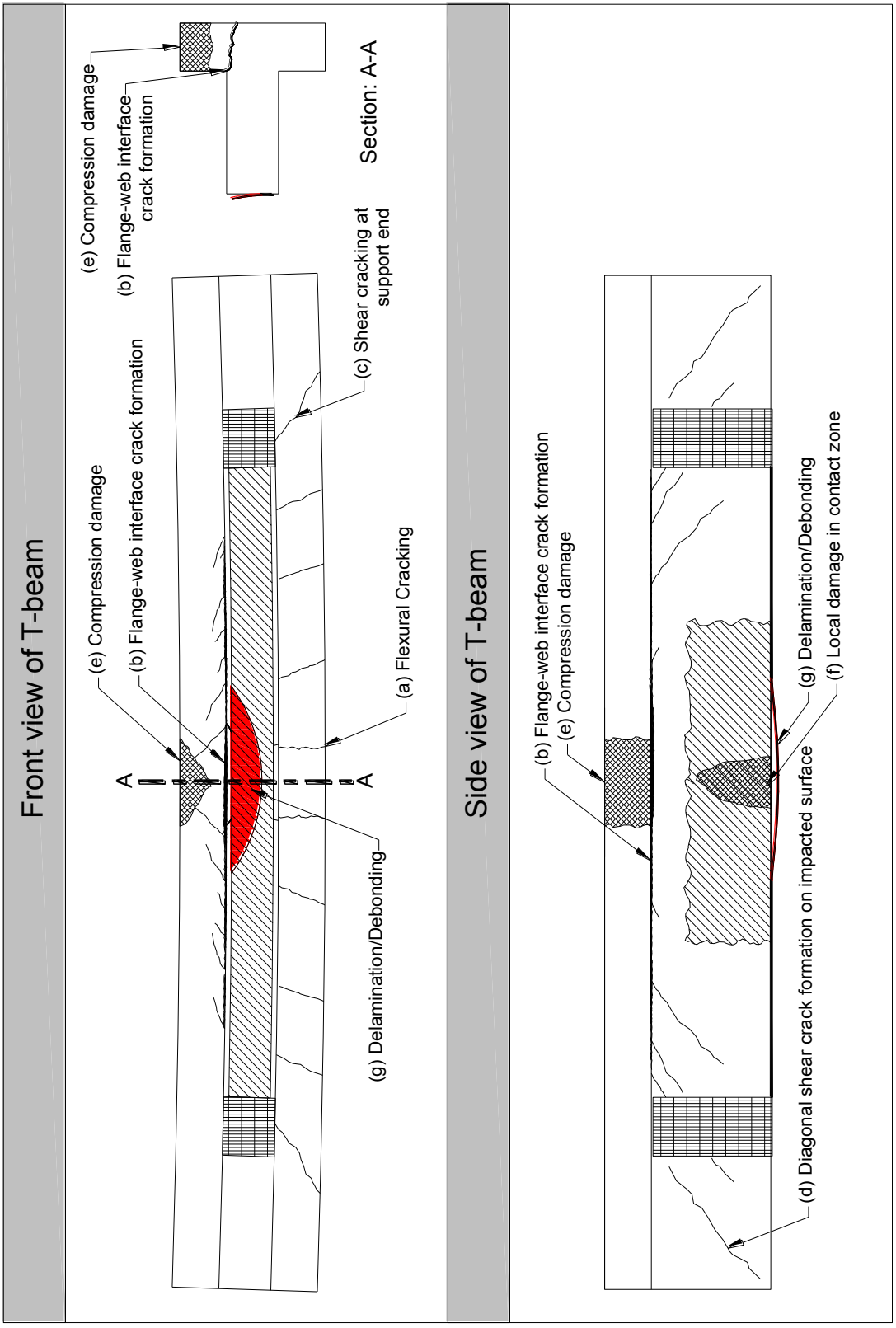

Figure 53: Damage observed due to consecutive impact loading

4.2.2 Progression of Damage: Beam C-80

The drop height range for the strengthened and repaired beams was selected based on the progression of damage observed in the control beam, C-80. Since beam C-80 was the first to be tested, certain aspects of the damage evolution were not observed during testing. Observations made after all the drop tests had been conducted revealed important information about the beam behaviour which enabled a more detailed account of the damage progression for the strengthened and repaired beams. Figures B5 to B9 in Appendix B capture the damage observed in beam C-80 after impact had been induced consecutively from varying drop heights (***h*** = 285mm, 555mm, 745mm, 1042mm, 1252mm and 1402mm).

During the testing of beam C-80, numerous flexural cracks were observed along the bottom part of the flange. These cracks initiated centrally and subsequently spread along the bottom of the beam. Figure B7 in Appendix B shows the most severe central cracks initiating from the bottom part of the flange. These central, flexural cracks were observed to extend well into the web, ultimately propagating to the front face of the web. The flexural crack formation is an indication of the overall response of the T-beam supported on its side. This is consistent with the findings of previous studies which affirm that an overall response, as opposed to a localised response, is the main concern when dealing with reinforced concrete beams subjected to impact loading (Fujikake et al. 2009; Hughes and Beeby 1982).

The beam ultimately failed due to crushing of the concrete in the compression zone (located centrally in the flange) during the fourth drop test (***h*** = 1042mm) as shown in Figure B6 of Appendix B. The crushing of the concrete was due to the development of high compressive stress in the flange and cannot be described as localised damage since the striker only makes contact with the web.

Further inspection of the beam after all the tests had been conducted indicated diagonal shear cracking in the bottom part of the flange at both support ends. A long horizontal crack formation was also observed along the flange-web interface as indicated in Figure B8 of Appendix B. This can be attributed to high shear stress development along the interface. The crack formation was observed to initiate along the flange-web interface and extend through the entire thickness of the flange. Diagonal shear cracks were also observed at the

support regions on the impacted surface (see Figure B9, Appendix B). Local damage, in the contact zone, was only observed after the final drop test.

The tests conducted on beam C-80, enabled the effective identification of various forms of damage to be expected during the testing of the remaining beams.

4.2.3 Progression of Damage: Beam R-80

Figure B1 in Appendix B is a diagram detailing the damage progression observed as a result of the consecutive drop tests conducted on beam R-80. Figures B10 to B12 in Appendix B are photographs taken of beam R-80 after the final drop test.

The progession of damage was gradual until the sixth drop test, during which crushing of the concrete in the extreme compression zone was observed. Thereafter the severity of damage intensified. The average spacing between flexural cracks (s_f), after the all the drop tests had been conducted, was determined to be $s_f \approx$ 160mm. The flexural cracks were observed to propagate from the bottom part of the flange well into the web, where significant branching was observed, and ultimately to the front face of the web underneath the CFRP laminate (see Figure B12, Appendix B). A total of six flexural cracks were observed to extend to this region.

Horizontal shear cracking at the flange-web interface initiated early and gradually propagated due to the successive drop tests. However, this crack formation was not considered to be of high severity. Diagonal shear cracks on the impacted surface were observed to propogate from the flange-web interface diagonally towards the support regions, creating a shear crack formation that was somewhat symetrical about the centre of the beam. The average spacing between these cracks (s_w) on the impacted surface was determined to be $s_w \approx$ 122mm. Local damage in the region of contact was only observed after the final drop test (see Figure B11, Appendix B)

The seventh drop test resulted in the delamination of a small area of CFRP located towards the left end of the beam (see Figure B1, Appendix B). The high speed camera footage captured a ripple like effect in the CFRP while the beam was approaching maximum deflection during the impact event. Since maximum deflection occurs at the beam centre, the CFRP laminate should experience maximum strain in this central region. However,

delamination was observed to occur off centre. Therefore the region of delamination could be attributed to imperfections in the epoxy bond. The extent of the delamination worsened during the final drop test. No cracking was observed to form along the repair concrete interface.

4.2.4 Progression of Damage: Beam RS-80

Figure B2 in Appendix B is a diagram detailing the damage progression observed as a result of the consecutive drop tests conducted on beam RS-80. Figures B13 to B16 in Appendix B are photographs taken of beam RS-80 after the final drop test.

Beam RS-80 experienced relatively few cracks during the initial five drop tests. The six drop test resulted in crushing of the concrete in the extreme compression region. Thereafter, the severity of the damage intensified greatly. The volume of concrete crushed during the final two drop tests, was the largest of all the tested beams. After all the drop tests had been conducted, the average spacing between the flexural cracks was determined to be $s_f \approx$ 139mm. Only one flexural crack was observed to to propogate to the front face of the web.

As with beam R-80, the extent of the horizontal shear cracking at the flange-web interface was considered minor. The diagonal shear cracks observed on the impacted surface was also considerd to be relatively minor with an average spacing of $s_w \approx$ 188mm. No local damage was observed around the region of contact.

The two additional laminates, used to strengthen beam RS-80 about the horizontal axis, debonded during the final drop test. Bond splitting failure was observed along the entire left side of both laminates. The debonding of the CFRP laminates is described as bond splitting instead of laminate peeling since large quantities of epoxy and concrete were found bonded to the loosened ends of the laminates. The debonding event can be likened to the release of a stretched elastic band (Erki and Meier, 1999). Strain energy was initially stored in the CFRP laminates as the beam approached maximum deflection. This was followed by an abrupt release of energy as debonding occurred. High speed camera footage captured shards of epoxy exploding from underneath the CFRP laminate. Figure B16 in Appendix B is a frame from the high speed camera footage which captures the release of energy during the debonding event. Figure B15 in Appendix B captures the extent of the debonding observed. The CFRP applied to the bottom of the T-beam remained intact without any form of bond

splitting or laminate peeling along its span. No cracking was observed to form along the repair concrete interface.

4.2.5 Progression of Damage: Beam R-160

Figure B3 in Appendix B is a diagram detailing the damage progression observed as a result of the consecutive drop tests conducted on beam R-160. Figures B17 to B19 in Appendix B are photographs taken of beam R-160 after the final drop test.

The beahaviour of beam R-160 was similar to that of beam R-80 in that the damage progression was initially gradual followed by an increase in severity after crushing in the compression zone was observed during the sixth drop test. The average spacing between flexural cracks was determined to be $s_f \approx$ 106mm, while the average spacing between the shear cracks on the impacted surface was determined to be $s_w \approx$ 100mm. The horizontal shear cracking observed at the flange web interface was considered to be more severe in terms of length and crack width than that of beams R-80 and RS-80. Figure B18 in Appendix B shows the extent of the shear cracking at the flange-web interface after all the tests had been conducted. Local damage in the region of contact was observed during the final drop test.

The CFRP at the bottom of the T-beam debonded due to bond splitting failure during the final drop test (see Figure B18, Appendix B). High speed camera footage indicated that the debonding initiated in the centre of the beam as the beam was approaching maximum deflection. A chunk of epoxy underneath the laminate separated from the concrete causing the surrounding CFRP to subsequently peel off over a small area. No cracking was observed to form along the repair concrete interface.

4.2.6 Progression of Damage: Beam R-240

Figure B4 in Appendix B is a diagram detailing the damage progression observed as a result of the consecutive drop tests conducted on beam R-240. Figures B20 and B21 in Appendix B are photographs taken of beam R-240 after the final drop test.

Crack formation was detected during the second drop test which is one drop test earlier than any of the other beams tested. The average spacing between flexural cracks was determined to be $s_f \approx$ 106mm. A total of seven flexural cracks were observed to extend to

the front face of the web. Beam R-240 exhibited the highest severity of shear damage of all the beams tested. This is apparent due to the extent of the shear crack formation on impacted surface; and the severity of the horizontal shear cracking along the flange-web interface. The average spacing between shear cracks on the impacted surface was determined to be $s_w \approx 95$mm. During the sixth drop test, the cracking at the flange-web interface was so severe that aggregate was exposed. The extent of the damage at the flange-web interface increased greatly during the final two drop tests. High speed camera footage of these tests indicates the separation of the top part of the flange and the rest of the beam, since the two parts were observed to oscillate and deflect separately during impact. The reduction in shear resistance effectively changed the mode of failure from the crushing of concrete in the extreme compression zone, as observed in the other tested beams, to shear failure along the flange-web interface. The extent of the separation due to the low shear resistance at the flange-web interface is clearly visible in Figure B20 in Appendix B.

The final drop test also resulted in the bond splitting failure and longitudinal splitting of the CFRP laminate bonded to the bottom of the T-beam. High speed camera footage indicates that the debonding initiated in the central region of the beam. Shards of epoxy exploded from underneath the laminate, also causing the laminate to split in the longitudinal direction. The entire right end of the CFRP delaminated (see Figure B21, Appendix B).

4.2.7 Comparative Analysis

The progression of damage, for each of the tested beams, initially began with the formation of flexural cracks and horizontal cracks along the flange-web interface. The subsequent drop tests however, resulted in clear differences in damage progression. This is evident due to the variations in crack formation and failure mechanisms observed for the various beams. These differences are illustrated in Figure 54 which compares the damage observed after the final drop test for repaired and strengthened beams. Table 9 quantifies the extent of the flexural and shear cracking observed for the various test specimens. Table 10 is a qualitative comparison of the repaired and strengthened beams with respect to the extent of concrete crushed during testing, the extent of the cracking at the flange-web interface and the extent of the damage induced in the CFRP laminates applied to the bottom of the T-beams.

Table 9: Quantitative account of cracking observed in the various test specimens

Beam No.	Average spacing between flexural cracks, s_f, (mm)	No. of flexural cracks propagated to front face of web	Average spacing between shear cracks on impacted surface, s_w, (mm)
R-01	160	6	122
RS-01	139	1	188
R-02	107	4	100
R-03	95	7	95

*Table 10: Qualitative account of damage observed in the various test specimens**

Beam No.	Extent of crushing in compression zone	Extent of cracking at flange-web interface	Extent of damage induced in CFRP laminates
R-01	***	*	**
RS-01	*****	*	-
R-02	**	***	***
R-03	-	*****	*****

*The various forms of damage are rated out of 5, with 5 being the worst in terms of damage induced.

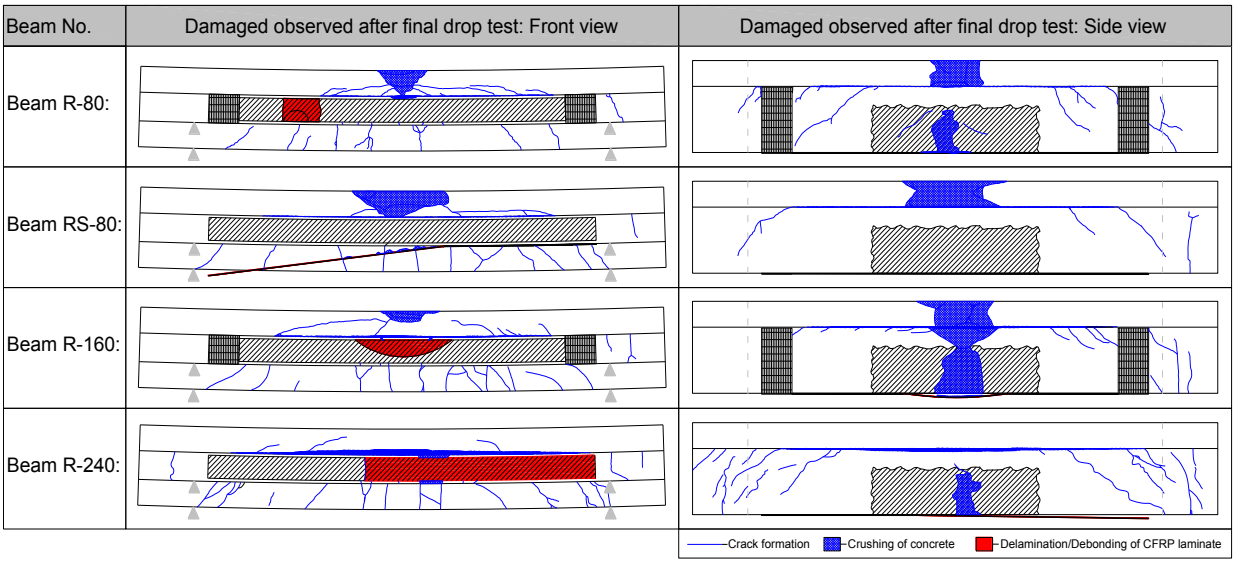

Figure 54: Damage observed after final drop test for the various beams tested

4.2.7.1 Effect of Repair and Strengthening Materials

An initial observation can be made with regard to the behaviour of the patch repair concrete used in all the beams with the exception of the control specimen. The interface between the patch repair concrete and the substrate was identified as a potential area of weakness. The performance at the interface depends specifically on the quality of the epoxy adhesive bond between the repair concrete and the substrate. Therefore, particular attention was paid to the development of cracks originating from the repair interface. The results indicate that none of the repaired and strengthened beams exhibited any form of crack propagation along their repair interfaces. This implies that under consecutive impact loading, the epoxy adhesive between the repair concrete and the substrate provided a continuous bond and did not have a noticeable effect on damage progression.

It was stated earlier that the off centre region of delamination, observed in the CFRP bonded to beam R-80, could have been due to the presence of imperfections in the epoxy bond. This suggests that such imperfections can increase susceptibility to the occurrence of delamination in the region of the imperfections, when subjected to impact loading. No noticeable damage was observed in the CFRP bonded to the bottom of beam RS-80. However, both beams R-160 and R-240 experienced bond splitting failure initiating in the central regions of the CFRP laminates. The bond splitting observed in beam R-160 was less severe than that observed in beam R-240. Table 9 and Figure 54 indicate that a larger proportion of damage was observed in the web of beam R-240 than that of beam R-160. This suggests that the extent of debonding induced in the CFRP laminates depends on the extent of the damage induced in the web. It should, however be stated that the severity of the debonding observed in beam R-240 is also attributed to the lack of anchorage at the ends of the laminate.

4.2.7.2 Effect of Additional Horizontal Strengthening (applied to Beam RS-80)

The damage progression observed in beam RS-80 can be compared to that of beam R-80 to analyse the effect of the additional CFRP laminates applied for horizontal strengthening. The flexural crack distribution observed along the bottom of beam RS-80 was noticeably larger than that of beam R-80 as indicated in Figure 54 and Table 9. However, only one flexural crack was observed to propagate to the front face of the web of beam RS-80 as compared to the six cracks observed in beam R-80. In addition to this, the main central flexural cracks

observed in beam RS-80 indicated smaller crack widths than that of beam R-80. This suggests that the CFRP applied for horizontal strengthening effectively reduced the propagation and widening of flexural cracks. Figure 54 and Table 9 also indicate that the distribution of shear cracking on the surface of the web for beam RS-80 was less than that observed in beam R-80, suggesting that the additional strengthening also limited the shear crack formation and propagation in the web. These findings are in agreement with those of previous studies which analysed the effect of CFRP strengthening on concrete beams subjected to impact loading (Erki and Meier, 1999; Tang and Saadatmanesh, 2003). The additional laminates applied to beam RS-80 also prevented the formation of local damage in the region of impact and effectively prevented the debonding of the CFRP applied to the bottom of beam RS-80. In effect, the additional strengthening reduced damage progression in the web of beam RS-80. However, the volume of concrete crushed, in the flange, due to the impact loading applied to beam RS-80 was larger than that observed in any of the other test specimens.

4.2.7.3 Effect of Stirrup Spacing

The damage progression observed in beams R-160 and R-240 can be compared to that of beam R-80 in order to analyse the effect of stirrup spacing. Beam R-160 exhibited similar behaviour in terms of damage progression to beam R-80. Both of these beams failed during the sixth drop test due to crushing of concrete in the compression zone. However, the volume of concrete crushed was less for beam R-160 and the horizontal shear cracking at the flange-web interface was worse in terms of length and thickness. The tests conducted on beam R-240 resulted in very little damage in the compression zone and severe damage at the flange-web interface. Since failure in the compression zone is part of the overall response of the T-beam, the increased stirrup spacing resulted in a reduction in the ability of the T-beam to respond as a whole, due to the lack of composite action between the flange and the web. In the case of beam R-240, this lack of composite action resulted in the complete separation of the top portion of the flange as discussed earlier. The web of beam R-240 exhibited the largest distribution of shear cracks of all the test specimens as indicated in Table 9. In addition to this, seven flexural cracks were observed to propagate to the front face of the web, which is also higher than that observed in the other specimens. The comparatively higher proportion of damage induced in the webs of beams R-160 and R-240

ultimately resulted in the debonding of the CFRP laminates applied to the bottom of the T-beams. Therefore the results suggest that high stirrup spacing, such as the 240mm stirrup spacing of beam R-240, results in low composite action between the flange and the web, which leads to excessive cracking at the flange-web interface and a larger proportion of damage induced in the web. Conversely, low stirrup spacing, such as the 80mm stirrup spacing of beam R-80, results in high composite action between the flange and the web, which enables the beam to respond as a whole.

4.3 Contact Force Response

4.3.1 Introduction

The current evaluation utilises data obtained via the loadcell connected to the drop hammer. The data recorded therefore represents the impulsive force introduced to the simply supported beam system. Figure 55 depicts the contact force response as well as secondary responses due to the rebounding of the drop hammer mass.

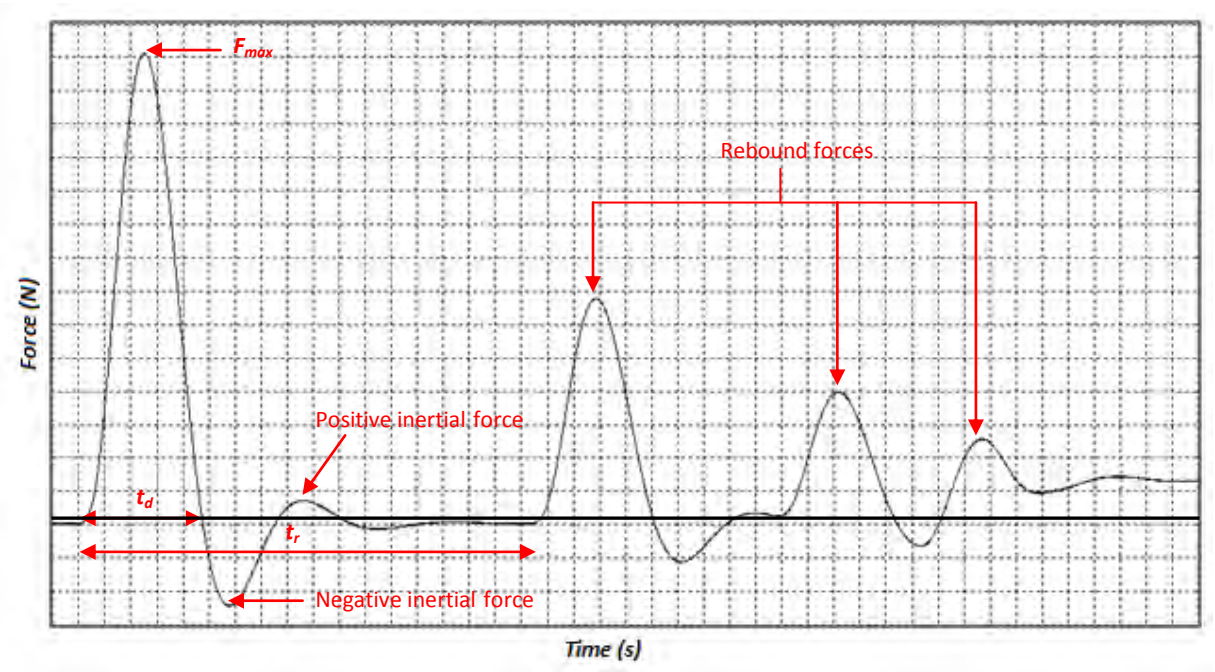

Figure 55: Typical response data obtained via loadcell

The contact force response for a particular drop height is represented by the initial recorded pulse formation. The contact force (F_{max}) corresponds to the amplitude of the initial pulse. The recorded duration of the impact event (t_d) is hence considered to be the duration of the initial pulse. Directly after the impulsive force is recorded the force oscillates between

negative and positive readings before returning to zero. This is attributed to the inertial forces generated after the striker loses contact with the beam and is propelled upwards (generating a negative inertial force) followed by the downward motion of the drop hammer (generating a positive inertial force). The impulsive forces generated by the rebounding of the drop hammer mass are depicted by the positive pulses occurring after the initial pulse as shown in Figure 55.

The recorded contact force represents the dynamic response of the load-cell and the excitation introduced to the simply supported beam system. The output is therefore the response of the system directly after contact is made. The magnitude of F_{max} depends primarily on the impact energy introduced to the system (governed by the drop height, h) as well as the stiffness and the reduced stiffness of the beam due to the consecutive impact tests. Therefore, the magnitude of the applied impact energy is proportionally related to the magnitude of F_{max} provided that the beam maintains its flexural rigidity. This depends on whether or not the applied impact load results in elastic or plastic deformation. If the applied impact load invokes a response that is within the linear elastic range of the beam, the impact energy transforms from kinetic energy into stored strain energy with minimal energy dissipation. However, if the magnitude of the applied impact load results in significant plastic deformation, the flexural rigidity and the capacity of the beam to store strain energy reduces. This then results in a reduction in the proportionality between the impact energy introduced and the contact force recorded. In addition to analysing the relation between impact energy and the contact force, the data obtained during testing also enables the analysis of the relation between the impact energy introduced and the recorded time to rebound (t_r). The time taken to rebound is representative of the strain energy released after impact. An analysis of this relation can provide useful information with regards to the dissipation of energy due to the consecutive impact tests. Therefore, each of the beams will be analysed based on the following relations:

- The relation between drop height, h, and the contact force, F_{max}.
- The relation between drop height, h, and the recorded time taken to rebound, t_r.

4.3.2 Results

Figure 56 below illustrates the contact force response for the patch repaired and CFRP strengthened beam R-80. The contact force response diagrams for the rest of the test specimens are provided in Appendix C, Figures C2 to C4.

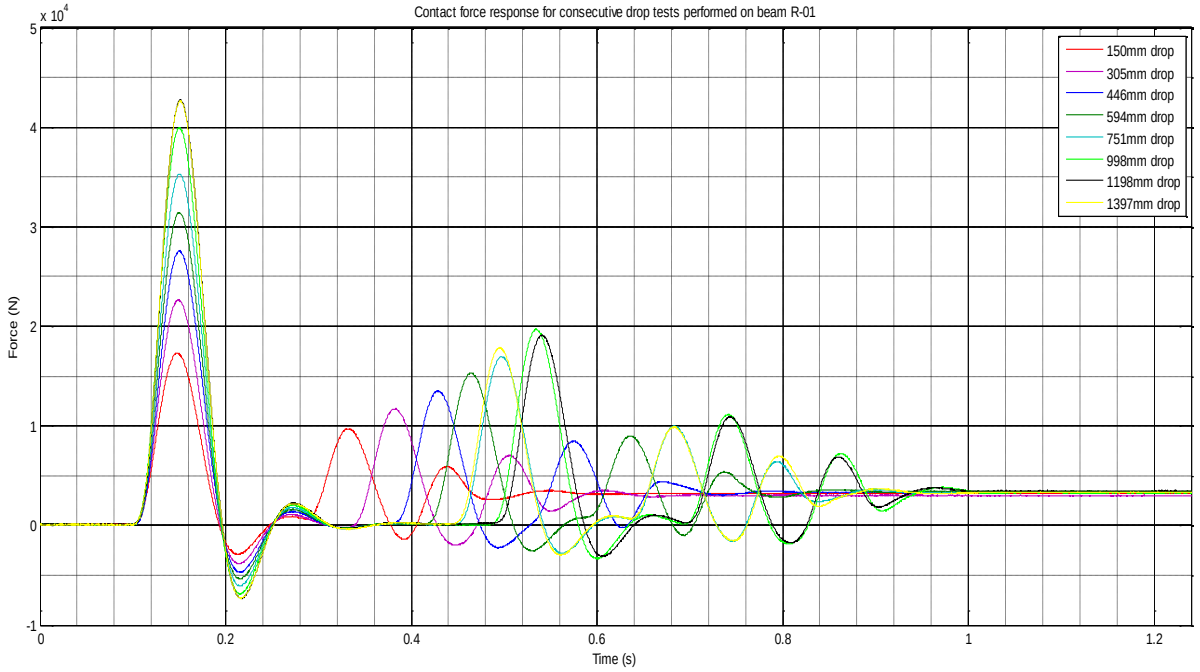

Figure 56: Loadcell response data for beam R-80

These diagrams indicate that the magnitude of the contact force generally increases with an increase in drop height, while the duration of the impulsive force is approximately $t_d \approx$ 0,095s regardless of the test specimen or of the drop height. The relation between the drop height and the maximum contact force for each of the tested beams is shown more clearly in Figure 57. Figure 57 indicates consistency in the the beahviour of the various test specimens. The rate of increase of the maximum contact force with respect to drop height decreases gradually. This can be attributed to the reduction of flexural rigidity within the beams resulting from quasi-plastic deformation incurred during the consecutive drop tests. The progression of damage varied according to the test specimen, as discussed previously. However the plastic deformation can generally be attributed to crack formation and propagation, concrete crushing, and CFRP delamination or debonding (in the case of the repaired and strengthened beams).

Figure 58 graphically indicates the relation between the impact energy introduced to the system (represented by the drop height) and the release of stored strain energy (represented by the time to rebound) for the various test specimens. The results depicted in Figure 58 are consistant with those of Figure 57 in that a noticeable reduction in the slope is observed due to the consecutive impact tests. The reduction in slope indicates the dissipation of strain energy attributed to a loss of flexural rigidity due to increasing plastic deformation.

The general similarity of the results for the various beams can be attributed to the fact that each beam was identical in terms of geometry and the flexural reinforcement provided. However, both Figures 57 and 58 indicate slight differences in the performance of the various test specimens, particularly due to the second half of the conducted drop tests, which can be attributed to the effects of the repair and strengthening materials.

4.3.2.1 Effect of Repair and Strengthening Materials

A comparison can be made between the behaviour of beams R-80, R-160 and R-240 to that of the control specimen, beam C-80. Figure 57 indicates that for similar drop heights the maximum contact forces recorded for beam C-80 are consistently lower than those of the strengthened and repaired beams. Since the magnitude of the contact force is dependent on the impact energy and the flexural rigidity of the beams, the results suggest that the repaired and strengthened beams have higher horizontal flexural rigidity than the control specimen, although this increase in capacity is considered minor. The patch repair concrete used to repair beams R-80, R-160 and R-240 has superior compressive and tensile strength properties than that of the substrate, as has previously been discussed. Additionally the CFRP laminates bonded to the bottom of the T-beams also provide additional resistance to bending providing that the laminates remain bonded to the repair concrete and the substrate. The increase in flexural capacity can therefore be attributed to the combined effect of the patch repair concrete and the CFRP strengthening. This is indicated further by comparing the time to rebound of beam C-80 to that of the other beams. The recorded time to rebound is consistently lower for beam C-80, for every drop test, with the exception of the final drop test. Since the recorded time to rebound is representative of the release of strain energy, the results suggest that the repaired and strengthened beams have a slightly larger capacity to store strain energy until the final drop test. Figure 58 indicates that the

repaired and strengthened beams experience a larger reduction in the recorded time to rebound during the final drop test than that of the control specimen. This is attributed to the high level of energy absorbed during delamination and the resulting loss of flexural rigidity.

4.3.2.2 Effect of Additional Horizontal Strengthening (applied to Beam RS-80)

The contact force response data also provides insight into the overall effect of the additional CFRP laminates bonded to the side of the web of beam RS-80. It has already been stated that the initial drop tests invoked similar responses for each of the repaired and strengthened beams. The final three drop tests however show differences in the performance of beam RS-80. Table 11 shows the recorded maximum contact forces for the final three drop tests for each of the repaired and strengthened beams. For equal impact energies, the results of the final three drop tests indicate that beam RS-80 exhibits the largest recorded contact forces of all the tested beams. The difference is most noticeable during the seventh drop test. This suggests that the application of the additional laminates resulted in an increase in the beams flexural rigidity and the beams capacity to withstand impact loads. This is consistent with findings of previous studies which specifically analyse the effect of externally bonded FRP laminates on the performance of RC beams subjected to impact loading (Erki and Meier, 1999; White et al, 2001; Tang and Saadatmanesh, 2003; Kabir and Shafei, 2009). It is important to note that the effect of the additional CFRP is only noticeable for the final three drop tests. This is due to the high degree of composite action between the flange and the web. The flange initially carried a large portion of the load during the first five drop tests. Once crushing initiated in the flange a large proportion of the load shifted to the additional CFRP laminates bonded to the web. The observed increase in capacity was however short lived due to premature debonding of the additional CFRP laminates during the final drop test. Figures 57 and 58 indicate that the debonding resulted in the largest reduction in contact force as well as the largest reduction in the recorded time taken to rebound of all the tests conducted on all of the beams. After debonding occurred the results recorded for beam RS-80 were closer to that of the other beams. Previous studies have shown that the occurrence of delamination/debonding can be prevented or prolonged by improving the degree of anchorage along the span of a laminate (Erki and Meier, 1999). Therefore the effect of the additional CFRP laminates could have been

enhanced if sufficient anchorage was provided. Even though the premature debonding affected the performance of beam RS-80, the additional laminates were still effective in significantly reducing the damage progression within the web, as previously discussed.

Table 11: Maximum contact forces recorded during final three drop tests

Beam no.	Maximum recorded contact force, F_{max} ,(kN))		
	Drop 6 (***h*** ≈ 1000mm)	Drop 7 (***h*** ≈ 1200mm)	Drop 8 (***h*** ≈ 1400mm)
R-80	39.9	42.73	42.65
R-160	39.8	41.74	43.97
R-240	41	43	43.72
RS-80	41.5	46	44.82

4.3.2.3 Effect of Stirrup Spacing

The damage progression observed in beams R-160 and R-240 can be compared to that of beam R-80 in order to analyse the effect of stirrup spacing. There seems to be very little difference in the behaviour of each of these beams with respect to the rate of increase of the maximum contact force after successive drops, or the rate of increase of the recorded time to rebound. This suggests that under consecutive impact loading the contact force response is independent of the amount of shear reinforcement. The similarity in the decay of the contact force observed in beams R-80, R-160 and R-240 implies that the degree of energy dissipation is also independent of the amount of shear reinforcement. However, the proportion and form of damage observed in the flange or the web is dependent on the degree of composite action between the flange and the web, which is dependent on the amount of shear reinforcement provided as discussed previously.

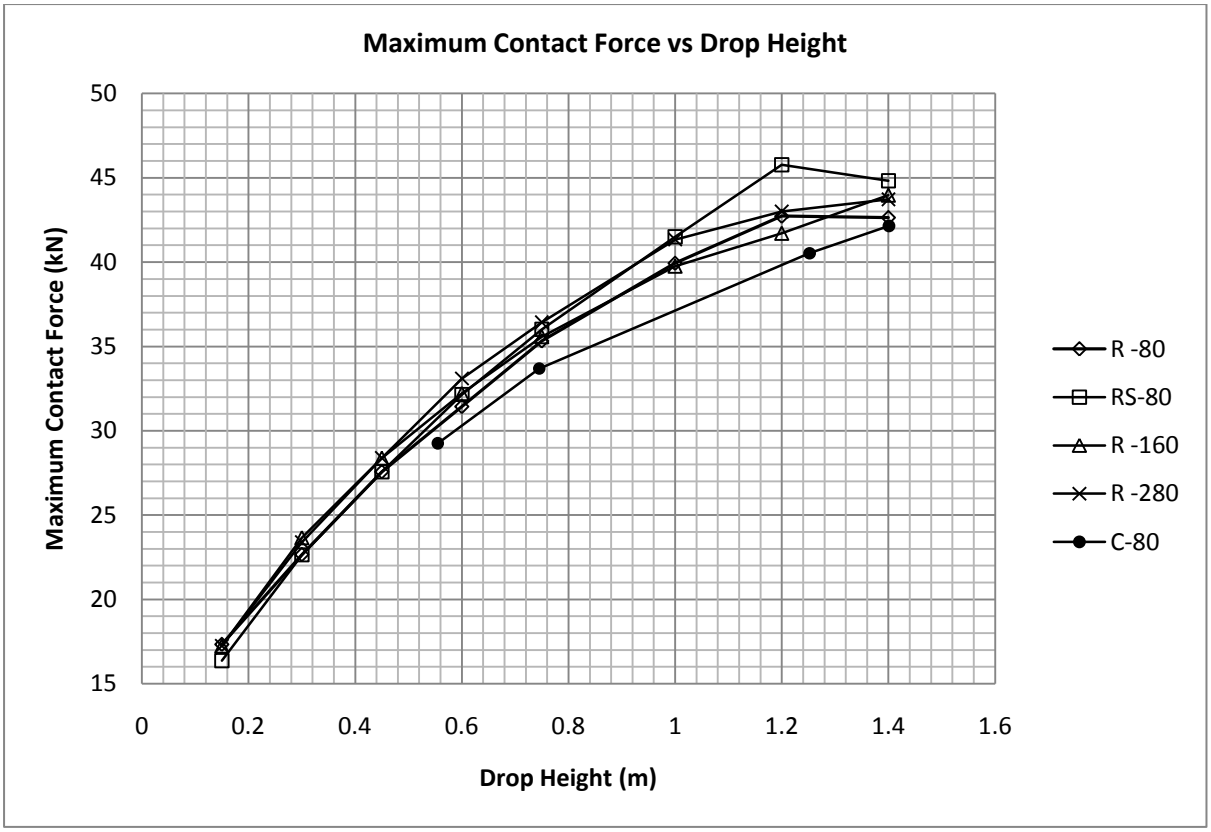

Figure 57: Contact force versus drop height

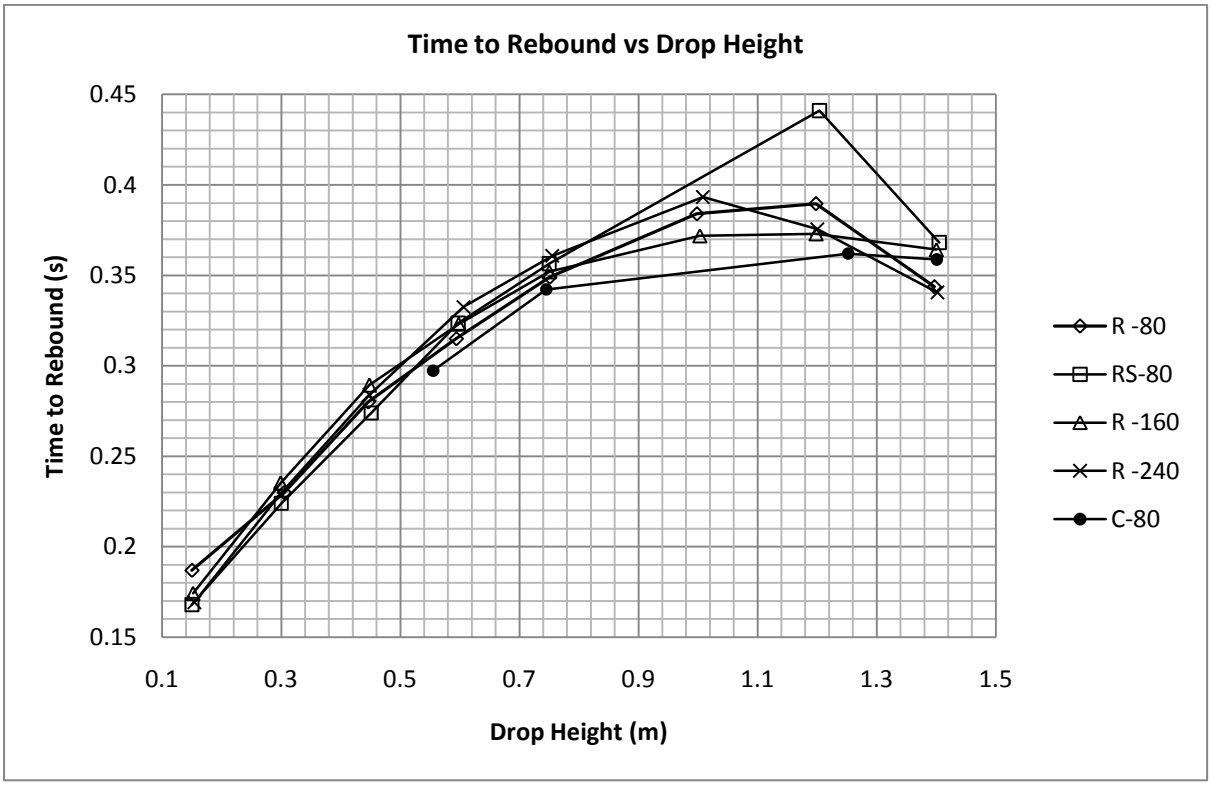

Figure 58: Time taken to rebound versus drop height

4.4 Deflection Response and Deterioration of Stiffness

4.4.1 Introduction

The deflection response data was obtained through detailed analysis of the high speed camera footage. This was done through the scaled tracking of the beams at midspan. Figure 59 illustrates a typical response of a simply supported beam subjected to low velocity impact loading. Limitations of the available equipment made it impossible to record the entire deflection response as depicted in Figure 59. However, the high speed camera footage enabled the determination of the maximum deflection and the duration of the initial deflection half cycle. Residual deflection was also recorded with a laser distance sensor and was confirmed using the high speed camera footage. The data captured is indicated in red on Figure 59.

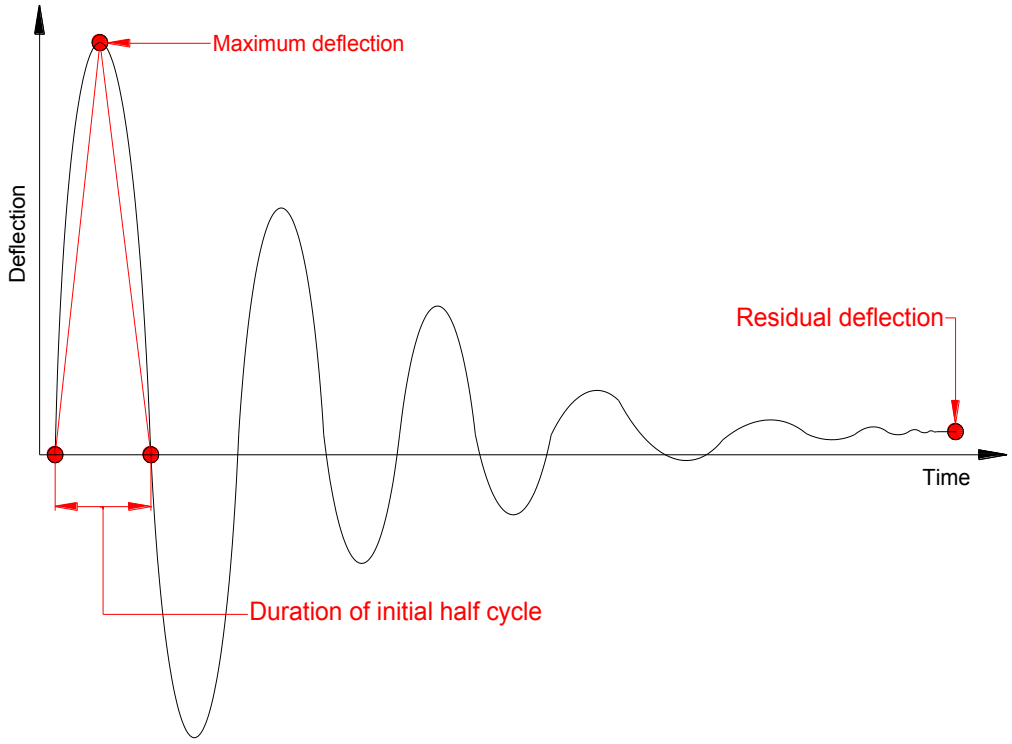

Figure 59: Typical deflection response (data captured by HSC indicated in red)

Deflection response data was only obtained for the four repaired and strengthened beams (such data was not obtained for the control beam, C-80). Therefore the analysis in this section will concentrate on the behaviour of the repaired and strengthened beams alone. The maximum deflection and residual deflection can provide insight into the effects of the

additional strengthening applied to beam RS-80 as well as the effects of the varying stirrup spacing within beams R-80, R-160 and R-240. The duration of the initial deflection halfcycle will provide insight into the performance of the repaired and strengthened beams with regards to stiffness. This will be discussed further by analysing the maximum deflection results in conjunction with the contact force results.

4.4.2 Results: Deflection Response

Figure 60 below shows the deflection response data for beam R-80. The diagrams for the rest of the repaired and strengthened beams are provided in Appendix D, Figures D1 to D3. Table D1 in Appendix D is a summary of the contact force and deflection results obtained. The general behaviour of each beam indicates an increase in maximum deflection and the duration of the initial halfcycle due to an increase in drop height. Figure 61 is a comparison of the maximum deflections of the various beams from varying drop heights. The results indicate that the increase in maximum deflection is roughly linear. The initial drops result in similar maximum displacements recorded for all beams, however noticeable differences can be observed during the final drop tests. Since deflection is largely dependent on beam stiffness, the similarity in the initial recorded displacement is attributed to the fact that the beams have identical longitudinal reinforcement and therefore should have identical flexural resistance. The differences in the recorded displacement, due to the second half of the consecutive drop tests, are therefore attributed to variations in the reduction of stiffness for the various beams due to variations in damage progression.

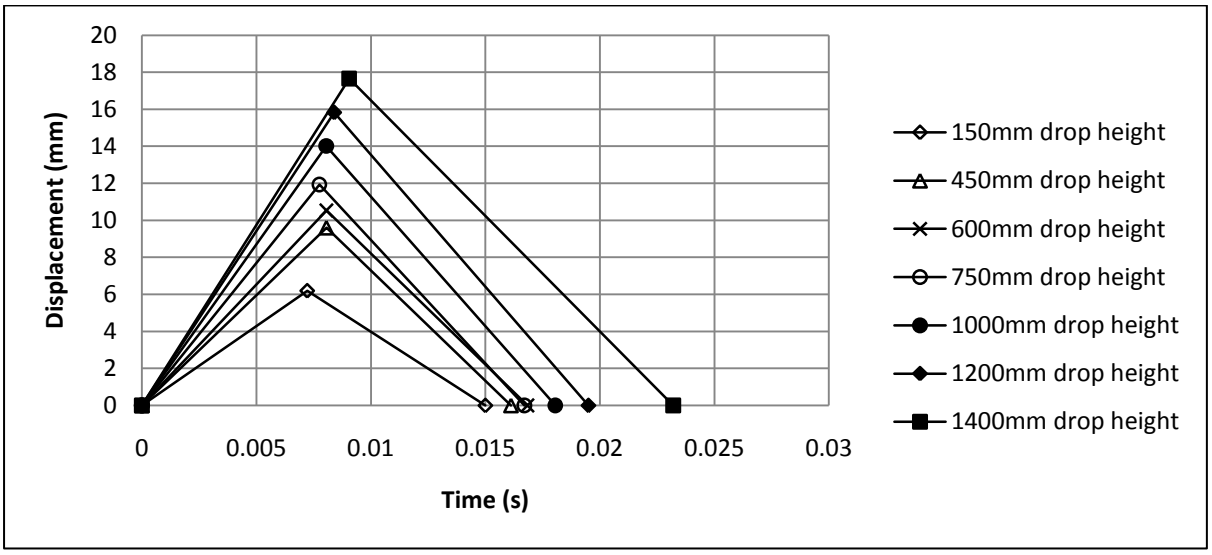

Figure 60: Deflection halfcycle data for beam R-80

Figure 62 shows the cumulative residual deflection for each of the repaired and strengthened beams due to the consecutive drop tests. Residual deflection depends on beam stiffness, material properties, the magnitude of the impact introduced and the extent of the damage observed as a result of the impact (Tang and Saadatmanesh, 2003). Residual deflection was observed after every drop test for each of the repaired and strengthened beams. This includes the first two drop tests during which visible cracks were mostly not detected on the beam surfaces. The initial residual deflection is therefore attributed to the presence of micro-cracking. The beams initially exhibit similar behaviour; however differences in residual deflection are noticeable due to the second half of the conducted drop tests.

4.4.2.1 Effect of Additional Horizontal Strengthening (applied to Beam RS-80)

An initial comparison can be made between the results obtained for beams R-80 and RS-80 to provide insight into the effects of the additional strengthening applied to the web of beam RS-80. Figure 61 shows that the maximum deflection recorded for both beams are similar. However, the final two drop tests resulted in higher displacement readings for beam RS-80. This could be attributed to a loss of stiffness due to the debonding of the additional laminates during the final drop test. It is also worth mentioning that the magnitude of the deflection is partly dependent on the magnitude of force introduced. Since the contact forces recorded for beam RS-80 observed during to the final three drop tests, were larger than that of beam R-80, this could also explain the larger deflections recorded for beam RS-80. Figure 62 indicates that contrary to the maximum deflection results, the cumulative residual deflection of beam RS-80 is consistently lower than that of beam R-80 or of beams R-160 and R-240. This suggests that the additional CFRP laminates applied to beam RS-80 had the effect of reducing residual deflection.

4.4.2.2 Effect of Stirrup Spacing

Figure 61 indicates clear differences in both beams R-160 and R-240 as compared to beam R-80, in that the maximum deflection is noticeably larger due to the second half of the consecutive drop tests. Beam R-240, having the largest stirrup spacing (240mm spacing between stirrups), shows the highest deflection of all the beams once sufficient damage is incurred. The difference in the magnitude of the deflection between beams R-240 and R-80 is initially noticeable as a result of the fifth drop test. At this stage beam R-240 had

undergone significant flexural damage and shear damage in the flange and the web as well as significant cracking at the flange-web interface as previously discussed (see Figure B4, Appendix B). After the fifth drop test the difference in magnitude intensified consistently. The maximum deflections recorded for beam R-160 were slightly less than beam R-240, however, greater than that of beam R-80. Beam R-160 deviates from the behaviour of beam R-80 as a result of the sixth drop test. This is also attributed to an increase in severity of the damage incurred due to the sixth drop test (see Figure B3, Appendix B). The results therefore suggest that larger stirrup spacing results in larger deflections once the beam has been sufficiently damaged. For beams with large stirrup spacing such as beam R-240, this occurs earlier due to excessive shear cracking and horizontal shear cracking along the flange-web interface. Figure 62 indicates that stirrup spacing also affects the magnitude of the residual deflection. Beam R-240 experienced the largest residual deflection of all the repaired and strengthened beams, which is once again reflective of the severity of the damage incurred within beam R-240. The residual deflection recorded for beam R-160 is, however, slightly lower than that of beam R-80 with the exception of the final drop test.

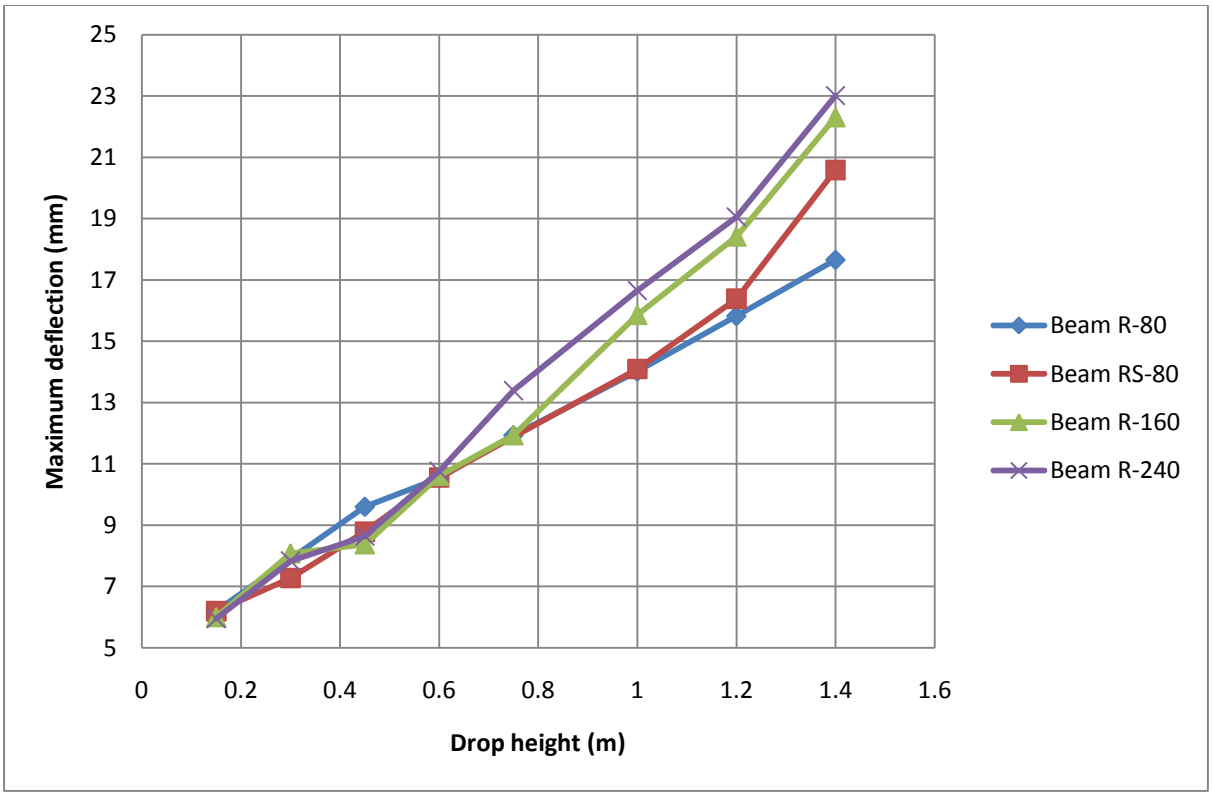

Figure 61: Maximum midspan deflection versus drop height

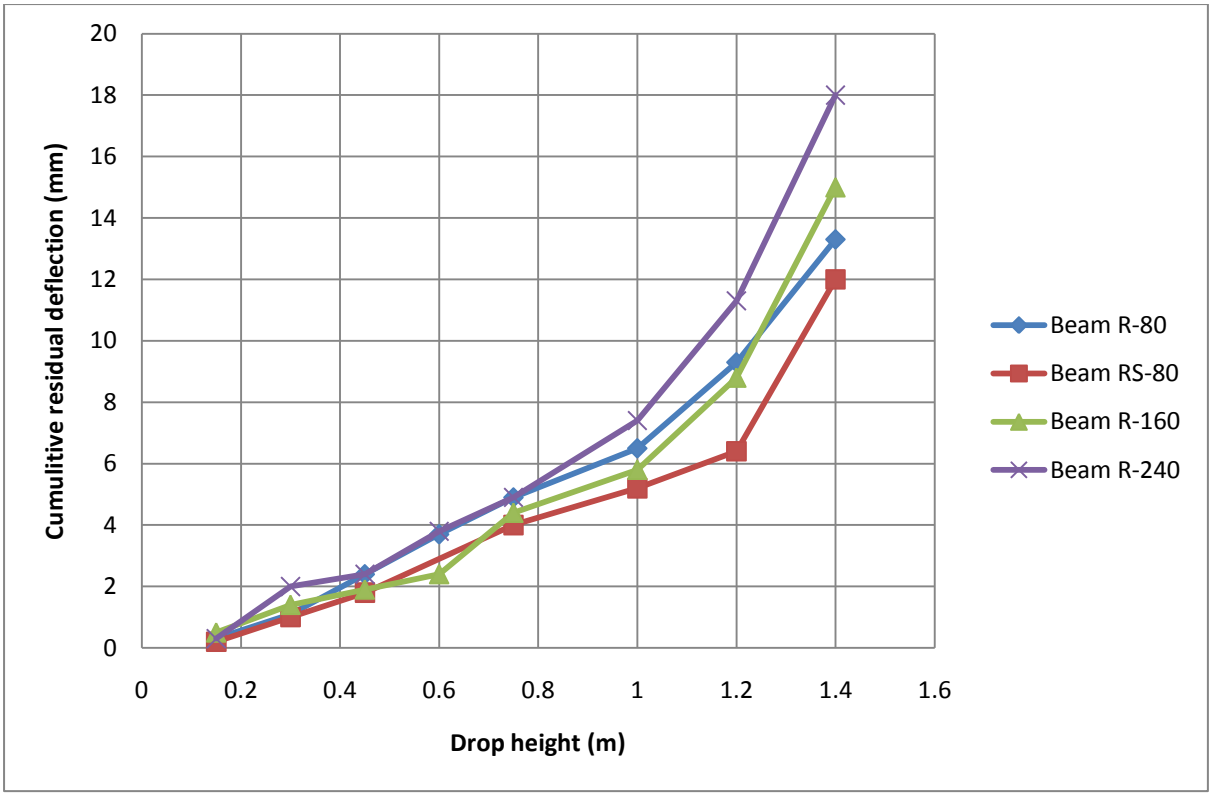

Figure 62: Cumulative residual deflection versus drop height

4.4.3 Deterioration of Stiffness

The increase in deflection and residual deflection is dependent on the reduction of stiffness after successive drop tests. An analysis of the comparative deterioration of stiffness within the repaired and strengthened beams can be accomplished by analysing the extent to which these beams resist deflection in response to the applied contact forces. Figure 63 shows the contact force versus deflection results of the repaired and strengthened beams. The changes in slope of the curves depicted in Figure 63 reveal information about the deterioration of stiffness. Traditionally the period of vibration and the natural frequency of a beam can be used to analyse damage progression and possible reductions in stiffness. Limitations in the available equipment did not enable the recording of the entire period of vibration. However the duration of the initial deflection halfcycle was determined using the high speed camera footage and can therefore also be used to analyse the deterioration of stiffness due to successive impact loads. The results depicted in Figure 64 confirm previous findings in that the initial stiffnesses of the beams are similar due to identical longitudinal reinforcement. Once the beams have been sufficiently damaged the slopes of the curves decrease, thus representing a reduction in the capacity of the beams to withstand impact.

4.4.3.1 Effect of Additional Horizontal Strengthening (applied to Beam RS-80)

The initial similarity of the slopes on the Figure 63 for beam RS-80 and R-80 suggests that the additional laminates applied to beam RS-80 did not increase the stiffness of the beam during the first five drop tests. Both beams experienced crushing in the compression zone during the six drop test. It was previously found that despite the damage incurred during the final drop tests, the rate of increase of the contact force of beam RS-80 remained consistent until debonding of the additional laminates occurred. After the crushing initiated, a large proportion of the load shifted to the additional laminates. The laminates therefore maintained the stiffness of beam RS-80 during the seventh drop test. Figure 63 clearly indicates that beam RS-80 had the highest load bearing capacity of all the beams. The load bearing capacity ultimately reduced due to the debonding of the additional laminates.

Figure 64 illustrates the growth of the halfcycle duration after successive drop tests. The results are consistent with the force versus deflection findings. Beams R-80 and RS-80 show similar increases in halfcycle duration, thereby confirming the similarity in their stiffness. The effect of the additional laminates can be seen during the stages when the duration of the halfcycle for beam RS-80 lies under that of beam R-80.

4.4.3.2 Effect of Stirrup Spacing

Figure 63 also indicates clear differences in stiffness deterioration due to the effects of the different stirrup spacing. The slopes of the curves for beams R-160 and R-240 depict similar reductions in stiffness. Beam R-80 maintains a steeper slope than beams R-160 and R-240 until the final drop test. This therefore suggests that higher stirrup spacing results in a faster deterioration of stiffness due to a higher severity of damage resulting from the consecutive impact loads.

Figure 64 indicates that both beams R-160 and R-240 have consistently higher halfcycle durations than that of beam R-80, particularly due to the second half of conducted drop tests. This confirms the previous findings which suggest that higher stirrup spacing results in faster deterioration of stiffness due to a higher severity of damage.

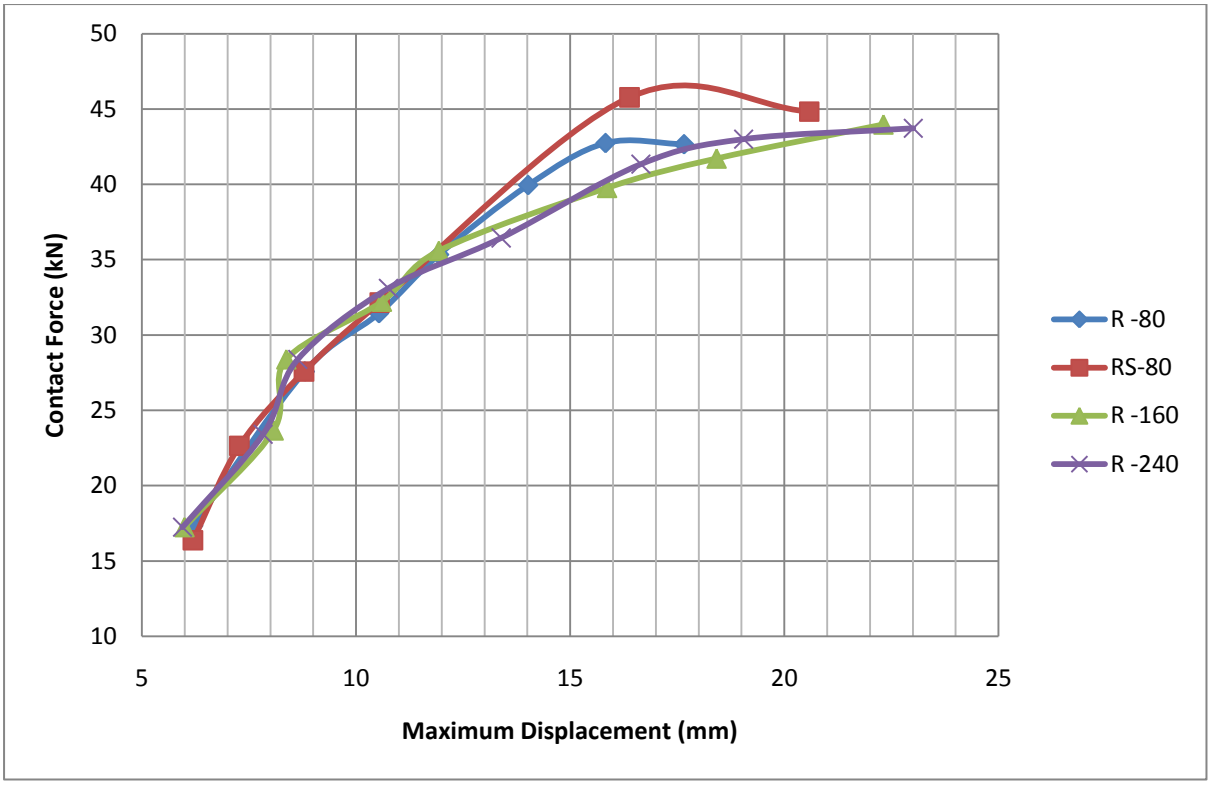

Figure 63: Contact force versus maximum midspan deflection

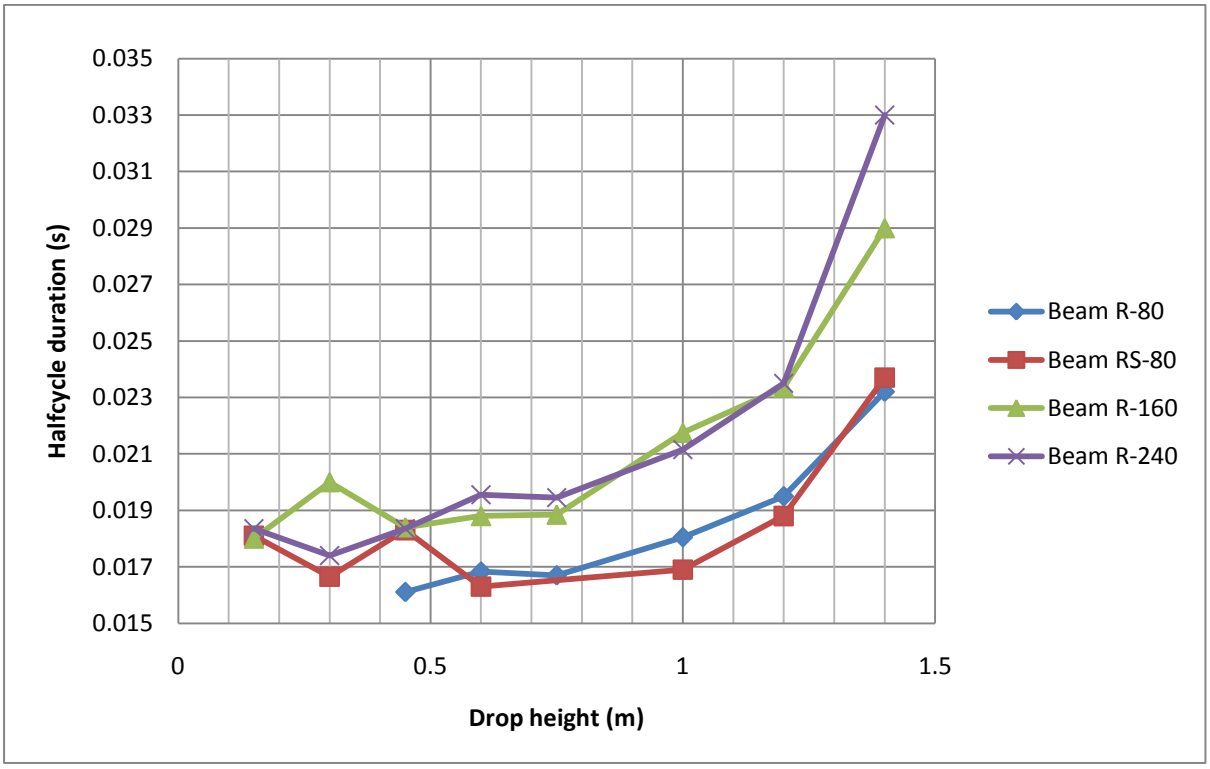

Figure 64: Deflection halfcycle duration versus drop height

5 Chapter 5: CONCLUSIONS

The current experimental study was conducted in order to investigate the behaviour of patch repaired and CFRP strengthened RC T-beams, under consecutive transverse impact loading. In addition to this, the effect of stirrup spacing on impact behaviour was analysed. The study was conducted on five RC T-beams with identical dimensions and longitudinal reinforcement, and varying stirrup spacing. Four of the beams were mechanically damaged at midspan, repaired with patch repair mortar and strengthened with CFRP laminates. The remaining beam was kept as a control specimen. The T-beams were simply supported on their sides and subjected to consecutive, transverse, impact loading applied to the web at the midspan of each beam. T-beams were specifically selected in order to simulate the bridge beam-deck interaction, where the flange of the T-beam is analogous of the deck and the web is analogous of the beam.

Prior to testing, four of the five test specimens were intentionally damaged through the exposure and grinding of the bottom reinforcing bars to a depth of approximately 4.8mm which correlates to 25% loss of cross-sectional area in the bottom tensile reinforcement. A cementitious patch repair mortar was used to repair each of the damaged beams and a CFRP laminate was bonded across the bottom of the T-beams to provide strengthening.

The experimental design was successful in acquiring the relevant data to validate the objectives of the dissertation. The data captured during the consecutive impact tests enabled the successful analysis of damage progression in each of the specimens as well as the successful recording of the contact force response and the displacement response.

5.1 Impact testing

Consecutive impact loading was induced on the sides of the T-beam specimens from varying drop heights. The beams were repeatedly impacted on their sides in order to analyze the behaviour of the test specimens as damage intensified. The impact loading was induced via a drop hammer impact machine. The beams were simply supported through the provision of a custom made support system that prevented uplift during impact without inducing restraint moments.

5.1.1 The objectives of the consecutive impact tests

- Capture damage progression and dynamic response of each test specimen.
- Determine the effects of the repair and strengthening materials on the damage progression and the dynamic response.
- Determine the effects of additional lateral strengthening, applied to the web, on the damage progression and the dynamic response.
- Determine the effect of stirrup spacing on the damage progression and the dynamic response.

All of the above mentioned objectives were achieved

5.1.2 Conclusions drawn based on research objectives

5.1.2.1 Effect of repair and strengthening materials

The patch repair mortar and the CFRP strengthening behaved well under consecutive impact loading. No cracking was observed to form along the interface between the repair mortar and the substrate thus indicating that the epoxy adhesive, used to facilitate adequate bond strength at the repair interface, provided a continuous bond and did not have a noticeable effect on the damage progression.

The integrity of the bond between the CFRP laminate applied to the bottom of the T-beams was observed to be dependent on the extent of the damage induced in the webs of the T-beams. Beams R-160 and R-240 displayed high levels of damage in their webs. Consequently the laminates applied to beams R-160 and R-240 failed during the final drop test due to bond splitting failure initiating at the centre of the beams.

Additionally, imperfections in the epoxy adhesive bond between the CFRP laminate and the concrete surface may result in premature laminate peeling failure at the location of the imperfection as was observed during the seventh impact test conducted on beam R-80.

The repaired and strengthened beams were also observed to have greater capacity to withstand consecutive impact loading, although this increase in capacity is considered minor. This is evident since the maximum contact forces observed in the control beam, C-80, was consistently lower than that of the repaired and strengthened beams with the exception of the final drop test. The slight increase in capacity is attributed to the combined

effect of the patch repair concrete (which has superior tensile and compressive strengths than the substrate) and the CFRP laminates. The repaired and strengthened beams were also observed to have a slightly higher capacity to store strain energy after consecutive drop tests. This is evident since the time taken to rebound, t_r, of the control specimen was found to be consistently lower than that of the repaired and strengthened beams.

5.1.2.2 Effect of horizontal strengthening (applied to beam RS-80)

The additional laminates bonded to the side of beam RS-80 effectively reduced the propagation and widening of flexural cracks into the web of the T-beam and prevented the formation and propagation of diagonal shear cracks on the impacted surface after successive drop tests. However, beam RS-80 also experienced a larger proportion of damage in the compression flange. Therefore the additional strengthening reduced damage in the web and increased the transfer of damage into the flange.

The additional laminates also prevented the delamination of the CFRP applied at the bottom of the T-beam for flexural strengthening. This is attributed to the reduced proportion of damage observed in the web.

The capacity of beam RS-80 to withstand impact loading was observed to increase only after significant plastic damage had been induced, which was observed to take place during the sixth drop test. This is evident since beam RS-80 exhibited the largest recorded contact forces of all the tested beams during the sixth and seventh drop tests before delamination occurred during the eighth drop test. The delayed effect of the additional CFRP laminates is attributed to the high degree of composite action between the flange and the web of the T-beam. The flange initially carried a large portion of the load during the first five drop tests. Once crushing initiated in the flange, during the sixth drop test, a large proportion of the load shifted to the additional CFRP laminates bonded to the web.

The additional laminates were observed to effectively reduce residual deflection upon the onset of severe plastic deformation. However, the maximum displacements observed in beam RS-80 were slightly larger than that of beam R-80. This is attributed to the larger contact forces associated with beam RS-80.

The additional CFRP laminates also resulted in increased stiffness properties between the fifth and the eighth drop tests. This is evident since beam RS-80 exhibited the shortest halfcycle durations of all the tested beams. Additionally, the results indicate that beam RS-80 exhibited the longest durations of the 'time taken to rebound', t_r, of all the tested beams during the sixth and seventh drop tests. This therefore suggests that the laminates enabled beam RS-80 to maintain its ability to store strain energy due to the additional stiffness provided by the additional laminates.

All of these improvements were however short-lived due to delamination of the additional laminates observed during the eighth drop test. The provision of anchorage systems for the additional CFRP laminates could result in further enhancement of the T-beam performance under impact loading. Such anchorage would supplement the epoxy bonding and prevent or delay the occurrence of delamination failure.

The increase in capacity and stiffness as well as the reduced residual deflections and the reduced damage observed in the web of beam RS-80 shows the potential for using CFRP as a means of energy absorption in bridge beams susceptible to transverse vehicular impact loading. Such a system would involve the bonding of CFRP laminates to the interior sides of vulnerable bridge beams. The additional horizontal strengthening could be effective in reducing damage and transverse deflection in the beam. Additionally the laminates could act as an effective energy absorber and increase the capacity of the bridge beam to withstand transverse impact loading. The additional laminates could also reduce the risk of bridge beam misalignment which is evident due to the reduced residual deflection observed in beam RS-80. Finally additional horizontal CFRP strengthening can be applied as a means of protecting CFRP laminates applied for conventional flexural strengthening purposes, from delamination during transverse vehicular impact. However, since the testing of beam RS-80 led to a large proportion of damage induced in the compression flange, impact loading on a bridge beam with horizontal strengthening could possibly result in an increase in the proportion of damage transferred to the deck-slab.

5.1.2.3 Effect of stirrup spacing

The stirrup spacing was observed to affect the damage mechanisms observed in the T-beams as well as the degree of composite action between the flange and the web of the T-

beams. Low stirrup spacing, such as the 80mm stirrup spacing of beam R-80, resulted in a large proportion of crushing in the compression flange with low levels of shear cracking and flexural cracking propagating into the web. Since a large proportion of the damage was transferred to the compression flange, the low stirrup spacing was observed to facilitate high composite action between the flange and the web. Conversely, high stirrup spacing, such as the 240mm stirrup spacing of beam R-240, resulted in low composite action between the flange and the web, which led to excessive cracking at the flange-web interface and a large proportion of damage induced in the web (both beams R-160 and R-240 displayed the highest concentrations of flexural cracks and shear cracks developing and propagating into the web). The beams with high stirrup spacing exhibited a lower proportion of damage in the compression flange.

The stirrup spacing was also observed to affect the failure mechanism of the CFRP laminate system applied to the bottom of the T-beams. Beams R-160 and R-240, were the only beams to experience bond splitting failure of the CFRP laminate applied to the bottom of the T-beam (as opposed to the laminate peeling observed in beam R-80). This is attributed to the comparatively high concentration of flexural and shear cracking observed in the webs of beams R-160 and R-240.

The contact force response due to the consecutive impact tests was observed to be similar irrespective of the stirrup spacing. This was however not the case for the deflection response. It was observed that larger stirrup spacing resulted in larger maximum deflections once sufficient plastic damage had been incurred. Beam R-240 exhibited higher maximum deflections than beam R-80 from the fifth drop test and the difference in magnitude intensified consistently. Beam R-160 exhibited higher maximum deflections than beam R-80 from the sixth drop test onwards. However, the maximum deflections recorded for beam R-160 were consistently less than that of beam R-240. The residual deflections were also observed to increase with increasing stirrup spacing.

Increased stirrup spacing was also observed to result in an earlier deterioration of stiffness due to consecutive impact loading. This is evident since the deflection halfcycle duration of beams R-160 and R-240 were observed to be consistently higher than that of beam R-80 with the difference intensifying continuously after successive drop tests.

Based on these observations, certain inferences can be made pertaining to the repair and strengthening of RC bridge beams which have been damaged due to transverse vehicular impact.

The observations made suggest, firstly, that stirrup/connector spacing can affect the proportion of damage induced in the beam and the deck-slab of a bridge. Beams with high stirrup/connecter spacing are likely to experience a lower degree of composite action between the beam and the deck-slab which would result in a greater proportion of damage in the beam as well as a greater possibility of reduced transverse stiffness in the beam. Beams with low stirrup/connector spacing may not experience the same degree of damage; however the high composite action between the deck-slab and the beam may result in a larger proportion of damage transferred to the deck-slab which could affect the transverse stiffness of the deck-slab. Damage assessment should therefore consider the effects of stirrup spacing on the damage mechanisms in the deck-slab as well as the beam.

Additionally the larger residual deflections observed in the T-beams with high stirrup spacing can be likened to an increase in susceptibility of bridge beam misalignment in the case of transverse vehicular collision. This would suggest that bridge beams with higher stirrup/connecter spacing have an increased susceptibility to misalignment.

5.2 Recommendations for future study

On the basis of the findings and conclusions, the following recommendations for future research are proposed;

- The use of laser type LVDT's to capture the midspan deflection would result in the capturing of the entire deflection response. This would enable a better understanding of the stiffness deterioration of the tests specimens.
- Additional loadcells at the support regions will enable the capturing of the reaction force response, which would enable an analysis of the stress wave propagation resulting from the applied impact, and energy absorption during the impact event.
- The same testing procedure could be conducted on beams with different repair mortars. This could provide additional insight into the effects of varying materials on the performance under transverse impact loading.

- Alternative FRP layouts could be considered to investigate possible enhancement of energy absorption and concrete confinement during testing.
- A wider range of stirrup spacing would result in an increase in the number of available test samples, therefore increasing the amount of data collected.
- Instead of casting the T-beam monolithically, the web and the flange could be cast separately using different concrete mix designs in order to further simulate the interaction between a bridge beam and deck-slab.
- The same tests could be conducted on beams with prestressed tendons in order to determine the additional effect of prestress on damage propagation and the dynamic response.
- A comparative study could be conducted between beams strengthened with CFRP and beams strengthened with steel plates.
- An in depth FEM analysis could be conducted in order to provide a better understanding of the damage mechanisms and failure modes.

References

Adhikary, S.D. Li, B. Fujikake, K. "Dynamic behaviour of reinforced concrete beams under varying rates of concentrated loading" *International Journal of Impact Engineering*, 2012: 24-38.

Bakis, C. E. Banks, L. C. Brown, V. L. Cosenza, E. Davalos, J. F. Lesko, J. J. Machida, A. Rizkalla, S. H. and Triantafillou, T. C. "Fibre-Reinforced polymer composites for construction-State-of-the-art review." *American Institute of Civil Engineers, 150th anniversary paper, 2002*

*Balaguru, P. "*FRP Composites for Reinforced and Prestressed Concrete Structures". New York: Taylor & Francis, 2009.

Beushausen, H. Alexander, M. "Fultons Concrete Technology." Midrand: Cement & Concrete Institute, 2009.

Bischoff, P.H. and Perry, S. H. "Compressive Behaviour of Concrete at High Strain Rates." *Materials and Structures*, 1991: 425-450.

Brara, A. and Klepaczko, J.R. "Experimental characterization of concrete in dynamic tension." *Mechanics of Materials*, 2006: 253-267.

Buyukozturk, O. "Failure behaviour of FRP bonded concrete affected by interface fracture." *National Science Foundation*, 2005.

Caprino, G. Lopresto, V. Scarponi, C. Briotti, G. "Influence of material thickness on the response of carbon fabric/epoxy panels to low velocity impact." *Composites Science and Technology*, 1999: 2279-2286.

Chen, J.F. Teng, J.G. "Shear Capacity of Fibre-Reinforced Polymer Strengthened Reinforced Concrete Beams: FRP Rupture." *Journal of Structural Engineering*, 2003: 615-625.

Cusatis, G. "Strain-rate effects on concrete behaviour." *International Journal of Impact Engineering*, 2011: 162-170.

Erki, M. A. and Meier, U. "impact loading of concrete beams externally strengthened with CFRP laminates." *Journal of Composites for Construction*, 1999: 117-124.

Fujikake, K. Li, B. Soeun, S. "Impact response of reinforced concrete beams and its analytical evaluation." *Journal of Structural Engineering*, 2009: 938-949.

Hollaway, L.C. "A review of the present and future utilisation of FRP composites in the civil infrastructure with reference to their important in-service properties." *Construction and Building Materials*, 2010: 2419-2445.

Hughes, G. and Beeby, A.W. Investigation of the effect of impact loading on concrete beams."*The Structural Engineer*, 1982: 45-52

Kabir, M.Z. and Shafei, E. "Analytical and Numerical Study of FRP Retrofitted RC Beams Under Low Velocity Impact." *Transaction A: Civil Engineering*, 2009: 415-428.

Keller, Thomas. "Use of Fibre Reinforced Polymers in Bridge Construction." Zurich: IABSE, 2003.

Kishi, N. Ikeda, K. Mikami, H. Yamaguchi, E. "Dynamic Behaviour of RC Beams under Steel Weight Impact Loading—Effects of Nose-shape of Steel Weight," *Proceedings of 3rd Concrete under Severe Conditions, Environments and Loading*, Vancouver, BC, Canada, 2001: 660-667.

Kim. Y.J., Green, M.F., Fallis, G.J. "Repair of Bridge Girder Damaged by Impact Loads with Prestressed CFRP Sheets." *Journal of Bridge Engineering*, 2008: 15-23.

Kulkarni, S.M. Shah, S.P. "Response of reinforced concrete beams at high strain rates." *ACI Structural Journal*, 1998: 705-715

Malver, L.J. and Crawford, J.E. "Dynamic increase factors for steel reinforcing bars", *Procedings from the 28th Department of Defence Explosives Safety Board*, Orlando, Florida, 18-19 Aug. 1998.

Mutsuyoshi, H. Machida, A. "Properties and failure of reinforced concrete members subjected to dynamic loading." *Transactions of the Japanese Concrete Institute*, 1984: 521-528

Norris, C.H. *Structural Design for Dynamic Loads.* Massachusetts: McGraw-Hill, 1959

Pajak, M. "Influence of the strain rate on the strength of concrete taking into account the experimental techniques." *Architecture Civil Engineering Environment*, 2011: 77-86

Reid, S. R. and Zhou, G. "Impact behaviour of fibre-reinforced composite materials and structures." Cambridge: Woodhead Publishing Ltd, 2000.

Ryall, M. "Bridge Management." Oxford: Butterworth-Heinemann, 2001

Saacti, S. and Vecchio, F. J. "Effects of shear mechanisms on impact behaviour of reinforced concrete beams." *ACI Structural Journal*, 2009a: 78-86

Sangi, A. J. "Reinforced concrete structures under impact loads." Unpublished Phd thesis. *Heriot-Watt University*, 2011

Snowy Mountain Engineering Corporation (SMEC), 2007, Photographs, viewed March 2014

Tachibana, S. Masuya, H. Nakamura, S. "Performance based design of reinforced concrete beams under impact." *Natural Hazards and Earth Systems Sciences*, 2010: 1069-1078.

Taljsten, B. and Elfgren, L. "Strengthening concrete beams for shear using CFRP-materials: evaluation of different application methods." *Composites Part B: Engineering*, 2000: 87-96.

Taljsten, B. *FRP Strengthening of Existing Structures.* Lulea: Lulea University of Technology, 2006.

Tang, T. and Saadatmanesh, H. "Behaviour of concrete beams strengthened with fibre-reinforced polymer laminates under impact loading." *Journal of Composites for Construction*, 2003: 209-218

Thabet, A. and Haldane, D. "Three-dimensional numerical simulation of the nonlinear response of reinforced concrete members subject to impact loading." *ACI Structural Journal*, 2000: 689-702.

Tigeli, M. "Effect of Structural Repair and Strengthening and Ultimate Capacity of Corrosion-Damaged RC Beams." Cape Town: University of Cape Town, 2010.

Vaysburd, M.A. "Holistic system approach to design and implimentation of concrete repair." *Cement & Concrete Composites*, 2006: 671-678.

Waheed, A. Kowel, E. Loo, T. "Repair manual for concrete bridge elements." Alberta: Infrastructure and Transportation, 2005

White, T. W. Soudki, K. A. Erki, M. A. "Response of reinforced concrete beams strengthened with CFRP laminates and subjected to high rates of loading." *Journal of Composites for Construction*, 2001: 153-162.

Zobel, R.S., Carrasquillo, R.L., Fowler, D.W. "Repair of impact damaged prestressed bridge girder using a variety of materials and placement methods." *Construction and Building Materials*, 1999: 319-326.

Chhabra, Y. "Photo 4 – External post tensioning" Photograph, viewed 16 February 2014,

<http://structuralretrofit.net.au/?page_id=272>

"Structural strengthening" n.d. Photograph, viewed 20 October 2013,

<http://www.sika.com/en/solutions_products/sika-markets.html>

APPENDIX A

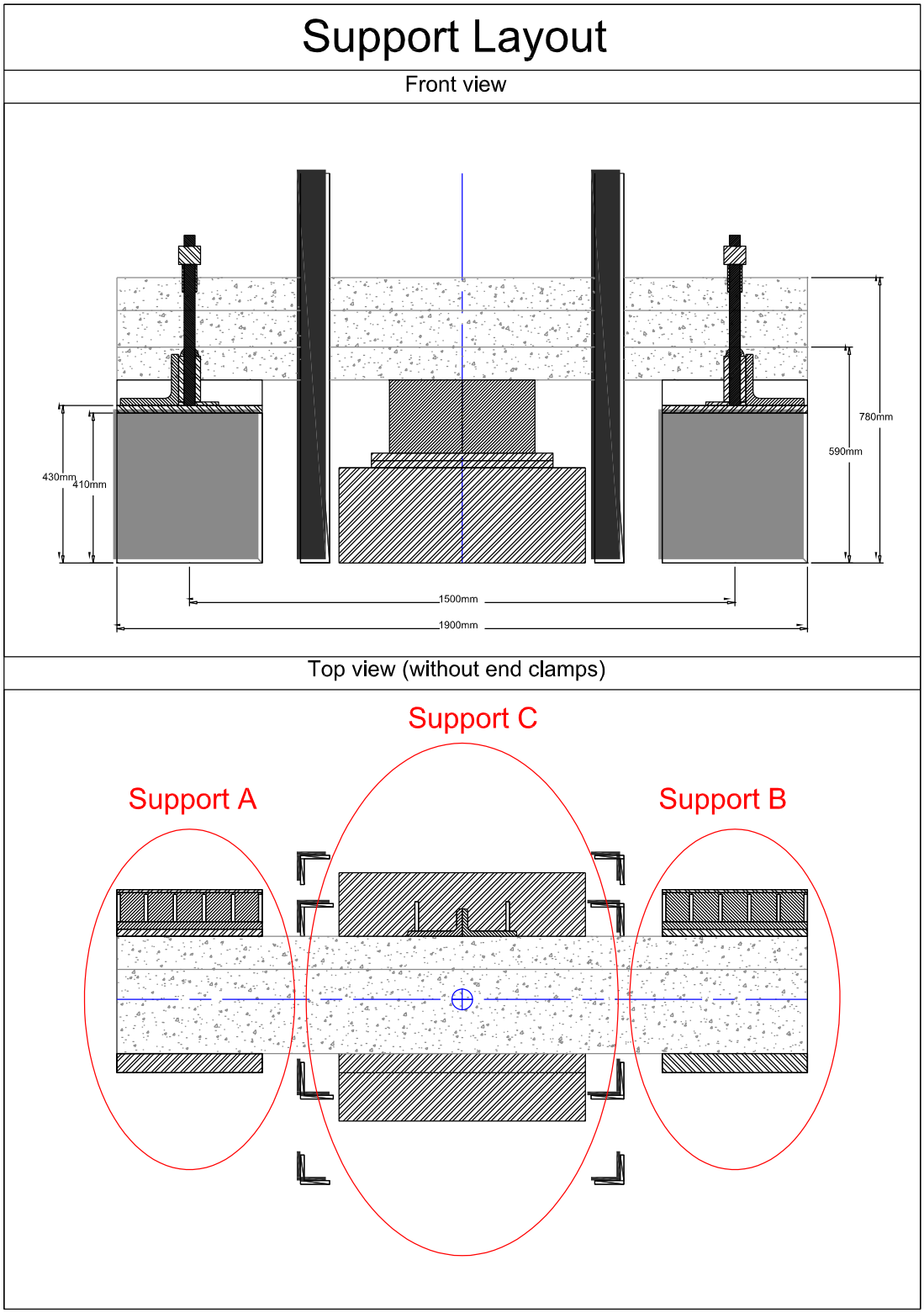

Figure A1: Design drawings for support system, front view and top view

Support A & B overview

Side view

Side view: Steel element details

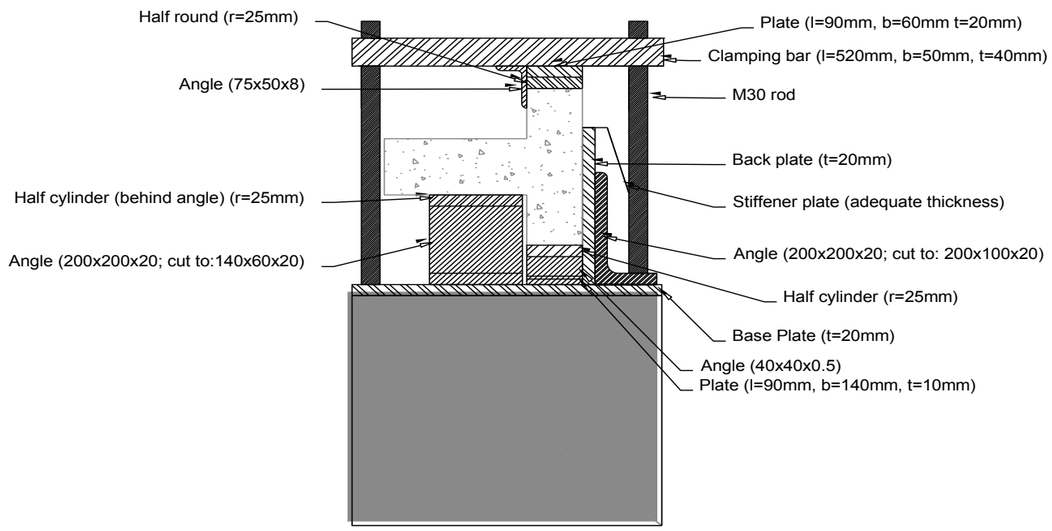

Side view: Relevant dimensions

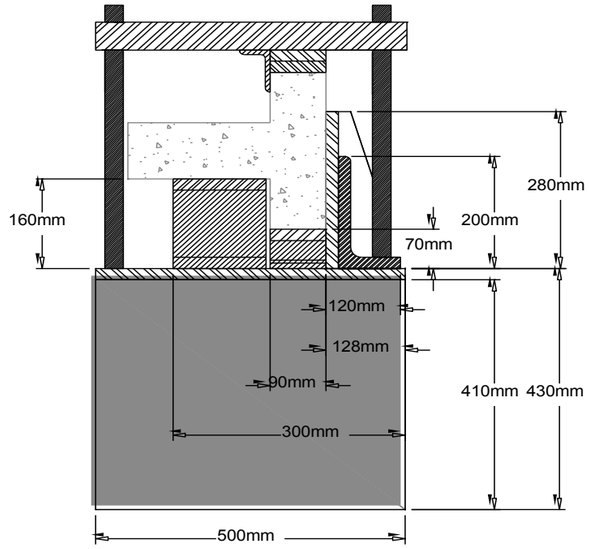

Front view

Front view: Without clamp for clarity

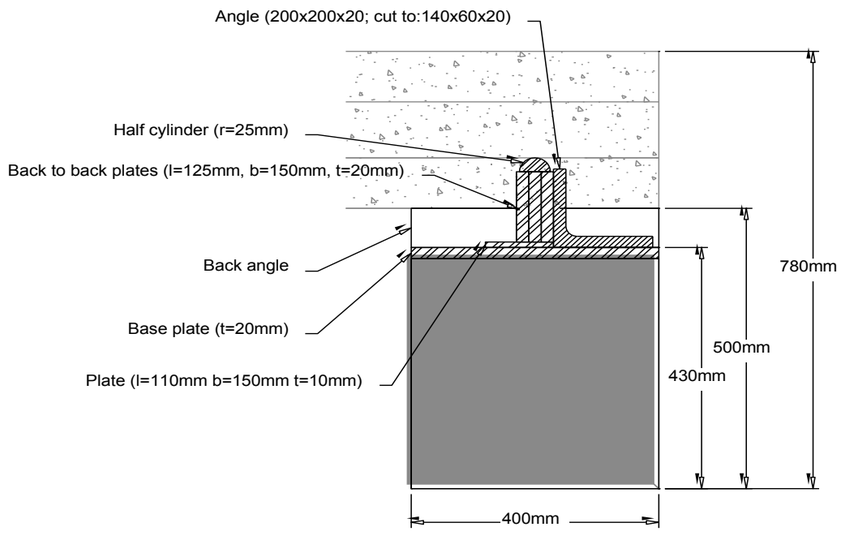

Front view: With clamp

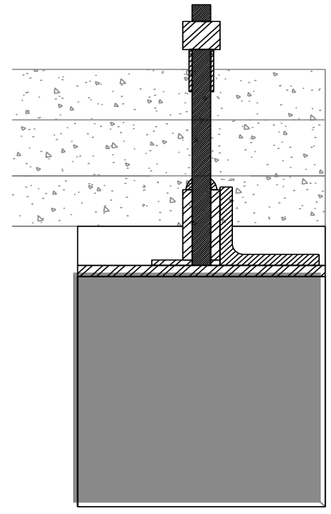

Figure A2: Design drawings for support system, side support

Support C

Front view

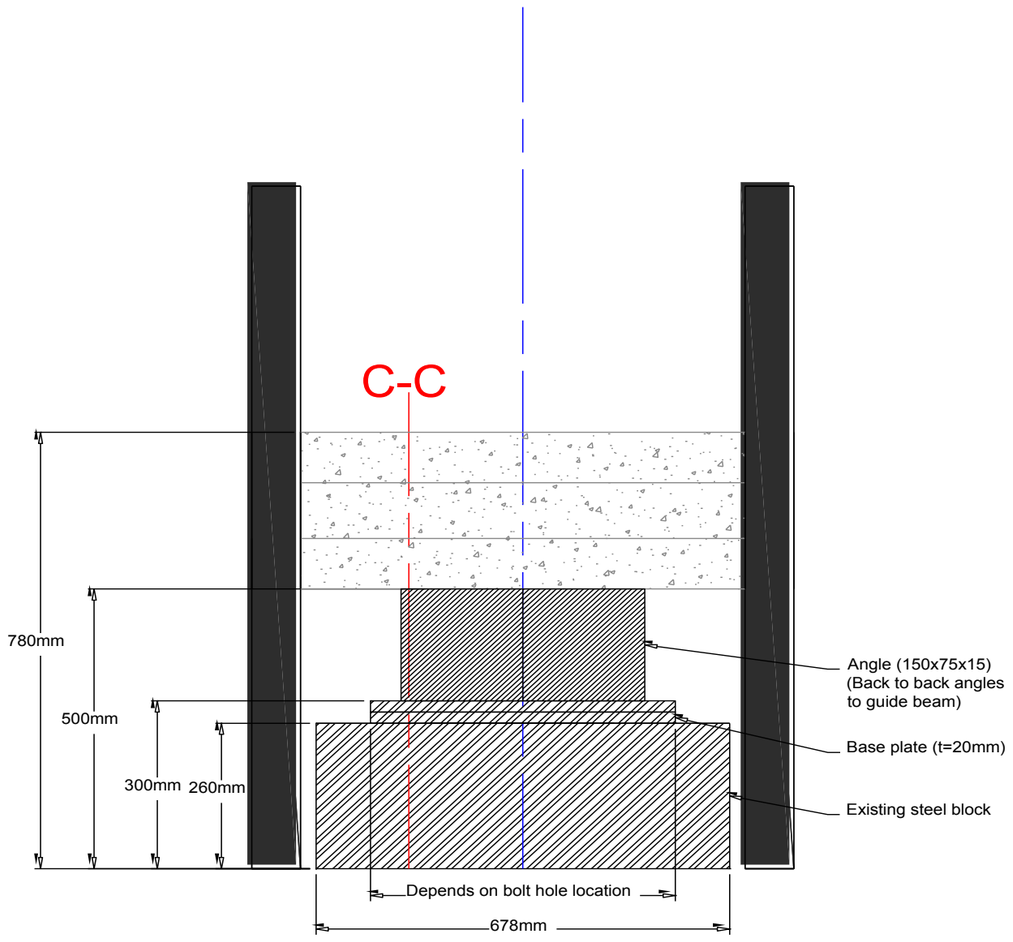

Side view

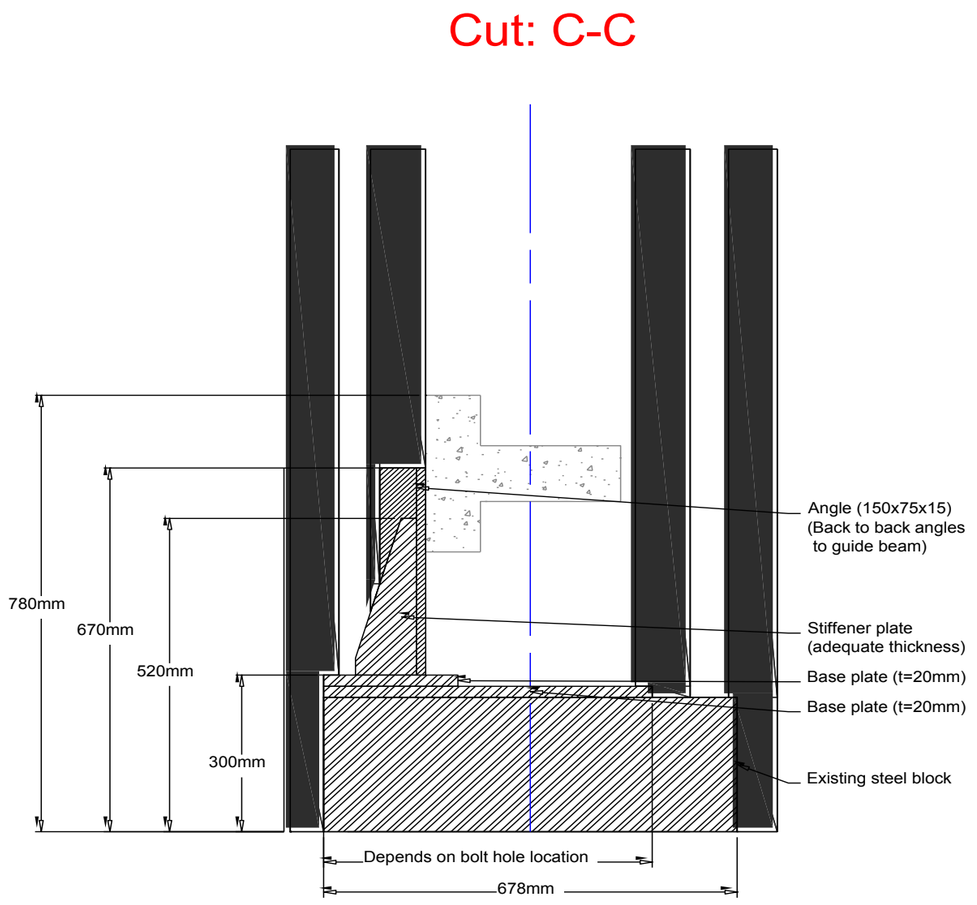

Figure A3: Design drawings for support system, middle support

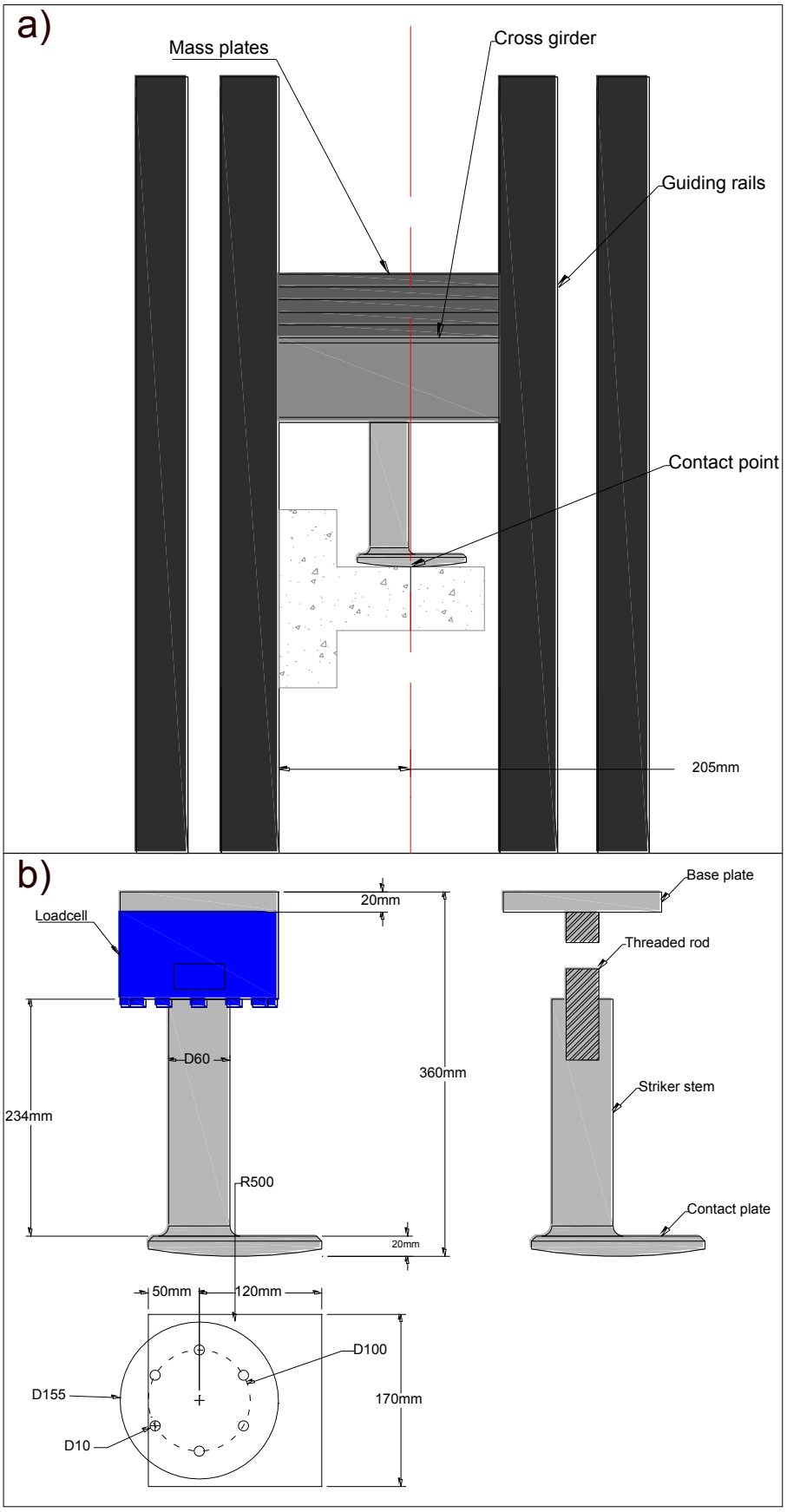

Figure A4: Design drawings for support system, middle support

Appendix B: Progression of Damage

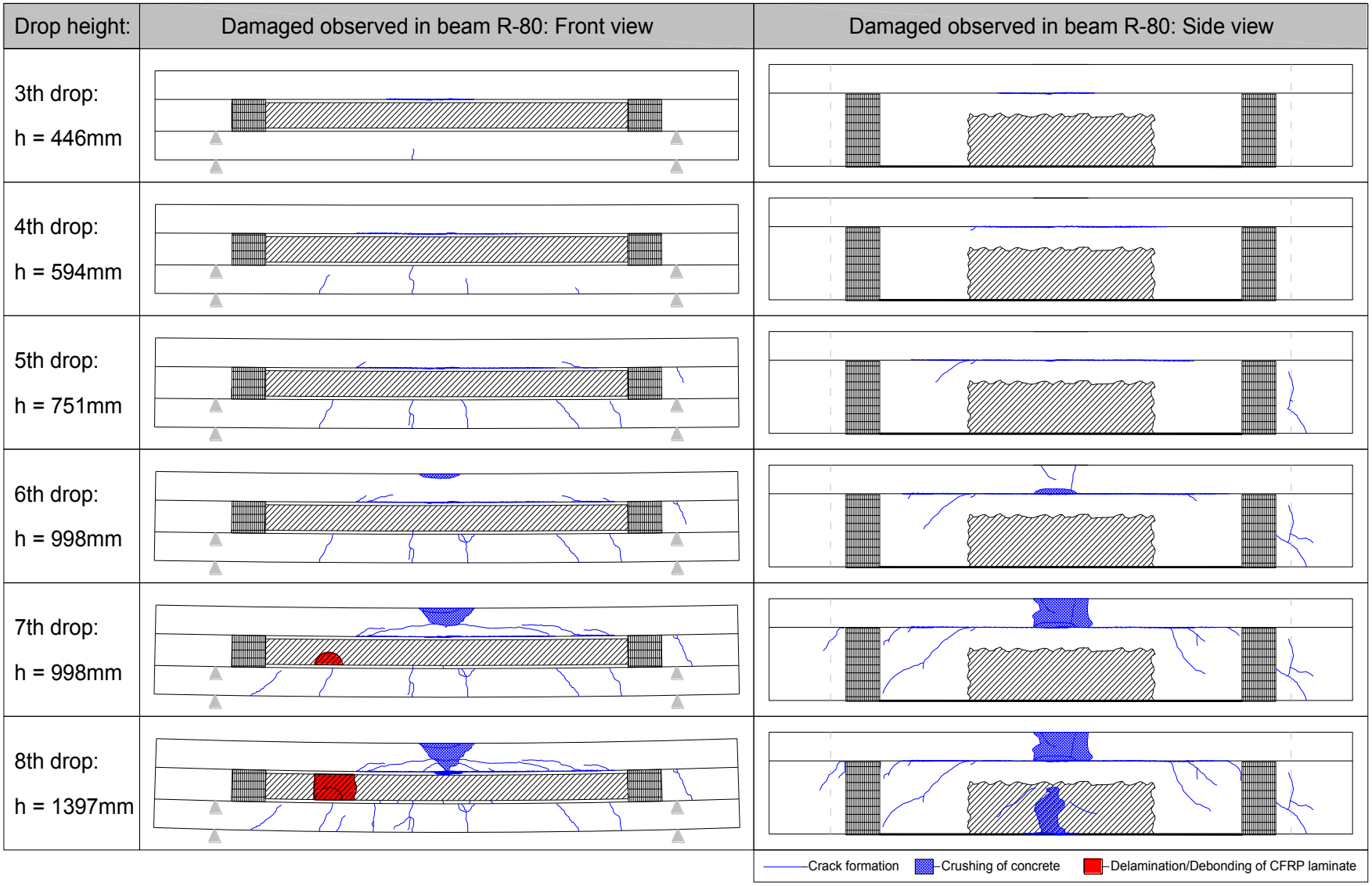

Figure B1: Progression of damage observed in beam R-80

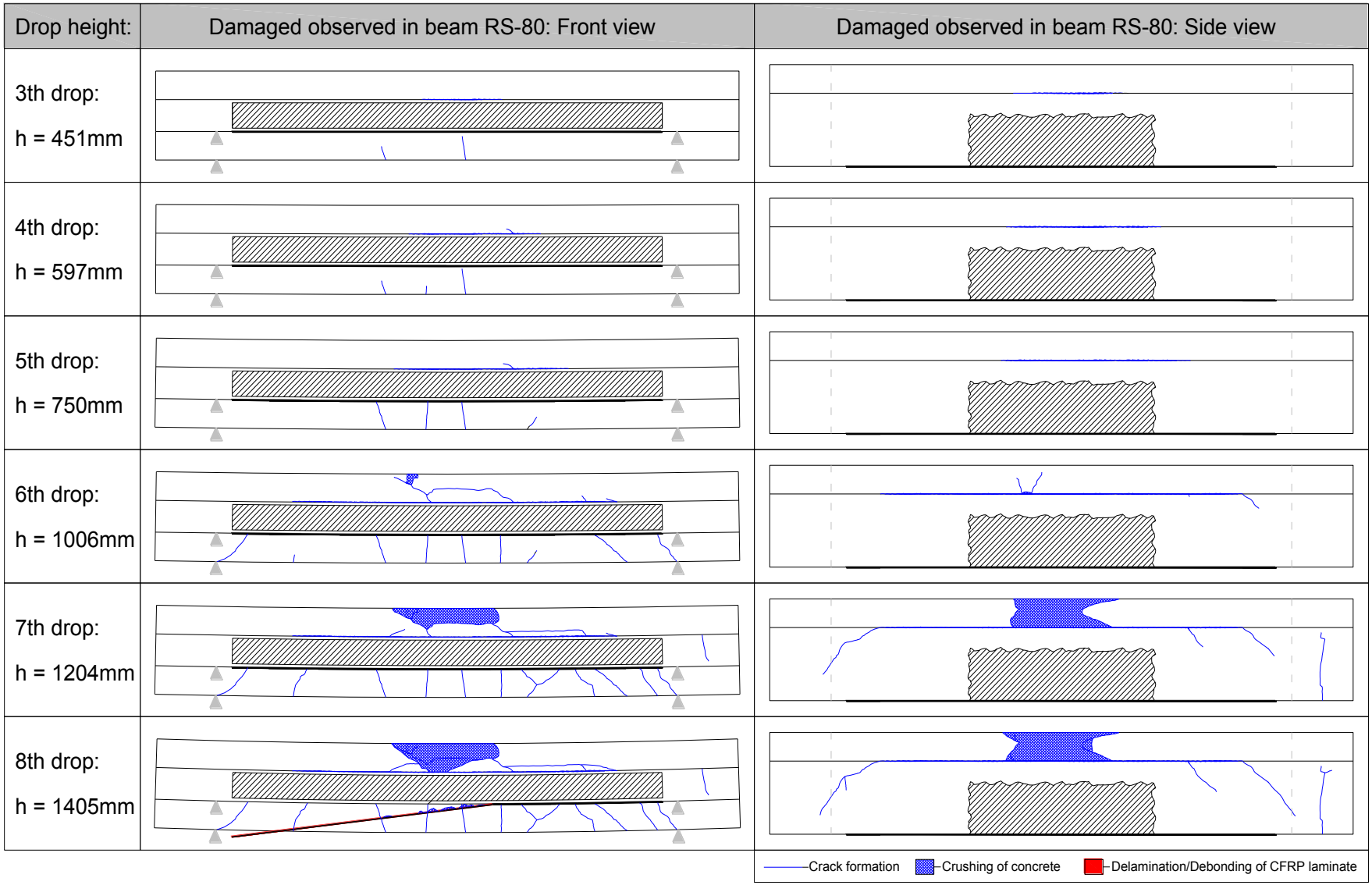

Figure B2: Progression of damage observed in beam RS-80

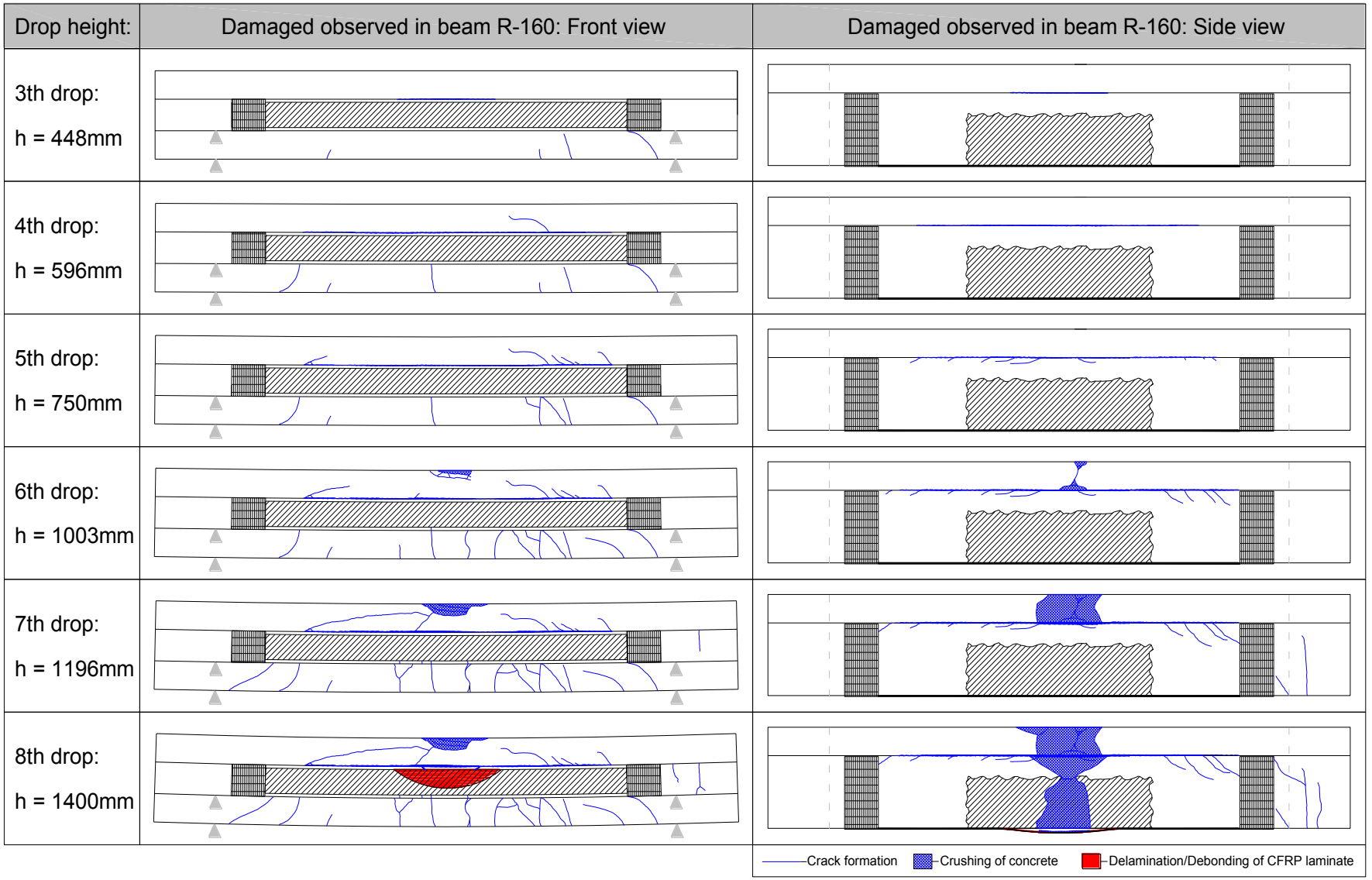

Figure B3: Progression of damage observed in beam R-160

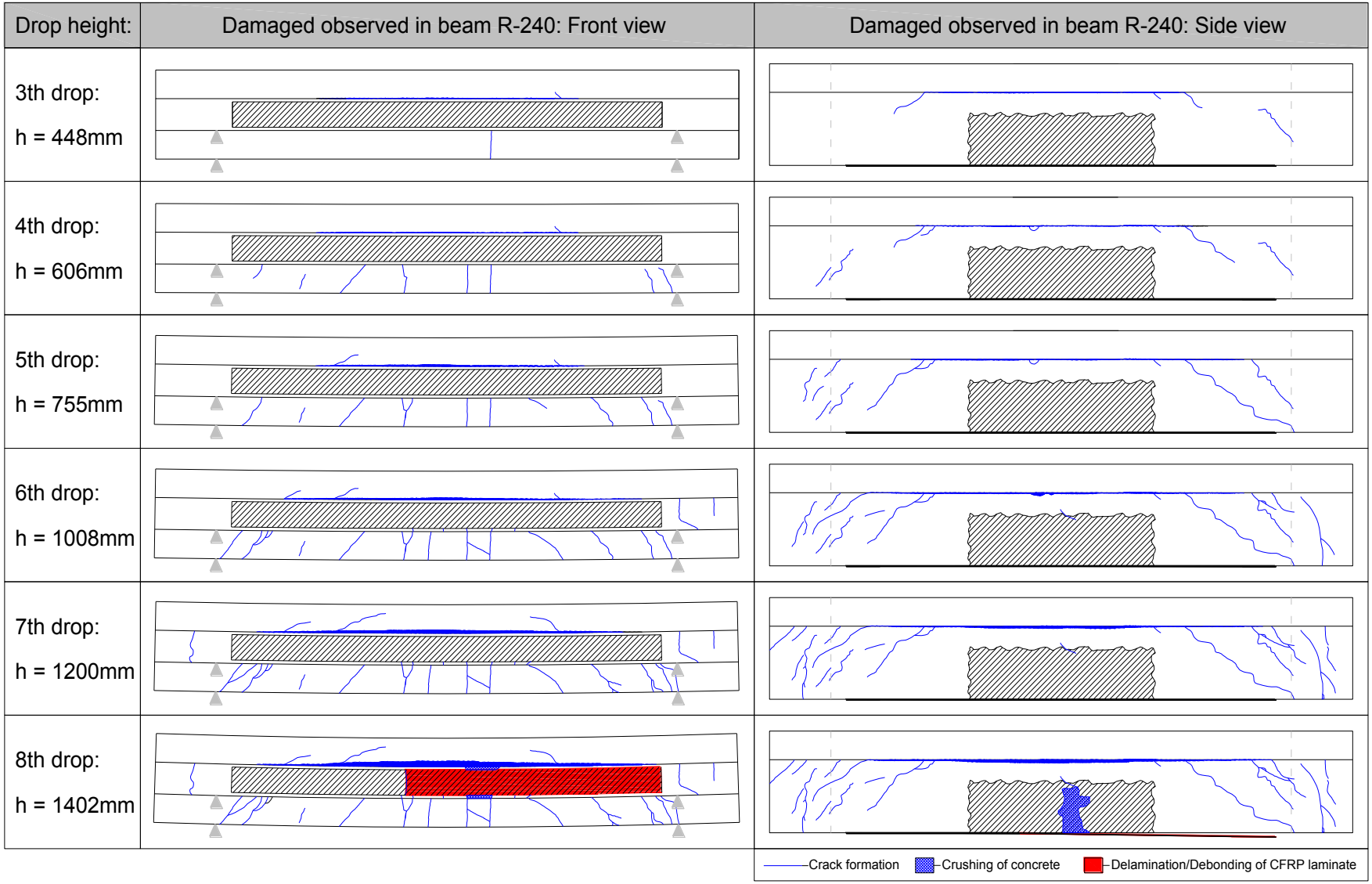

Figure B4: Progression of damage observed in beam R-240

Figure B5: Damage observed after consecutive drop tests conducted on beam C-80

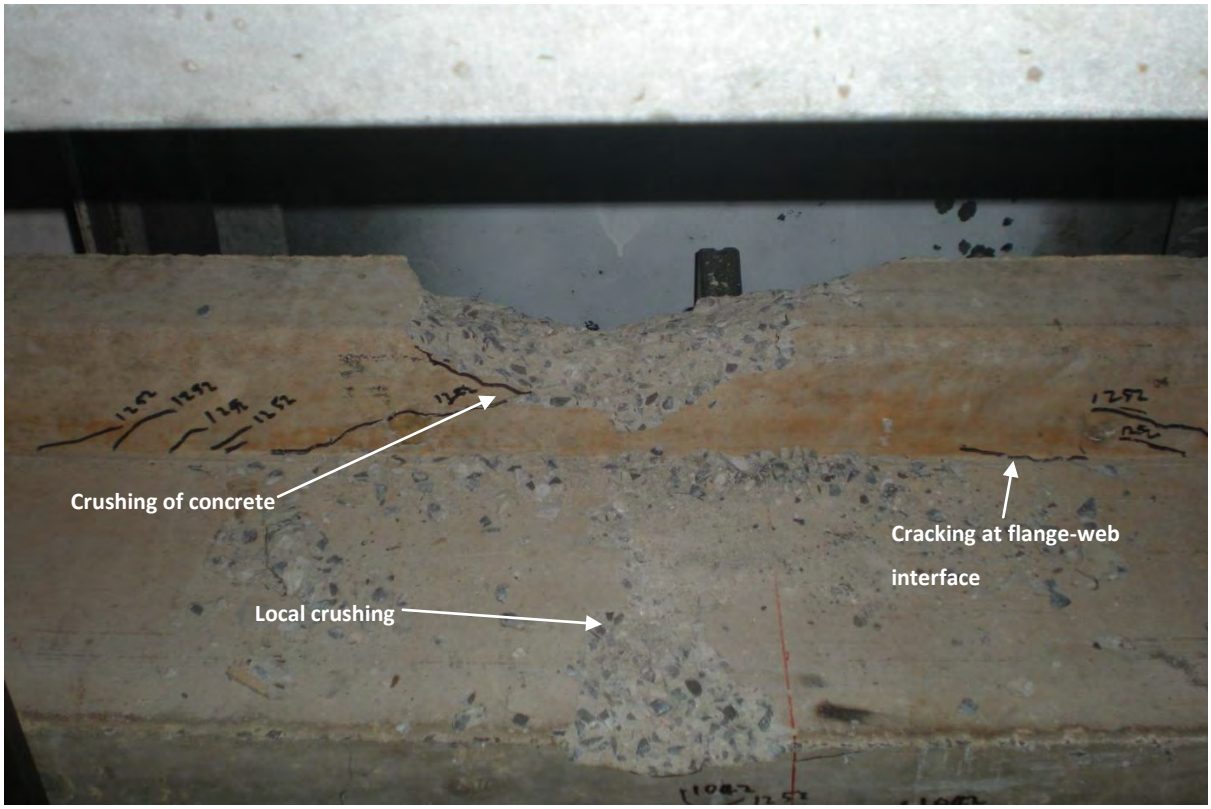

Figure B6: Compression damage and local damage (beam C-80)

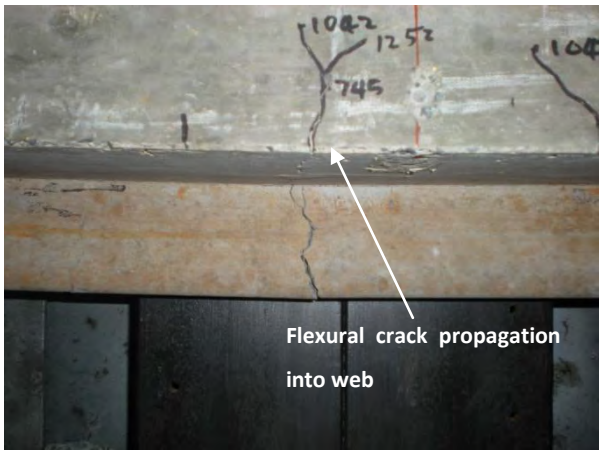

Figure B7: Flexural crack propagation

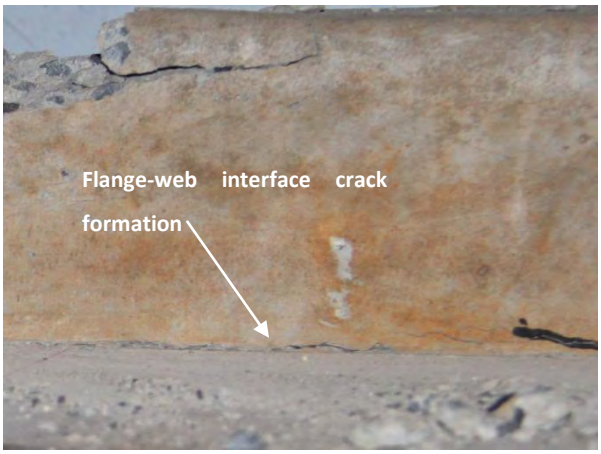

Figure B8: Cracking at flange-web interface

(a)

(b)

Figure B9: Diagonal cracking on impacted surface of beam C-80: (a) left support region (b) right support region

Figure B10: Damage observed after consecutive drop tests conducted on beam R-80

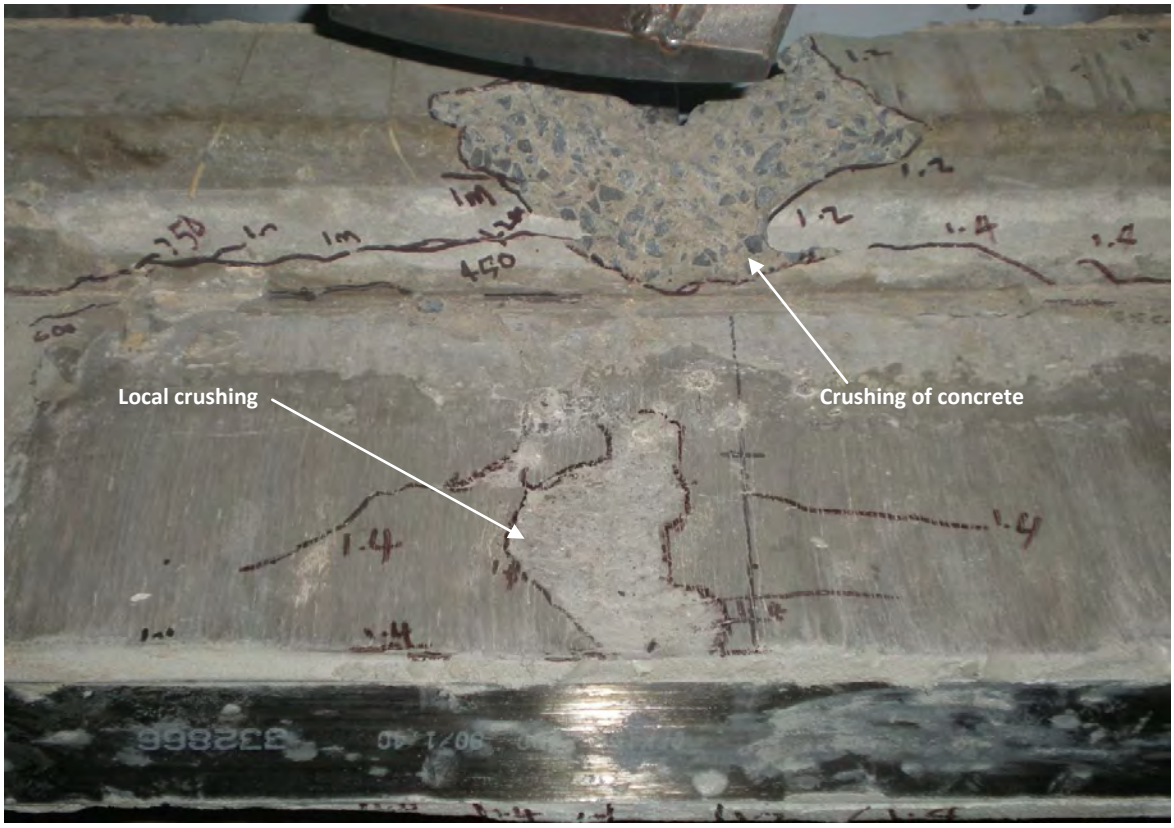

Figure B11: Compression damage and local damage (beam R-80)

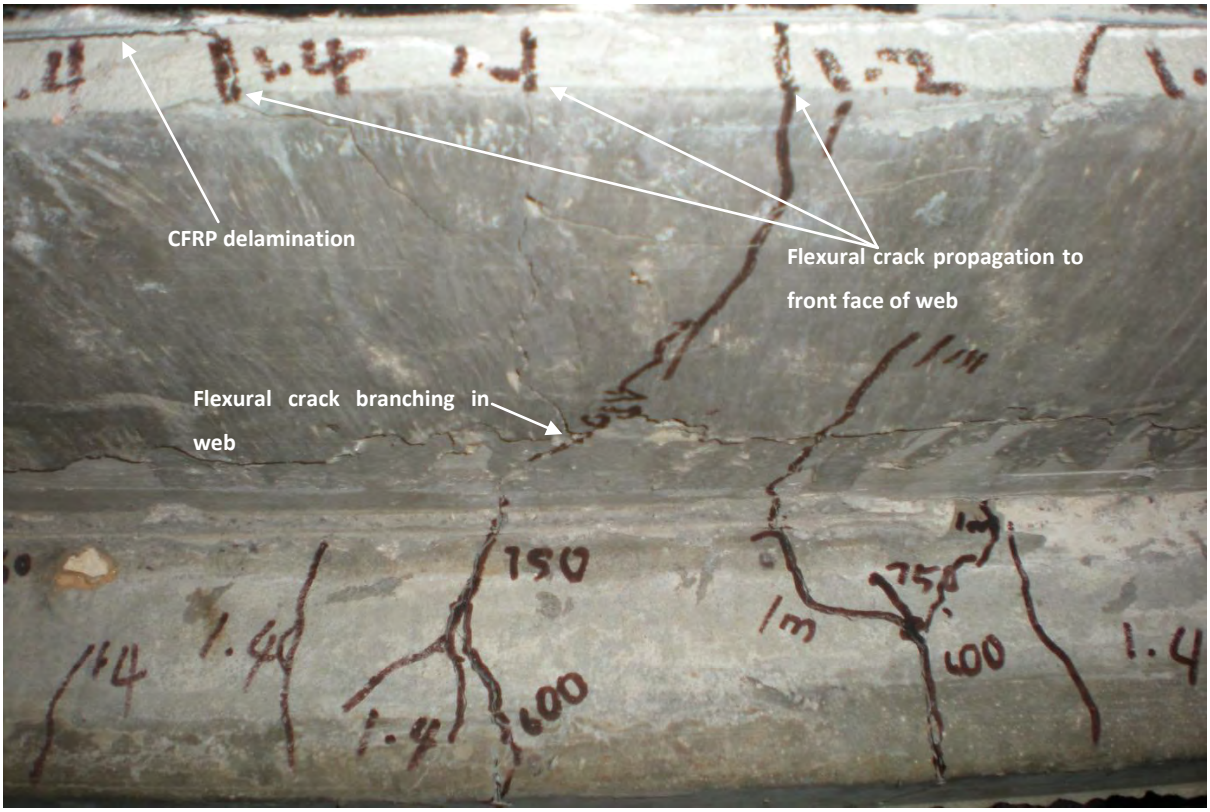

Figure B12: Flexural crack propagation and delamination of CFRP (beam R-80)

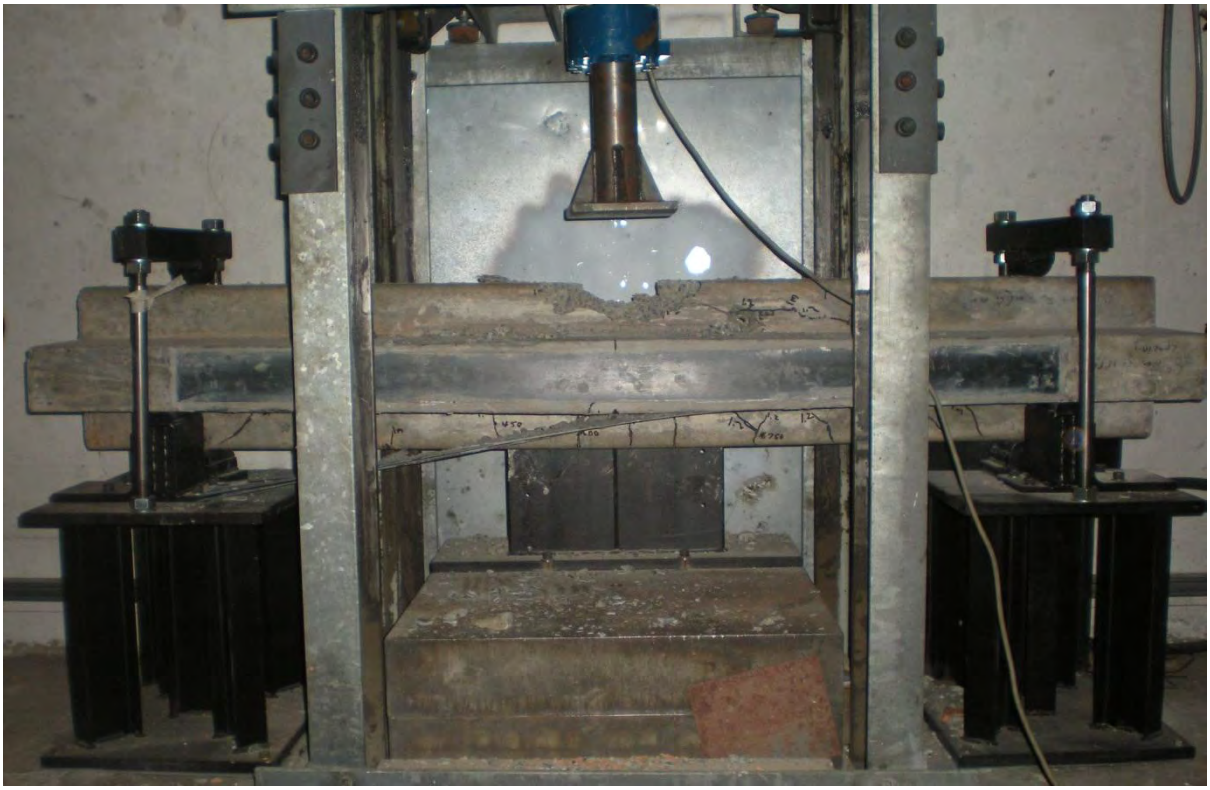

Figure B13: Damage observed after consecutive drop tests conducted on beam RS-80

Figure B14: Compression damage and local damage (beam RS-80)

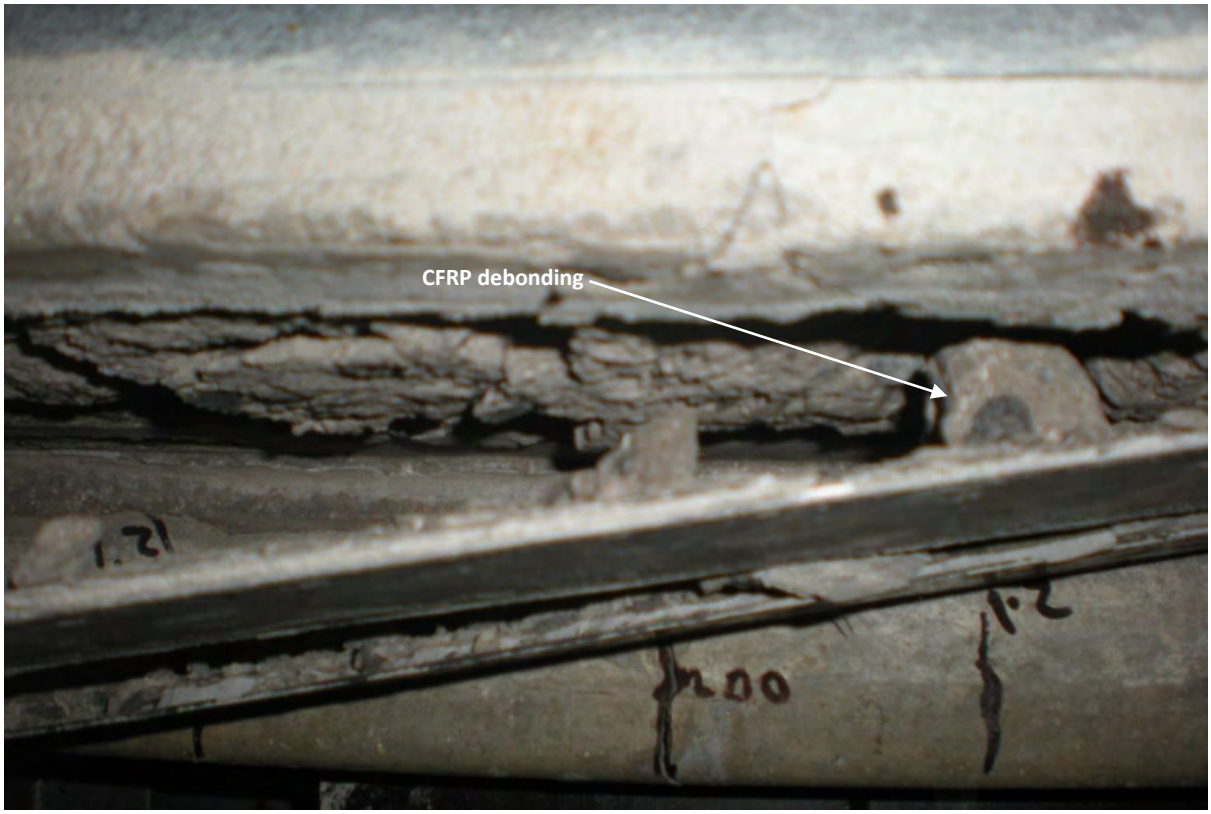

Figure B15: Debonding of additional CFRP applied for horizontal strengthening (beam RS-80)

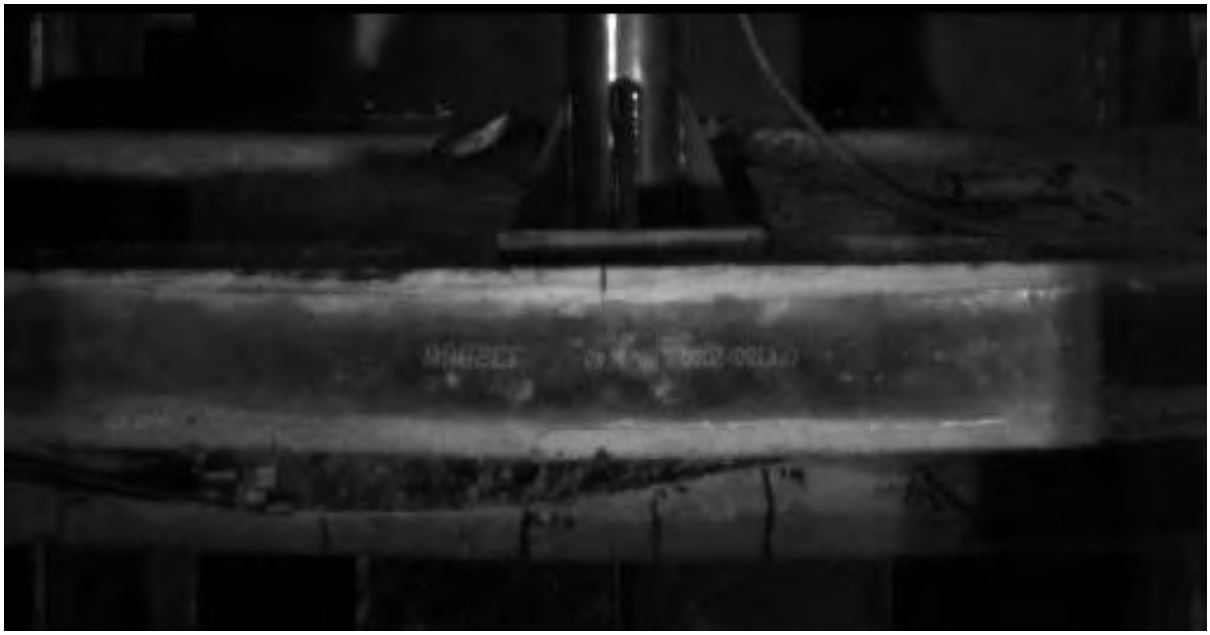

Figure B16: HSC frame showing debonding of CFRP during final drop test (beam RS-80)

Figure B17: Damage observed after consecutive drop tests conducted on beam R-160

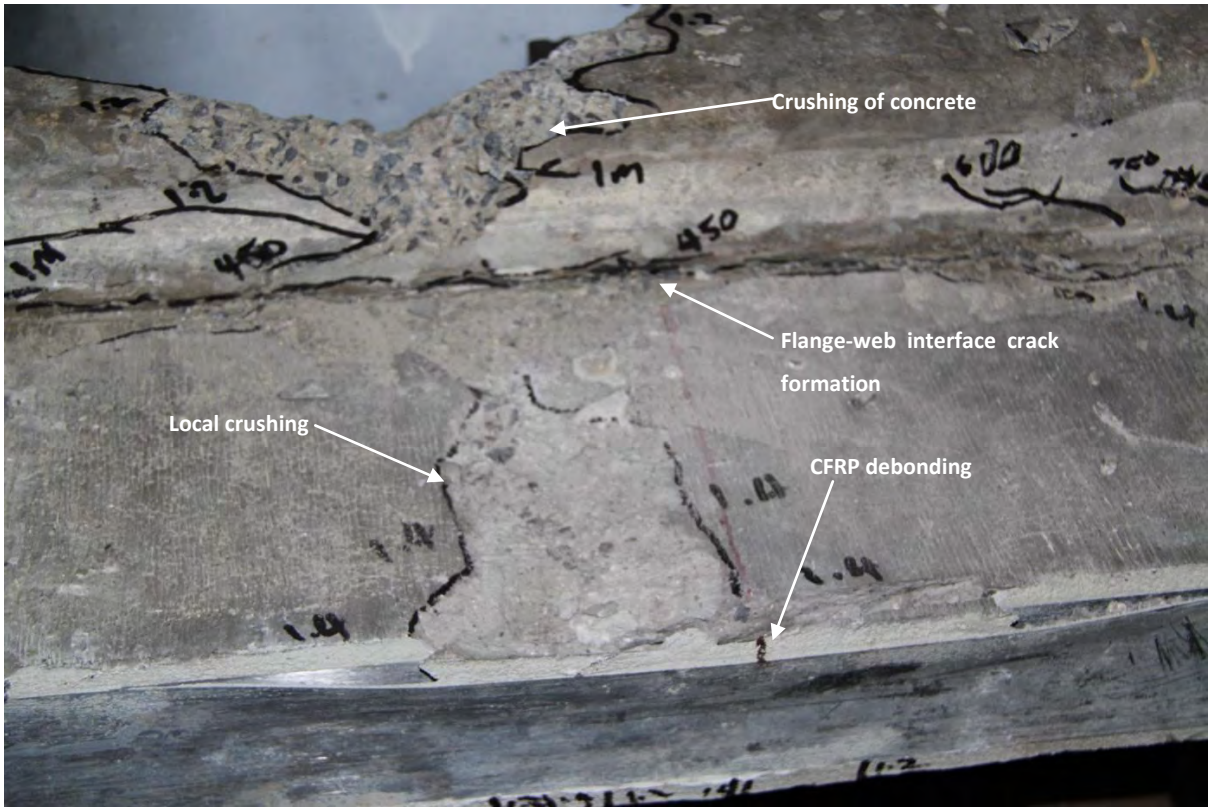

Figure B18: Compression damage, local damage and debonding of CFRP (beam R-160)

Figure B19: Flexural crack propagation (beam R-160)

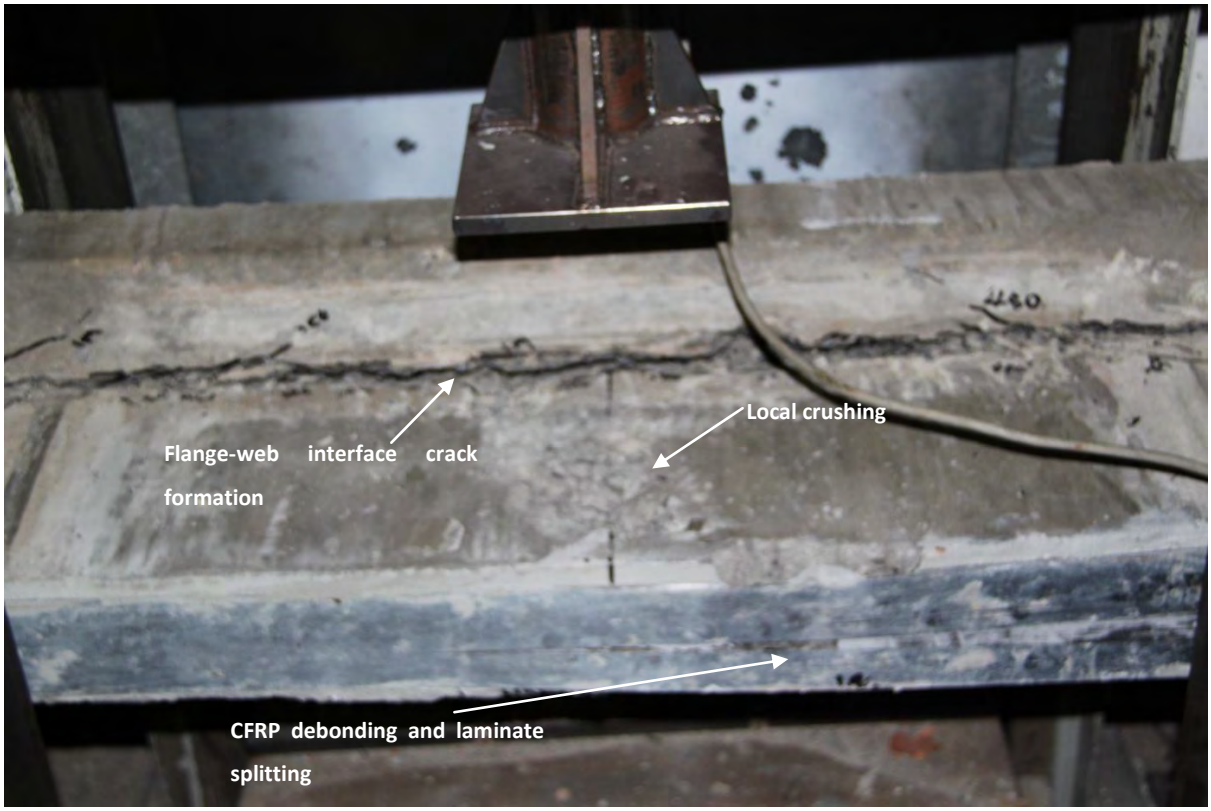

Figure B20: Excessive cracking at flange-web interface (beam R-240)

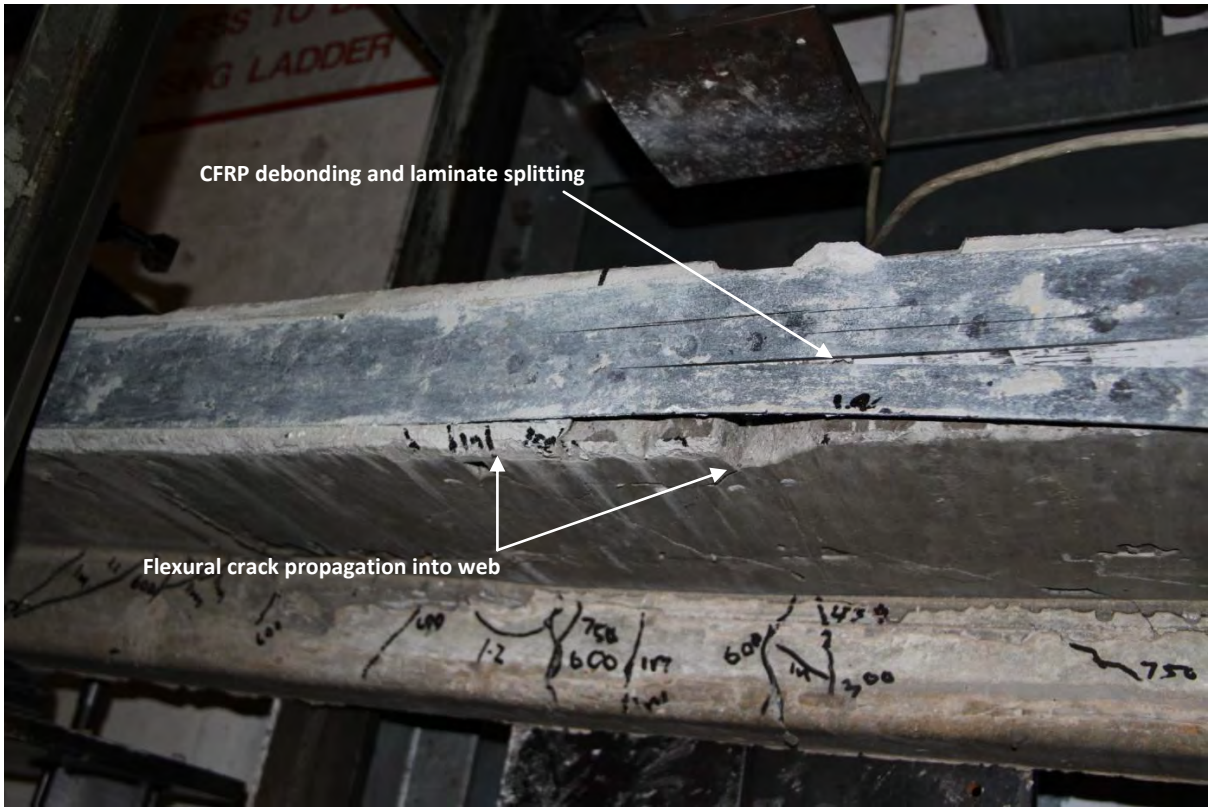

Figure B21: Debonding and laminate splitting (beam R-240)

Appendix C: Contact force response diagrams

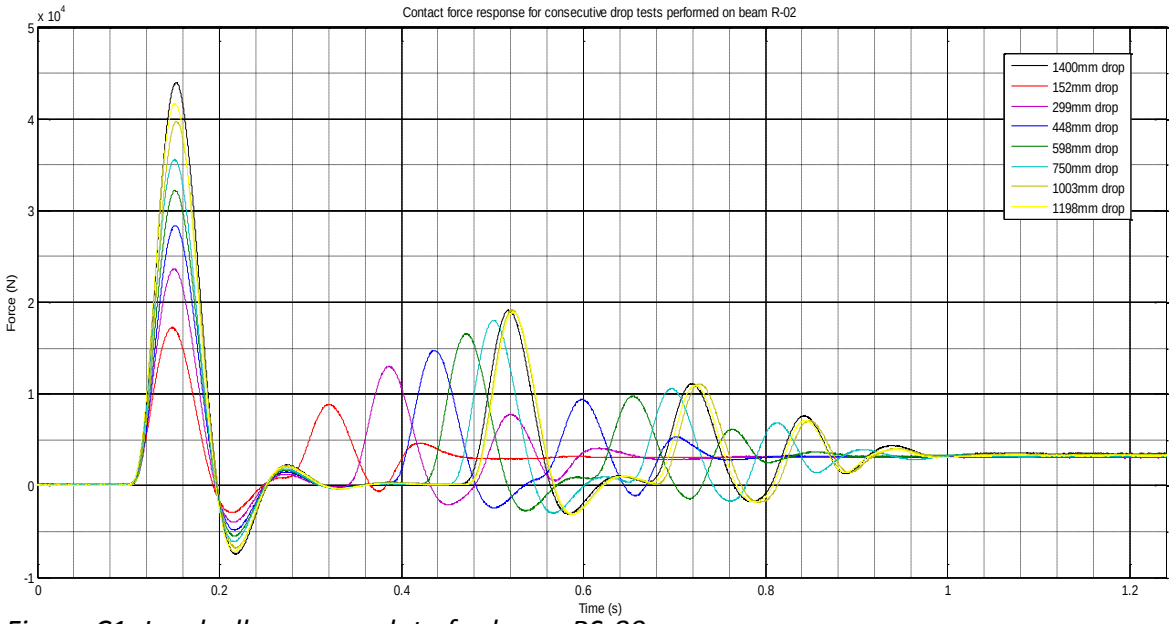

Figure C1: Loadcell response data for beam RS-80

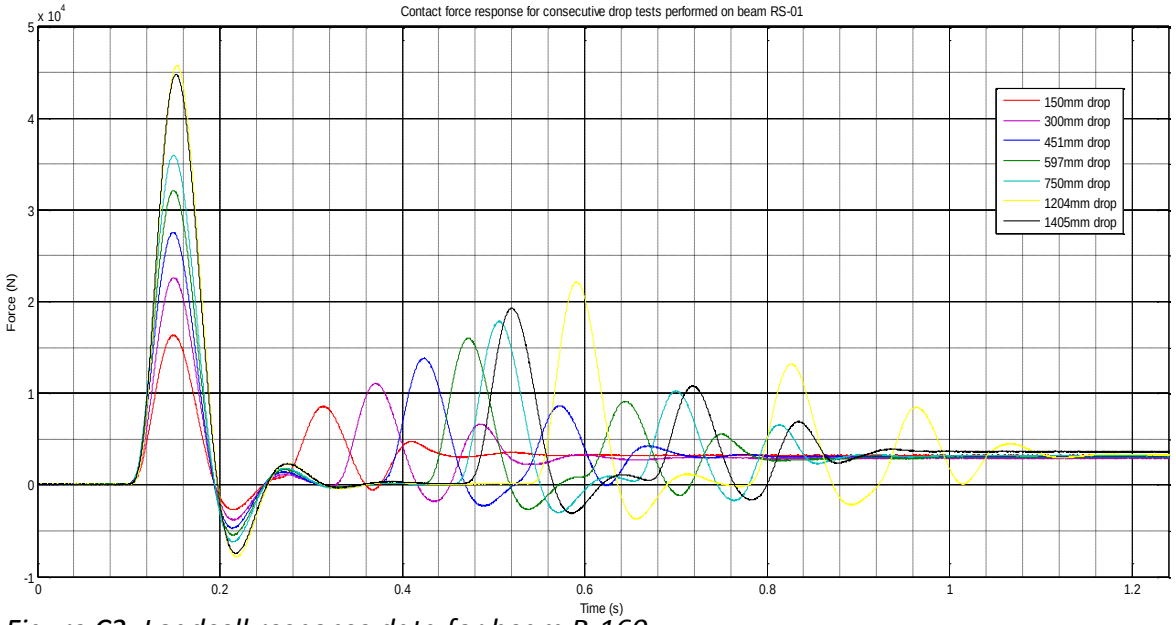

Figure C2: Loadcell response data for beam R-160

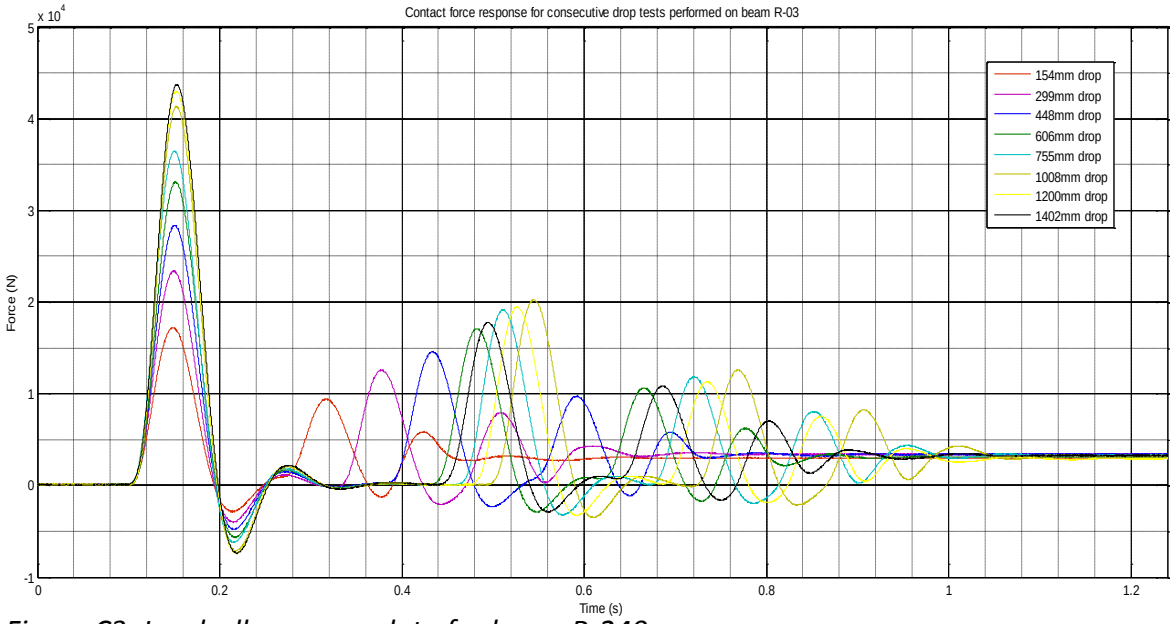

Figure C3: Loadcell response data for beam R-240

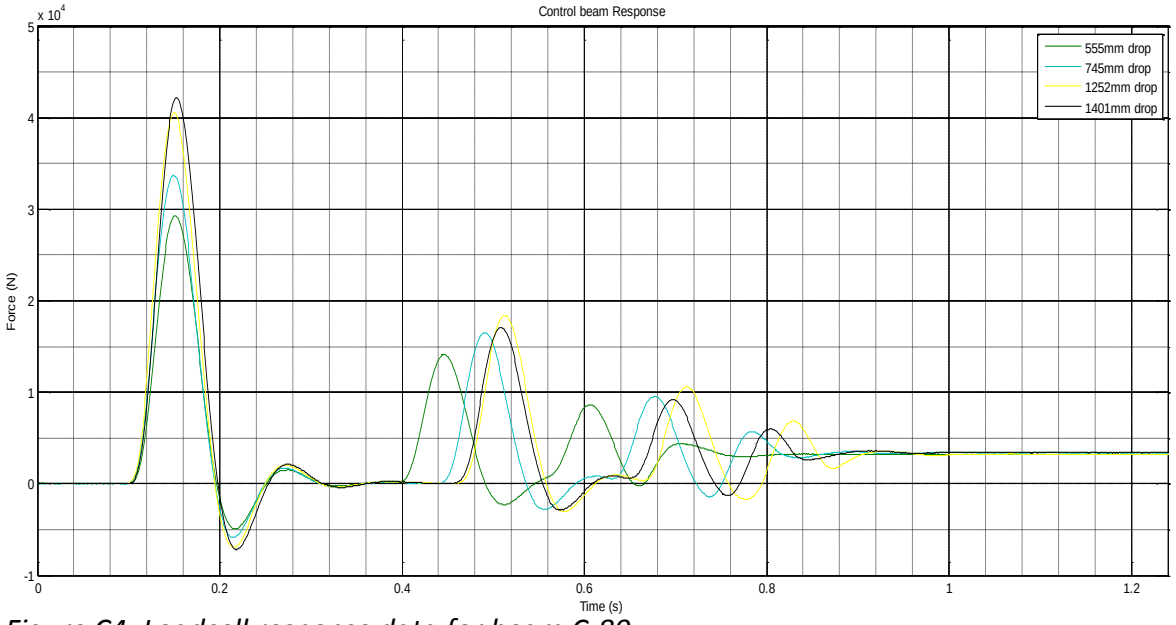

Figure C4: Loadcell response data for beam C-80

Appendix D: Deflection response diagrams

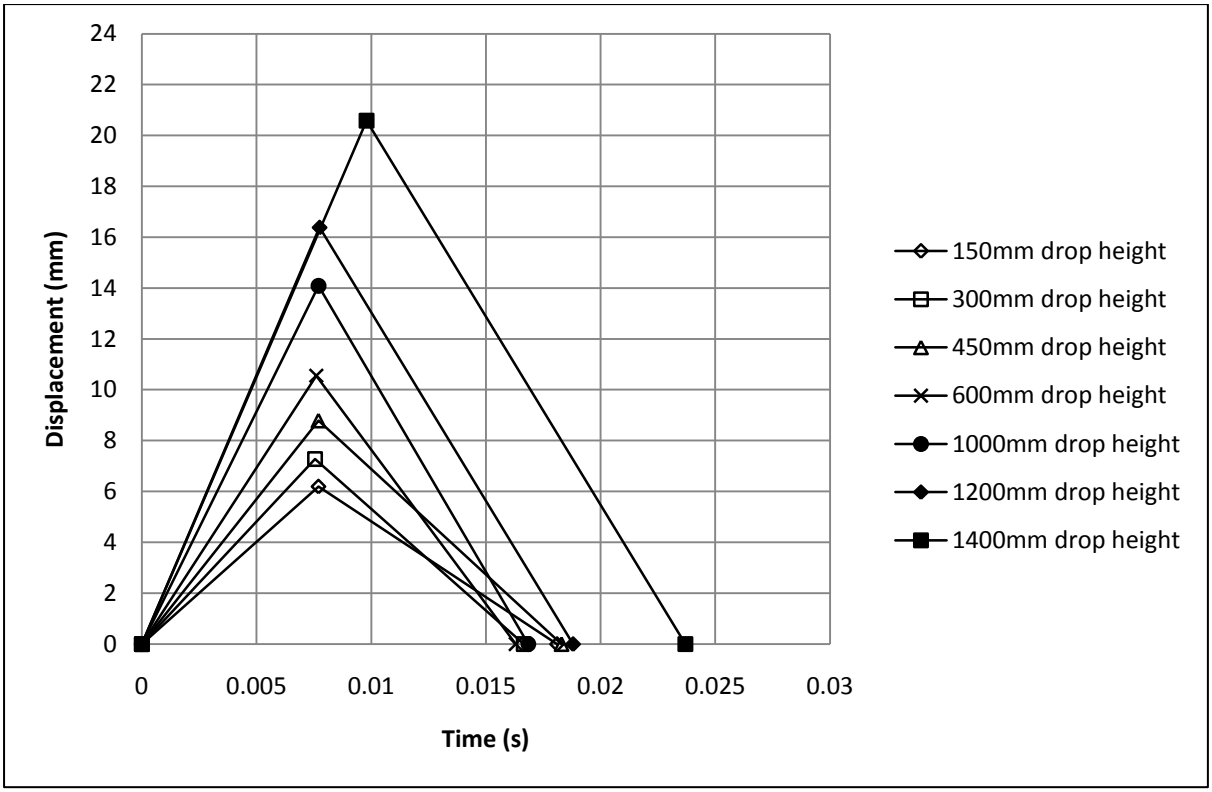

Figure D1: Deflection halfcycle data for beam RS-80

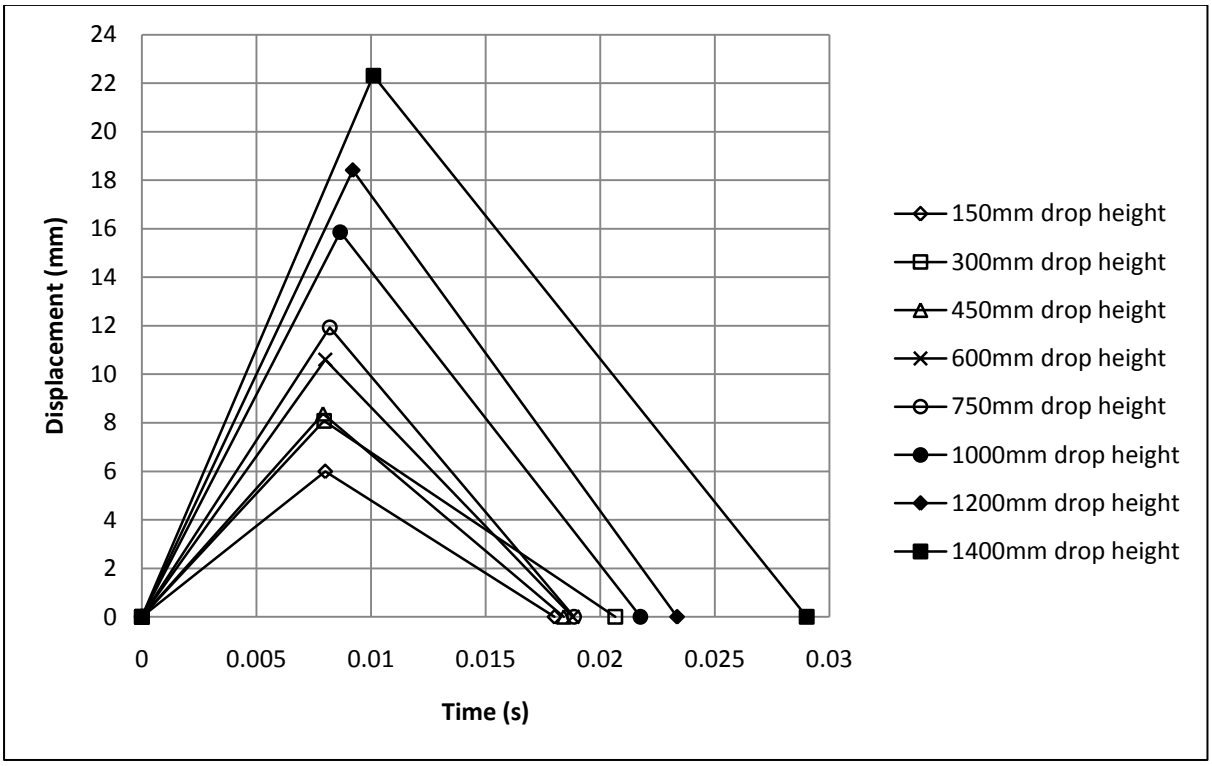

Figure D2: Deflection halfcycle data for beam R-160

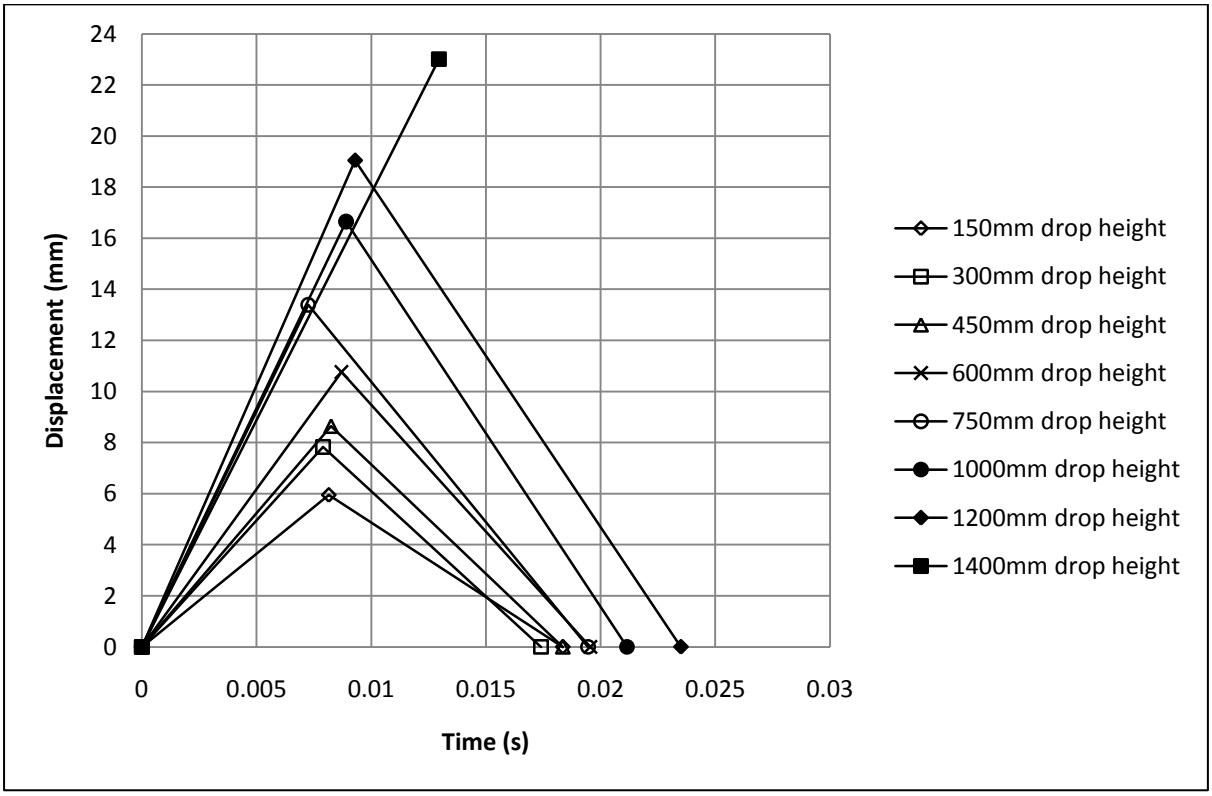

*Figure D3: Deflection halfcycle data for beam R-160**

*During the final drop test (h≈1400) beam R-240 did not return to its original resting place due to excessive plastic deformation.

Table D1: Contact force and displacement data

Beam no.	Drop height (mm)	Contact force (kN)	Midspan Deflection (mm)	Halfcycle duration (s)
R-01	150	17.33	6.193	0.015
	300	22.66	-	-
	450	27.57	8.800	0.0161
	600	31.44	10.533	0.0168
	750	35.33	11.935	0.0167
	1000	39.94	14.016	0.0181
	1200	42.73	15.823	0.0195
	1400	42.65	17.656	0.0232
RS-01	150	16.37	6.191	0.0181
	300	22.64	7.275	0.0167
	450	27.57	8.783	0.0183
	600	32.15	10.552	0.0163
	750	36.01	-	-
	1000	-	14.089	0.0169
	1200	45.77	16.384	0.0188
	1400	44.82	20.583	0.0237
R-02	150	17.24	5.996	0.018
	300	23.66	8.078	0.020
	450	28.38	8.373	0.0184
	600	32.21	10.605	0.0188
	750	35.58	11.933	0.0189
	1000	39.76	15.86	0.0218
	1200	41.71	18.417	0.0234
	1400	43.97	22.312	0.0290
R-03	150	17.24	5.949	0.0184
	300	23.4	7.830	0.0174
	450	28.38	8.640	0.0184
	600	33.1	10.756	0.0196
	750	36.44	13.388	0.0195
	1000	41	16.650	0.0212
	1200	43	19.050	0.0235
	1400	43.72	23.009	0.0330
C-01	150	-	-	-
	300	-	-	-
	555	29.26	-	-
	745	33.69	-	-
	1252	40.53	-	-
	1401	42.15	-	-